GE Research & Development Center

Laser Processing for Interconnect Technology

Final Report

Original contains color plates: All DTIC reproductions will be in black and white

Prepared by

H.S. Cole, Y.S. Liu, and K. Paik
General Electric Research and Development Center
Schenectady, NY 12345

Prepared for

U.S. Office of Naval Research/Strategic Defense Initiative Office
Contract No.: N00014-85-C-0890
Period: January 1, 1988–November 30, 1991

February 27, 1992

92SRD001

Unclassified
SECURITY CLASSIFICATION OF THIS PAGE

REPORT DOCUMENTATION PAGE

Form Approved
OMB No. 0704-0188

1a. REPORT SECURITY CLASSIFICATION
Unclassified

1b. RESTRICTIVE MARKINGS

2a. SECURITY CLASSIFICATION AUTHORITY

3. DISTRIBUTION / AVAILABILITY OF REPORT

2b. DECLASSIFICATION / DOWNGRADING SCHEDULE

4. PERFORMING ORGANIZATION REPORT NUMBER(S)

5. MONITORING ORGANIZATION REPORT NUMBER(S)

6a. NAME OF PERFORMING ORGANIZATION
General Electric Company
Corporate Research & Development

6b. OFFICE SYMBOL (*If applicable*)

7a. NAME OF MONITORING ORGANIZATION
Office of Naval Research

6c. ADDRESS (*City, State, and ZIP Code*)
P.O. Box 8
Schenectady, NY 12301

7b. ADDRESS (*City, State, and ZIP Code*)
800 N. Quincy Street
Arlington, VA 22217-5000

8a. NAME OF FUNDING / SPONSORING ORGANIZATION
Strategic Defense Initiative Office

8b. OFFICE SYMBOL (*If applicable*)

9. PROCUREMENT INSTRUMENT IDENTIFICATION NUMBER
N00014-85C-0890

8c. ADDRESS (*City, State, and ZIP Code*)
1717 H Street N.W.
Washington, DC 20006

10. SOURCE OF FUNDING NUMBERS

PROGRAM ELEMENT NO.	PROJECT NO.	TASK NO.	WORK UNIT ACCESSION NO.

11. TITLE (*Include Security Classification*)
Laser Processing for Interconnect Technology

12. PERSONAL AUTHOR(S)
H. S. Cole, Y. S. Liu, K. Paik

13a. TYPE OF REPORT	13b. TIME COVERED	14. DATE OF REPORT (*Year, Month, Day*)	15. PAGE COUNT
Final Technical Report	FROM 10/1/85 TO 11/30/91		

16. SUPPLEMENTARY NOTATION

17. COSATI CODES			18. SUBJECT TERMS (*Continue on reverse if necessary and identify by block number*)
FIELD	GROUP	SUB-GROUP	

19. ABSTRACT (*Continue on reverse if necessary and identify by block number*)

Laser-assisted metal deposition and photoetching on low dielectric constant substrates were investigated for applications in direct write adaptive interconnect technology. In addition, critical materials issues such as metal/polymer interface properties, adhesion and metal interdiffusion in new polymers, including benzocyclobutene and polyquinoline were studied. Laser-activated copper deposition on polyimide was demonstrated using an argon ion laser at 351 nm; writing speeds up to 10 cm/s with 10-μm-wide Cu lines and resistivities of 3 Ω-cm were demonstrated. A process to selectively electroplate copper was discovered in this program. Copper lines on polyimide dielectrics used in high density interconnect structures were demonstrated using this process in conjunction with a laser direct write patterning technique. Copper lines 4 μm thick and 8 μm wide were achieved. Photoetching of polymers and high-speed via formation in polyimide dielectrics was investigated using a frequency-quadrupled YAG laser at 266 nm.

20. DISTRIBUTION / AVAILABILITY OF ABSTRACT
☐ UNCLASSIFIED/UNLIMITED ☐ SAME AS RPT. ☐ DTIC USERS

21. ABSTRACT SECURITY CLASSIFICATION
Unclassified

22a. NAME OF RESPONSIBLE INDIVIDUAL	22b. TELEPHONE (*Include Area Code*)	22c. OFFICE SYMBOL
Dr. Wallace Smith	(703) 696-0284	Code 431N

DD Form 1473, JUN 86 *Previous editions are obsolete.* SECURITY CLASSIFICATION OF THIS PAGE

Table of Contents

Section ..... **Page**

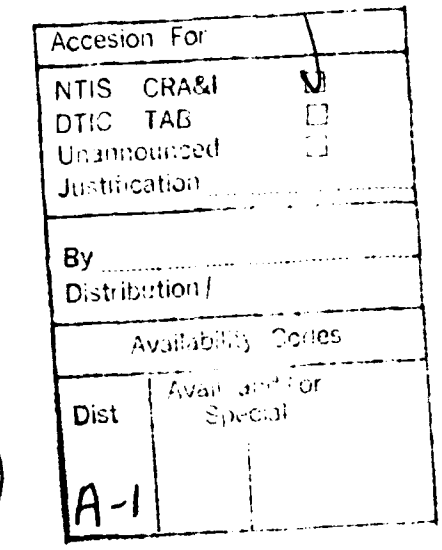

Statement A per telecon
Dr. Wallace Smith ONR/Code 1132
Arlington, VA 22217-5000

NWW 3/31/92

List of Figures

Figure *Page*

List of Tables

ACKNOWLEDGEMENT

This work was sponsored by the Strategic Defense Initiative Office (SDIO) under the direction of Dr. Kepi Wu and Dr. Dwight Dustin of the Innovative Science and Technology Section. The program was administered by the Office of Naval Research under Contract No. NOOO14-85C-0890 and managed by Dr. Wallace Smith. This report covers work performed during the second phase of this program, January 1988 to November 1991.

The authors wish to acknowledge R. Guida and J. Rose for their excellent technical capabilities in performing the experiments in this program. Experiments on gold metallization were carried out by T. Ali.

Technical discussions with Dr. H. R. Philipp and Dr. L. M. Levinson during the early phase of this work are greatly appreciated. Rutherford backscattering carried out by Professor H. Bakhru of the Physics Department at the State University of New York at Albany, New York; x-ray photoelectron spectroscopy, and cross section transmission electron microscopy measurements by Dr. M. Burrell, J. Chera and G. Hutchins of CRD are also acknowledged. In addition, discussions with Dr. B. Karas and Dr. D. Foust on various metallization processes and with Professor G. D. Mahan of the University of Tennessee on ablation theory have been very helpful to this work.

Section 1

SUMMARY

The overall objective of this program has been to investigate laser-activated chemistry for fabrication of metal lines on low dielectric constant substrates. The need to provide highly conductive metal on polymeric substrates (with $\varepsilon < 3.5$) is essential for high-speed interconnect technology. Using lasers to fabricate these interconnects offer unique possibilities and advantages over more conventional lithography approaches. Since the laser can be put under computer control, the possibility exists for rapid design modifications.

Initial results of work performed on this contract were reported in a Phase I final report entitled, "Laser-Activated Metal Deposition," January 31, 1988. This Phase I report covers work during the period of October 1, 1985 to December 31, 1987. Work carried out during that time period included a survey of laser-driven processes for metal deposition from organometallic compounds and investigations into various gas phase and thin film metal deposition processes. The key output of that activity was the development of a process to selectively deposit copper on polyimide. The approach uses a CW laser at 351 nm to irradiate organometallic palladium compounds to selectively deposit catalytic amounts of palladium on polyimide. Subsequent immersion of the irradiated samples in an electroless copper solution resulted in selective copper deposition. Since only a few monolayers of palladium were needed to catalyze the electroless copper process, fast writing speeds of up to 10 cm/s were achieved. Copper lines with 1.5-μm thickness and resistivities of 3 μ Ω-cm were produced. This process is reviewed in Section 3 of this report.

The scope of this program was expanded during the second phase of this contract covering the period from January 1988, to September 30, 1991. The area of study during this period covered the topic, "Laser Processing for Interconnect Technology." Areas of study included additional development on direct-write metal deposition processes, laser photoetching of polymers, metal/polymer interface studies, and selected studies on very low dielectric constant polymers for applications in the GHz region.

Following is a summary of the major accomplishments of this program:

- A new process was developed for high-speed fabrication of microvias in polyimide. A frequency quadrupled YAG laser was developed using a tandem-doubling technique to generate UV pulses at 4.6 eV at a high-pulse repetition rate to 5 kHz. The UV-pulsed YAG is used to fabricate 10-μm-diameter vias in 25-μm thick polyimide at a drilling speed of 20 ms per via hole.
- A new selective electrolytic copper deposition process was discovered. This process, referred to as selective electrolytic deposition (SED), used a metal primer layer such as titanium, which when properly treated, will prevent electroplating. Thus, a laser-patterned copper layer on titanium can be selectively electroplated in

the regions containing the copper pattern. Copper lines 8 μm wide and 3 μm thick were produced on polyimide using this novel SED process. (A patent, US #4,988,412 was granted on Jan. 29, 1991.)

- A process to plate gold on ceramic substrates for use as power and ground connections in a high-density interconnect package was demonstrated. The process uses deposition of a palladium compound to produce a catalytic surface for electroless nickel and electrolytic or electroless gold.

In addition, various in-depth studies relating to surface catalysis, metal/polymer interfaces, laser photoetching, electroless and electroplating, and interconnect metallization processes were investigated. The results of some of these studies can be found in reference papers published under this program.

During the course of this work, a novel high-density interconnect packaging system (HDI) has been under development at GE Research and Development (CRD). This approach uses a polyimide overlay layer over bare chips on a ceramic substrate where the polyimide layer functions as the insulating layer, and the connection to the integrated circuit chips is accomplished through via holes to the individual bonding pads. Via hole formation and interconnect metallization are accomplished using a laser lithography system. The unique capability, which is not feasible in conventional interconnect approaches, allows partitioning of complex systems for testing with subsequent removal and replacement of nonfunctioning chips. The key to the system performance is the use of a direct-write adaptive laser lithography system, which increases interconnect density by an order of magnitude over that achieved by conventional packaging techniques. High-density interconnect structures are currently being fabricated with 100-μm pitch and up to 4 levels of interconnect structure. In addition, a prototype facility at CRD has been established for the production of limited quantities of devices. The current baseline process uses polyimide dielectrics, and the interconnect structure is copper fabricated using photoresist technology.

The results and developments of this program can significantly advance the state of the art of high-density interconnect technology in general and in particular the developments of the current GE-HDI process described above. A major goal of the ONR/SDIO-sponsored research has been the development of non-resist processes for use in interconnect structures. Conventional resist processing is limited to 4-mil pitch design rules because of nonuniform surface topography and other fundamental issues associated with laser equipment, throughput, and thick film resist materials considerations. Laser-direct write metal deposition processing has been demonstrated and may improve line resolution and pitch in HDI structures. As the on-chip device density increases, a higher resolution interconnect technology is required to take advantage of the improved chip performance. Higher resolution interconnects provide higher density chip packages resulting in reduced interconnect length, propagation delay, and higher speed circuits. Improvements in speed, yield, reliability, and lightweight packages can be accomplished by improved interconnect resolution. In addi-tion, processes for direct-write metal interconnect for in situ repair of opens can further offer process yield advantages.

Studies of new low dielectric constant polymers and structures developed under this sponsorship will impact device performance as we move to higher frequency device

fabrication. Furthermore, the results of metal/polymer interface studies and laser photo-etching experiments have pointed the direction of process related developments in this high frequency regime.

Section 2

PHASE II OBJECTIVES

The fabrication of metal lines by laser-induced deposition techniques offers several advantages over other thin film deposition processes because the process is noncontact, maskless, low temperature, selective, and relatively simple. In addition, the ability to interface a laser with computer offers unique advantages in circuit design as well as in process implementation.

Phase I studies focused on selective deposition of copper on polyimide. A two-step laser catalized copper deposition process was developed and demonstrated. Additional studies addressed issues such as metal/polymer adhesion and laser photoetching of polymers.

Based on results obtained in Phase I, the objectives of this program were broadened to include all aspects of laser processing for high-density interconnect technology. The objectives of the Phase II extension of this program are grouped into four basic areas of research:

1. Continued development of direct-write metal depostion processing on polyimides.
2. Basic understanding of metal/polymer interfaces as a means to develop processes to provide improved adhesion of metal/polymer systems.
3. Understand mechanism of laser photoetching for development of rapid laser via fabrication process.
4. Investigation of low dielectric constant polymers for use in high-density interconnects in the GHz regime.

Section 3

TECHNICAL ACTIVITIES

3.1 Laser-based Processing Technologies for High-Density Interconnect

3.1.1 Introduction

As electronic devices become faster and more complex, the chip-to-chip delay begins to limit the electronic system performance. To reduce the chip-to-chip interconnect length and improve circuit performance, high-density interconnect multichip module (MCM) packaging is considered to be a key technological solution. Various MCM technologies have been developed in recent years and are summarized in Table 3.1-1 in terms of substrate, metal, dielectric materials, method of patterning, chip attachment, and interconnect technology. [1] As shown in Table 3.1-1, copper and aluminum are the most commonly used metals for high-density multichip interconnect, and polyimide is the preferred dielectric material. The polymeric materials are compatible with the standard IC processing technology, have good thermal stability, and more important, have lower dielectric constants suitable for higher frequency applications.

Among those HDI technologies listed in Table 3.1-1, GE [2] and Livermore [3] employed lasers as the main processing tool for fabrication of the interconnect structures. Although the dielectric materials and interconnect structures employed in these two processes differ considerably from each other, both processes employ the adaptive and maskless laser techniques which make them particularly suitable for quick turnaround and prototype design. In the following sections, we will discuss several novel processing technologies developed for advanced electronic packaging applications under the present program.

Laser processing has been shown to be a viable technology for depositing and/or etching a variety of metals and dielectric materials and has been the subject of many research activities. [4-7]. Laser metal patterning on polymers, either direct-write or projection patterning, is of particular relevance to high-density interconnect. In electronic packaging, the surface topography is not aways perfectly planer, the relatively long depth of field provided by a laser beam is an important property. In the earlier phase of this program, we investigated various laser-induced metal deposition processes with emphasis on a two-step approach for improving the writing speed. In this phase, in addition to direct metal processing, we extended the study to investigate photo-etching of polymeric materials and applied laser ablation to fabricate interconnect structures such as micro-vias and metal interconnects.

3.1.2 Laser Photo-etching of Polymers

3.1.2.1 UV Laser Sources for Photo-etching

Several laser sources are available for photo-etching of polymers: excimer lasers, argon ions laser, and solid state YAG laser. Each of these laser sources has its own unique properties, and the selection of each type of laser mainly depends upon specific application requirements.

Table 3.1-1

High Performance Interconnect Technologies Multi-Chip Hybrid Module [1]

USER	SUBSTRATE	CONDUCTOR				INSULATOR	CHIP ATTACH	MODULE I/O
		MATERIAL	WIDTH	THICKNESS (μm)	PITCH			
MOSAIC	Si	Al	11	2	22	SiO_2	WIRE-BOND	WIRE-BOND
IBM	Al_2O_3	Cu	8	6	25	POLYIMIDE	SOLDER-BUMP	PIN-GRID-ARRAY
HONEYWELL	Si	Cu	50	5	125	POLYIMIDE	WIRE-BOND TAP-BOND	WIRE-BOND
ATT	Si	Cu	25	5	50	POLYIMIDE	SOLDER-BOND	PIN-GRID-ARRAY
RAYCHEM	Si	Al	40	5	100	POLYIMIDE	WIRE-BOND	WIRE-BOND
GE	Al_2O_3	Cu	25	5	75	POLYIMIDE	OVERLAY THIN FILM	WIRE-BOND
LIVERMORE	Si	Au	15	3	25	SiO_2	BEVELED EDGE THIN FILM	WIRE-BOND

Excimer Lasers

The excimer lasers have many unique features: high power, high efficiency, and high brightness and are powerful UV laser sources useful for a wide range of microfabrication applications such as lithography, surface modification, and micromachining of both organic and inorganic materials. The presence of a large number of transverse modes scrambles the spatial coherence and thus eliminates the speckle noises frequently observed in images formed from coherent illumination seen in other kinds of lasers. Figure 3.1-1 shows the available powers obtained from excimer lasers and several other UV lasers. The figure also includes the spectral output from a 1-kW medium-pressure incoherent mercury arc lamp measured at 1-m distance away from the lamp.

Argon Ions Lasers

The high power visible and UV argon ion lasers are frequently used in microelectronic processing for imaging and scanning applications. The argon ions laser emits visible radiation between 454.5 to 514.5 nm and UV radiation between 351.1 to 363.8 nm. The commercially available argon lasers are operable to 20-W multiple lines in the visible, about 10-W single line at 514.5 nm, and 7-W at 488 nm. UV argon lasers with multiline UV outputs of 7 W (351-364 nm) are now available. The Argon ion lasers are typically operated continuously. They can also be operated in the pulsed and mode-locked modes to produce pulses to about 100 ps duration at a repetition rate equal to c/2L, where L is the laser cavity length and c is the speed of light. A visible argon laser can be frequency doubled to generate cw UV output at 257 nm using nonlinear optical crystals KDP, ADP, or BBO. Efficient doubling requires phase-matching, which can be accomplished either by properly orienting the crystal or by adjusting the crystal temperature. The output from a frequency doubled cw argon laser is typically on the order of several mW's.

Solid State YAG Lasers

The solid-state Nd:YAG laser is a versatile laser source capable of CW, pulsed, Q-switched or mode-locked operation. The solid state YAG laser can be operated at a pulsed mode with a pulse rate to several thousand pulses per second; as a result, it can be used as a laser source for direct writing applications. We have constructed a cw pumped, acousto-optically Q-switched frequency-doubled YAG to produce a visible output at 0.53 μm using a KTP or LBO crystal as the doubling crystal. A versatile UV laser source at 266 nm was also developed during this program for photoetching study using a two-stage frequency doubling process. The cavity configuration is shown schematically in Figure 3.1-2. In a typical experiment, an average UV power of about 50 mW at 266 nm and about 500 mW at 530 nm were generated. The solid-state YAG laser has several advantages including its reliability, ease of handling, and frequency agility. In addition, the YAG laser can be miniaturized and pumped by a diode laser.

3.1.2.2 Optical Properties of Polymers

At the beginning of this program, little information was available on the optical UV properties of polymeric materials of interest to electronic applications in spite of the fact that there was significant interest and activities in polymer processing using lasers. A systematic study was therefore initiated to measure the UV optical properties of a selected number of polymers of interest. By applying Kramers-Kronig analysis, complex indices of refraction of polymers were derived in the spectral range from IR to near

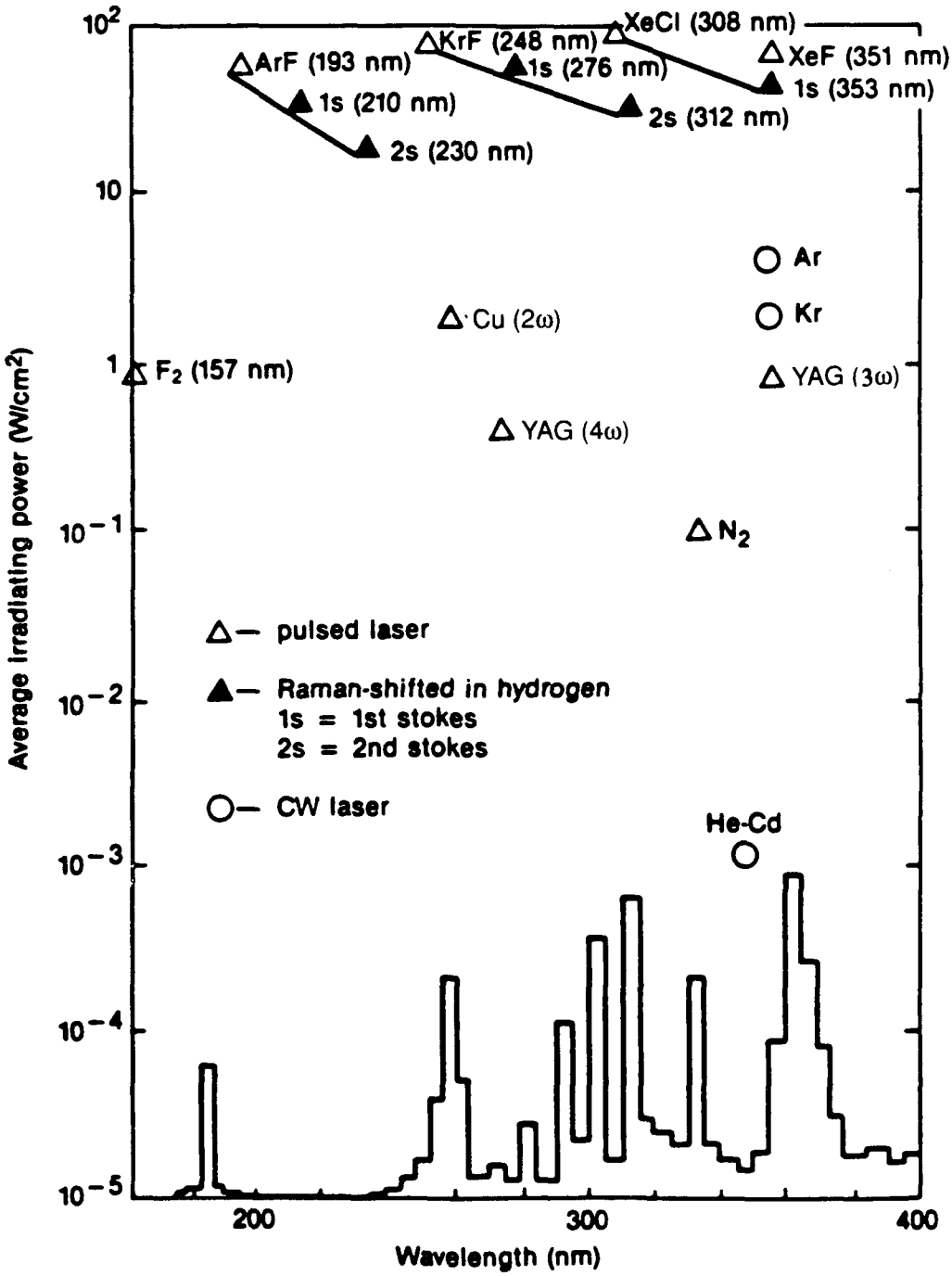

Figure 3.1-1. The spectral output powers from various UV laser sources compared with those from an incoherent Hg lamps.

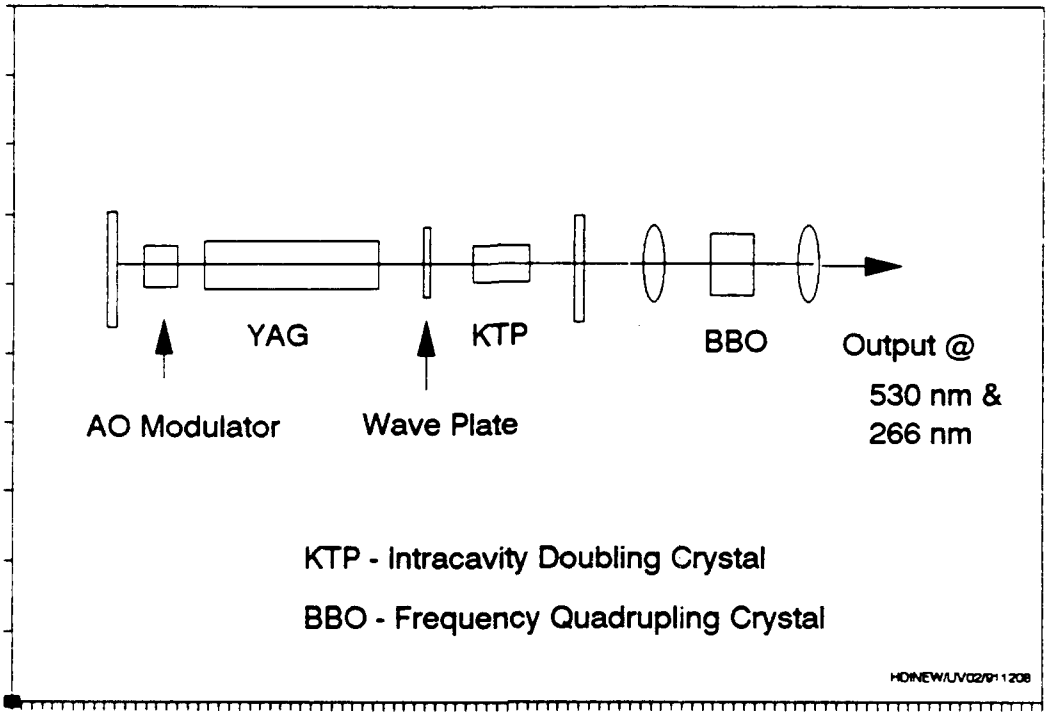

Figure 3.1-2. A schematic of a frequency quadrupled YAG laser.

100 nm and were reported earlier [8,9]. In this section, the relevant optical data useful for laser processing are briefly summarized.

The optical absorption of several useful polymers was measured in the spectral range of 200 nm to about 400 nm using a vacuum UV spectrometer. The absorption coefficients, α (cm^{-1}), for various polymers were determined including polyimide (PI), poly(methyl-methacylate) (PMMA), poly(vinylacetate) (PVA), poly(a-methyl styrene) (PS), poly(tetrafluoreoethylene) (PTFE), polyproylene (PP), nitrocellulose, copolymer styrene allyl alcohol (SAA) and polymer-monomer mixtures PVA plus 25% (weight) byphenyl carnonitrile. The details of these measurements were discussed in the ealier phase of the study. Table 3.1-2 lists the optical absorption coefficients of polymers at 193, 248, 308 and 351 nm, which correspond, respectively, to ArF, KrF, XeCl and XeF excimer laser wavelengths. As shown in Table 3.1-2, the optical absorption coefficients of polymers in this spectral range vary by as much as four orders of magnitude. For example, the optically thin polymers such as PMMA have an absorption coefficient of 2×10^3 cm^{-1} and PTFE, 2.6×10^2 cm^{-1} at 193 nm, respectively, while optically thick polymers such as polyimide have an absorption coefficient, e.g., 4.2×10^5 cm^{-1} at 193 nm and 2.8×10^5 cm^{-1} at 248 nm.

Table 3.1-2

Optical Absorption Coefficients of Selected Polymers (cm^{-1})

POLYMER	193 nm	248 nm	308 nm	351 nm
Polyimide	4.2×10^5	2.8×10^5	1.2×10^5	2.6×10^4
Polysulfone	4.0×10^5	1.5×10^5	8.1×10^2	$\sim 10^1$
Polycarbonate	5.5×10^5	1.0×10^4	2.2×10^1	4×10^0
Poly(a-methyl)styrene	8.0×10^5	6.5×10^3	8.0×10^1	$\sim 10^1$
Poly(methyl-methacrylate)	2.0×10^3	6.5×10^1	$< 10^1$	$< 10^1$
Poly(vinylacetate)	1.0×10^3	$< 10^2$	$< 10^1$	$< 10^1$
Polyethylene	6.3×10^2	$< 10^1$	$< 10^1$	$< 10^1$
Polypropylene	5.3×10^2	$< 10^1$	$< 10^1$	$< 10^1$
Polytetrafluoroethylene	2.6×10^2	1.4×10^1	$< 10^1$	$< 10^1$

3.1.2.3 Photo-etching Rates Studies

In this investigation, our first attempt was to correlate the photo-ablation characteristics such as photo-etching rates of a polymer with its optical absorption property. To control the optical absorption property of a polymer, we devised a method to alter the absorption coefficient by blending together two polymers of distinctive optical absorption coefficients. For example, PMMA and PS (polymethyl-styrene) mixtures were prepared with different compositions and their etching rates were measured as functions of irradiation fluence. PMMA and PS are mutually soluble and by adjusting the concentration of PS in PMMA, absorption coefficients can be varied from 2×10^3 cm^{-1}

for the pure PMMA, to 1.5×10^4 cm^{-1} for 2% PS in PMMA, 7×10^4 cm^{-1} for 20% PS in PMMA, and 8×10^5 cm^{-1} for pure PS. The etched depths per pulse of PMMA and its mixtures measured as a function of various laser fluence levels are shown in Figure 3.1-3, where the vertical axis, defined as the etch depth per pulse, was the total etched depth measured using a surface profilometer divided by the total number of pulses irradiated upon the sample surface over a given area. The x-axis is defined as the laser energy per pulse over the irradiated area. In the measurements, the laser pulse duration was constant at about 20 ns.

From these measurements, the initial results suggested that, once the laser fluence is above a certain threshold value, the etched depth per pulse increased almost linearly as a function of the incident laser fluence to about 0.5 J/cm^2. Above this fluence level, the etching rate started to saturate. The saturation level depended upon the degree of absorption of the polymer mixtures and the inflection point was observed to vary reciprocally with the absorption coefficient of the material.

If we used the irradiation laser fluence as a variable and plotted the measured photo-etching rates as a function of the absorption coefficient by reconstructing the data shown in Figure 3.1-3. This representation is shown in Figure 3.1-4. In this figure, the absorption depth, $1/\alpha$, where the intensity of incident light attenuates to e^{-1} of its incident value at the surface is also drawn. We observed in the region where the mixture has a low optical absorption ($< 10^4$ cm^{-1}), the etched depth per pulse was smaller than the optical absorption depth of the sample mixture; on the other hand, in the high absorption region ($> 10^4$ cm^{-1}), the observed etched depth is larger than the optical absorption depth. These data suggested: (1) that the etching depth in a polymer can be controlled by modifying its optical properties, and (2) that the Beer's law does not satisfactorily describe the observed photo-etching behaviors in PMMA and PS mixtures.

To determine if these measurements were material-dependent, similar measurements were performed over a variety of polymers whose absorption coefficients vary from 10^3 cm^{-1} to 10^6 cm^{-1}, and the etched depths measured at 0.2 J/cm^2 using both an ArF laser (193 nm) and KrF laser (248 nm) were plotted in Figure 3.1-5. In this figure, the straight line represents the corresponding optical absorption depth. This result is in good agreement with those measured in PMMA/PS mixtures. Considering the fact that the absorption coefficients of those polymers vary by more than three orders of magnitude, the etched depths measured at about 200 mJ/cm^2 using either the ArF (193 nm) or KrF(248 nm) laser varied only by less than factor of five. Similar to that observed in the PMMA/PS mixtures, the data confirmed that the etched depths for strongly absorptive polymers were generally larger than the absorption depths defined by the Beer's law while the etched depths of weakly absorptive polymers were smaller than their absorption depths.

Real-Time Photo-etching Measurements: Experimentally, photo-etching rate measurements, described in previous section as well as reported by others, have been usually determined by measuring the etched depth averaged over many laser pulses. To accurately determine the photo-etching rate on per pulse basis, a real-time dual-beam method was developed by monitoring the transmitted intensity of a probe laser beam. The experimental setup is shown schematically in Figure 3.1-6. A He-Ne probe laser was aligned to the ablation laser and focused upon the sample, then imaged onto a photodiode. The samples were prepared by spin-coating polyimide films on a quartz substrate. The smooth uniform polymer films of several micron were vacuum-baked to

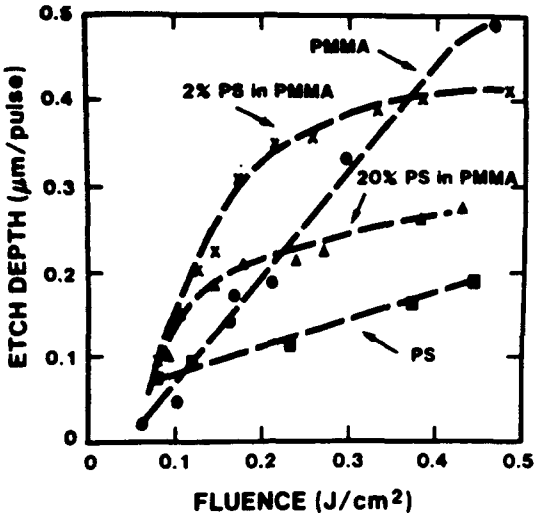

Figure 3.1-3. Photoetching rates of mixtures of PMMA and PS are shown as function of the incident laser fluence.

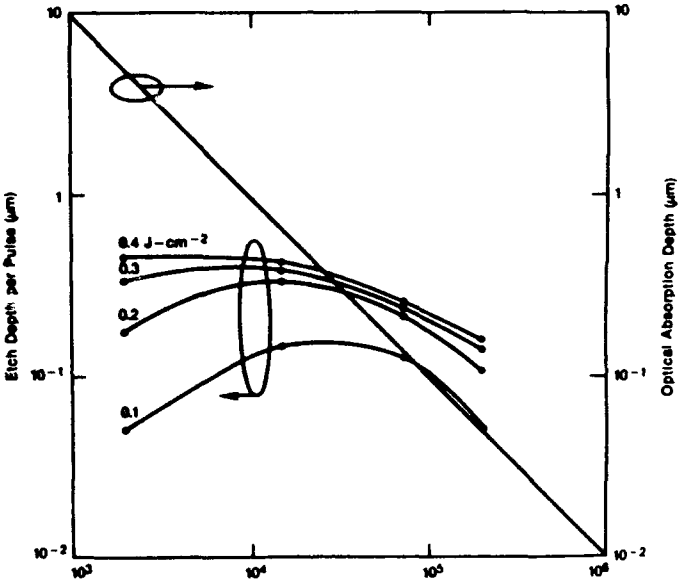

Figure 3.1-4. Photoetching rates measured in PMMA and PS mixtures and are plotted as functions of the absorption coefficients.

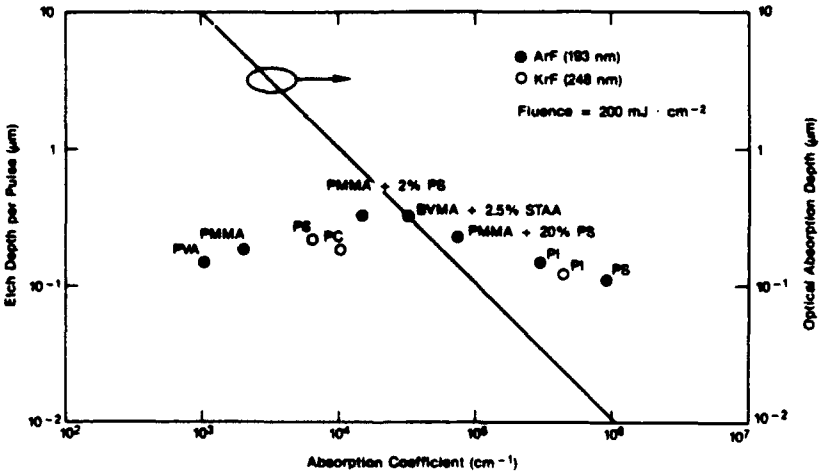

Figure 3.1-5. Photo-etching rates at 0.2 J/cm^2 for various polymers plotted as function of the absorption coefficient of the polymers. The straight line represents the corresponding absorption depth.

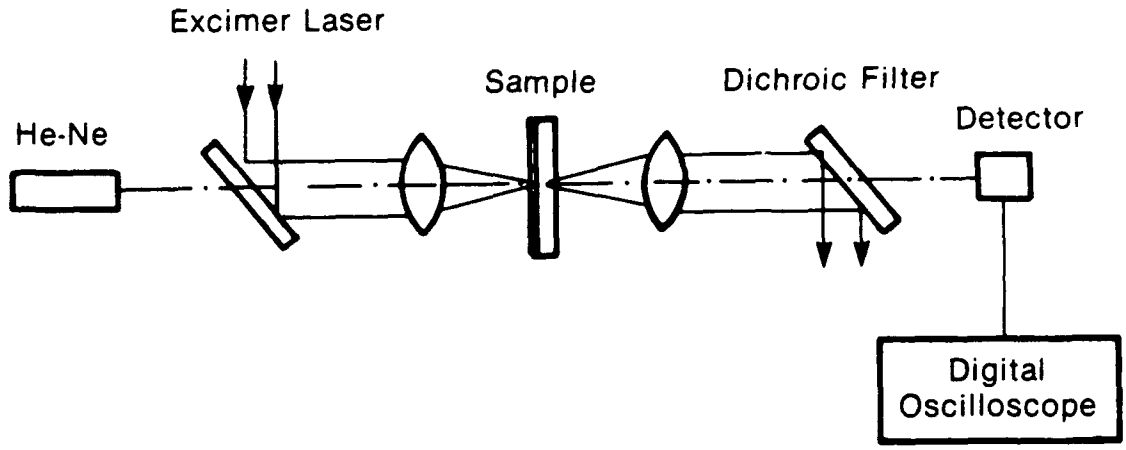

$$\text{Phase Difference } \delta = \frac{4\,\pi\,n\,d\,\text{Cos}\,\theta}{\lambda_o}$$

$$\text{Maximum Transmission at } \delta = 2m\,\pi$$

$$\Delta d = \frac{\lambda_o}{2n\,\text{Cos}\,\theta}$$

Figure 3.1-6. A schematic of setup for the real-time transmission measurement during excimer laser ablation.

remove the residue solvent. As the thickness of the sample changed during ablation, the transmitted optical signal was modulated as a function of sample thickness according to,

Polyimide

For a polyimide sample, typical transmitted signals measured during ablation are shown in Figure 3.1-7 for three different ablation laser fluence levels at a constant repetition frequency of 2 Hz. The bottom trace (at 80 mJ/cm^2) shows the transmitted probe beam signal was strongly modulated as the ablation process proceeded. Each cycle represented the removal of polymer by an optical thickness equal to half the wavelength of the probe laser beam at 0.63 μm. Under this condition, the sample was ablated layer by layer during ablation with a thickness less than one fourth of the wavelength at 0.63 μm. The total transmitted signal intensity decreased, however, as ablation proceeded deeper into the sample. This was due to the fact that at this relatively low ablation fluence level, the sample surface became graphitized upon repeat irradiation. As a result, the total transmitted signal intensity decreased as ablation proceeded. As the polymer thin film was totally ablated through, the transmitted signal returned to its maximum value. From this end point, one can determine the average photo-etching depth per pulse by dividing the film thickness by the total number of pulses required to remove the whole layer.

When the laser fluence increased, the period between the transmitted signals shortened and the time required to ablate through the total film decreased as shown in the middle (middle figure at 110 mJ/cm^2 and the top trace at 146 mJ/cm^2) in Figure 3.1-7. It is interesting to note that as ablation proceeded to the substrate, the period for the transmitted signal to complete a full cycle became longer. This was particularly pronounced in the bottom trace where the ablation fluence was the lowest. This suggested that the ablation rate decreased as the ablation reached the very last thin layer which was in contact with the substrate. Since the absorption depth of polyimide at 248 nm is much smaller than 0.6 m, the reduction of the observed etch rate could not be attributed to the reduction of laser energy absorbed by the sample. The reduction of etch rate observed at the interface was attributed to better heat dissipation at the interface near the substrate. This data strongly suggests that thermal process is the dominant mechanism which contributed to the material removal for the optially thick polymer-like polyimide.

PMMA

When the same measurement was applied to a PMMA sample, a distinctively different characteristic was observed, and typical transmitted signal traces are shown in Figure 3.1-8 for PMMA. We observed when the ablation beam was first turned on that there was an incubation period during which there is little change in the probe beam transmitted signal. As the number of pulses irradiated upon the sample reached a certain value, the transmitted signal dropped suddenly to a level almost distinguished. As the sample was continuously exposed to the excimer laser pulses, the transmitted signal was finally recovered when the PMMA film was completely ablated away. As the excimer laser fluence increased, the incubation period decreased, and the total duration for removing the whole film also decreased, as shown in the middle and the top two traces in Figure 3.1-8. In this case, even long after the PMMA film was mostly removed, some residual materials still remained on the substrate as was manifested by the spikes observed in the transmitted signals.

From a thermal analysis, the temperature rise at the surface of the PMMA sample is about 100 °C at an irradiation fluence of about 0.2 J/cm^2 at 248 nm. In materials such as

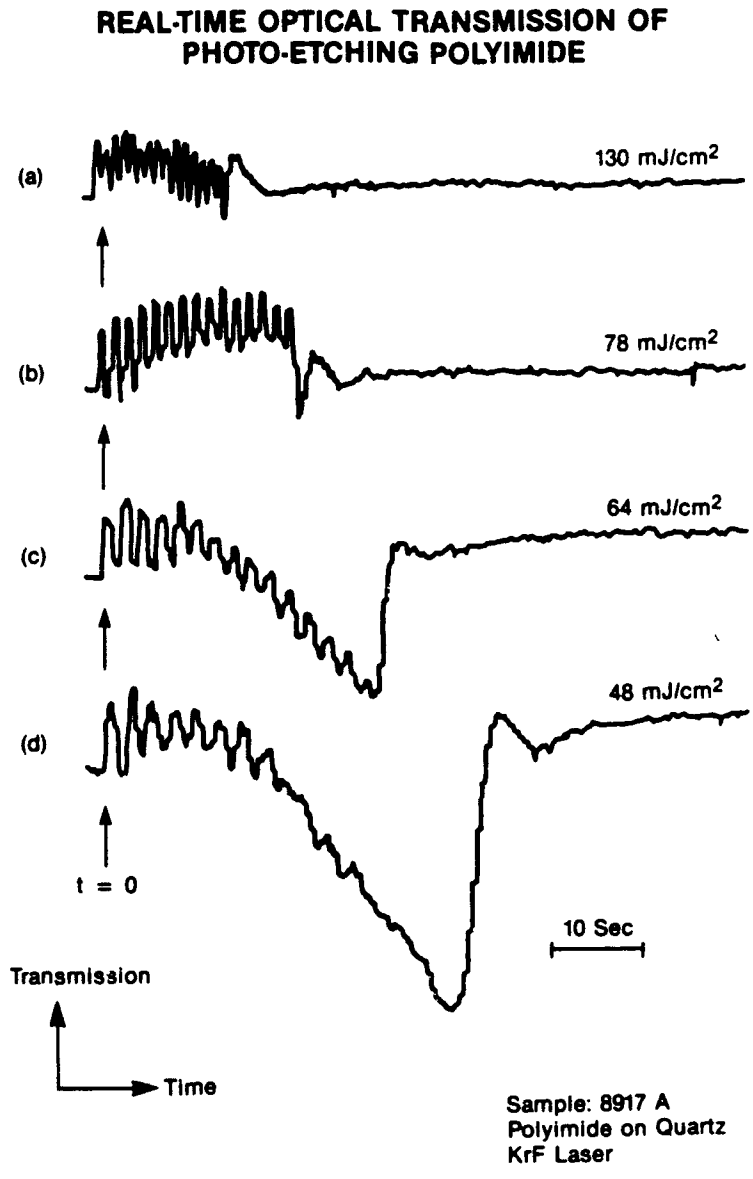

Figure 3.1-7. Typical transmitted signal of the probe beam measured during the excimer laser ablation of a polyimide thin film spun on a quartz substrate..

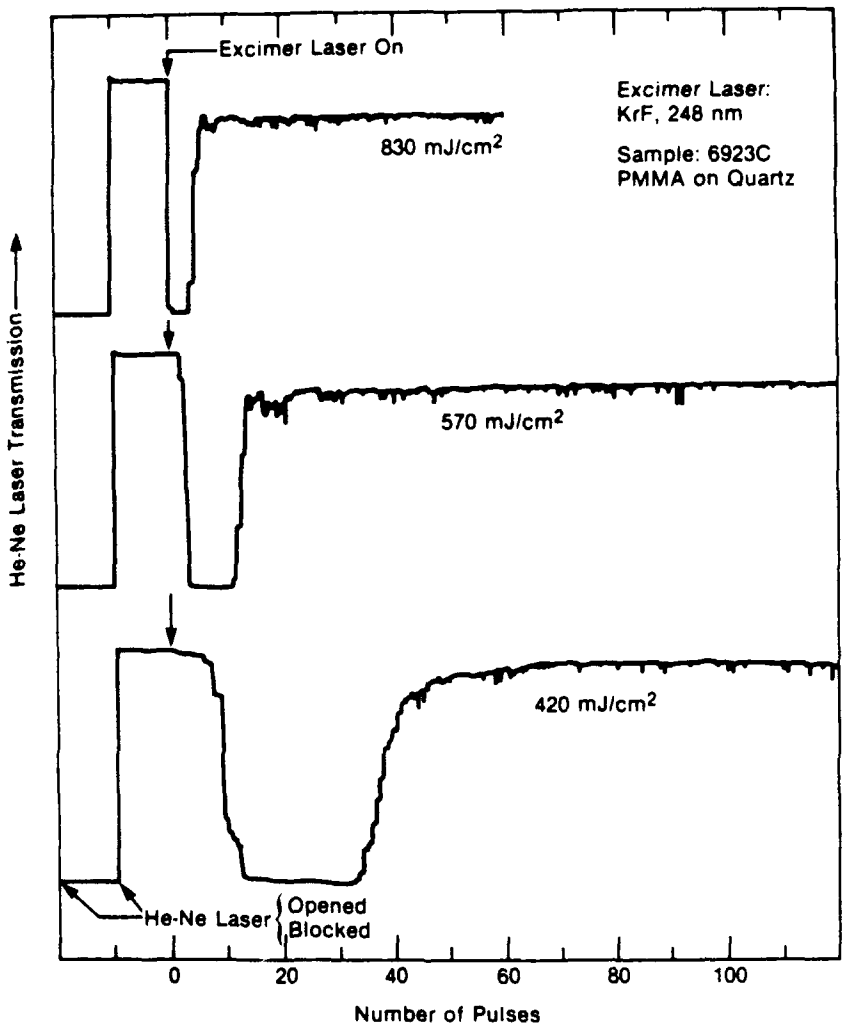

Figure 3.1-8. The real-time transmitted signals of a PMMA sample during the excimer laser ablation.

polyimide, which has a much higher absorption coefficient, the theoretical temperature rise can be as high as 15,000 °C (without taking into account of ablation) under the same laser irradiation condition.

3.1.2.4 Morphology of Photo-ablated Polymers

The morphology of a polymer after photoetching depends strongly on its optical absorption coefficient as well as the laser ablation fluence. In general, we found that for strongly absorptive polymers like polyimide, the ablated surface shows charring when the laser fluence is relatively low. As the irradiation laser fluence increases, the degree of charring reduces and the irradiated surface area becomes smoother. At high laser fluence, the irradiated polymer has a very smooth surface morphology. Figure 3.1-9 shows SEM micrographs of the surface morphology of a polyimide film irradiated under three different laser fluence levels using an excimer laser at 248 nm. At the relatively low fluence level (top photo), the ablated surface was charred and darkened. As the irradiation fluence increased, the ablated surface looked smoother and charring reduced (middle photo). At high fluence level, a very smooth surface was observed after ablation (bottom photo). These findings are in agreement with the real-time optical probing data discussed earlier. At a low laser fluence, we observed that the transmitted probe beam decreased gradually during ablation, and the reduction became more pronounced as ablation reached to the polymer-substrate interface because of thermal conduction through the substrate, thus reducing the effective temperature during ablation.

For polymers with a lower absorption coefficient such as PMMA, we observed distinctively different surface morphologies after UV irradiation. Figure 3.1-10 shows a typical result in which a 4-m thick PMMA film was irradiated at 0.4 J/cm^2 for various pulses. The film was deformed because of volumetric expansion caused by photodecomposition of PMMA into low molecular weight polymeric fragments of MMA. This is consistent with an earlier x-ray photoelectron spectroscopic study in which no apparent changes in the XPS spectra were observed in PMMA sample after excimer laser irradiation with an ArF excimer laser at 193 nm at a fluence to 300 mJ/cm^2. [10] The lack of observable changes in the surface chemical composition resulting from the laser ablation process indicates that the mechanism of material removal does not involve the formation of surface intermediates that are chemically different from the staring materials such as photo-oxidation reactions. A possible mechanism includes a simple thermal degradation of the polymer into monomers and/or oligermeric fragments. Such a mechanism for PMMA is known and could contribute to material ablation for specimens under laser irradiation. [11]

The surface deformation of PMMA after excimer laser irradiation was further confirmed by the surface profile measurements using a Dektak profilometer. Figure 3.1-11 in which the surface profiles of a PMMA sample were measured under different irradiation conditions. If the irradiated sample was immersed in methyl iso-butyl ketone (MIBK) for 30 s, the irradiated volume was preferentially dissolved and the sample was left with etched pits whose depths and sizes were determined by the irradiation dose. These results are shown in Figure 3.1-12 for a PMMA sample irradiated repeated at 0.6 J/cm^2 and then dissolved in MIBK solution for 30 s. These results suggest that PMMA behaves like a positive photoresist under the excimer laser irradiation. PMMA is thermally degraded into monomers which leads to volumetric expansion. Under repeatedly pulsed irradiation, the PMMA sample will be slowly ablated away and will result in photo-etched pits similar to the development in a developing agent such as MIBK.

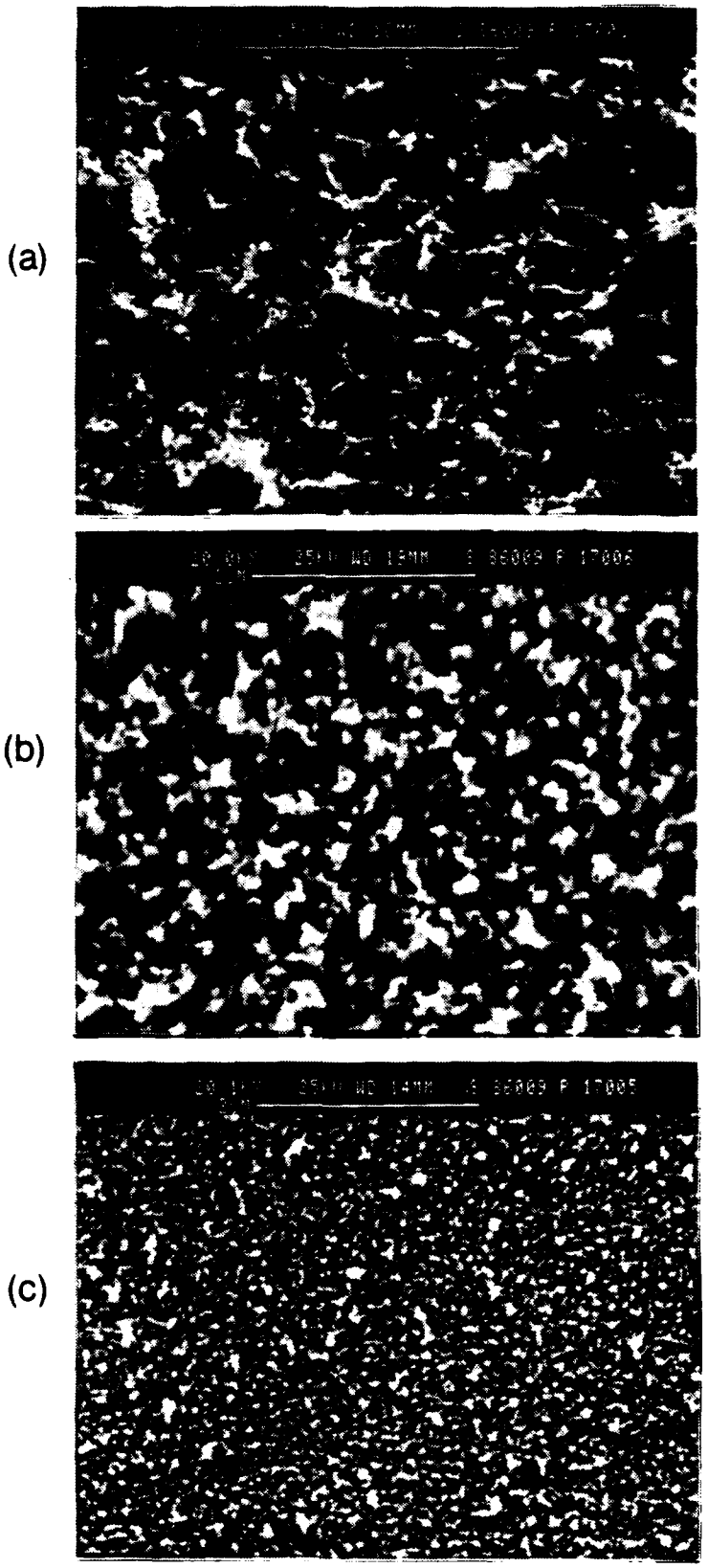

Figure 3.1-9 A SEM micrograph of polyimide irradiated with a KrF laser at three different laser fluence levels of less than 100 mJ/cm^2 (top), 150 mJ/cm^2 (middle) and exceeding 300 mJ/cm^2 (bottom).

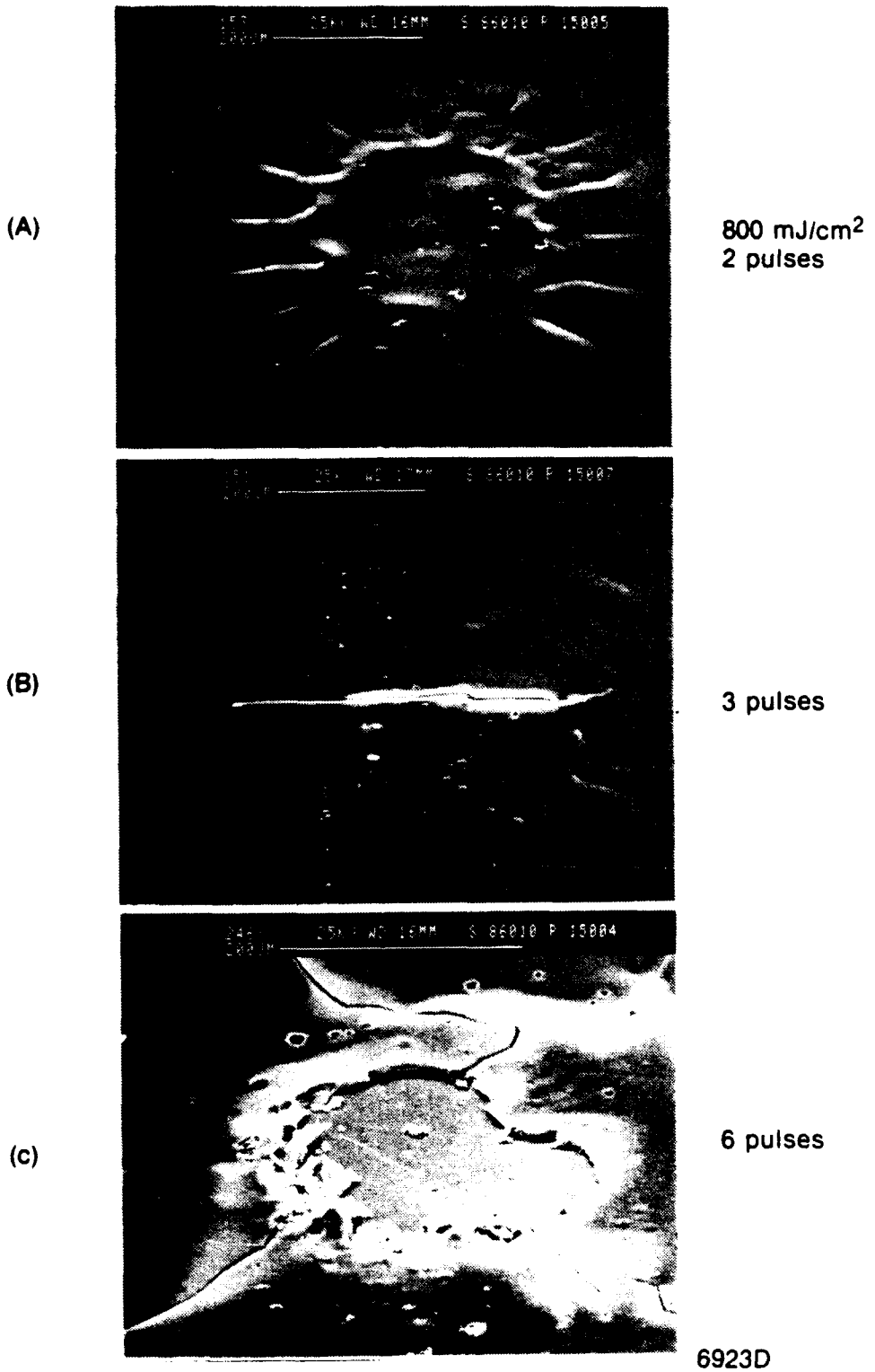

Figure 3.1-10. A SEM micrograph of a PMMA sample which was irradiated with an excimer laser at a fluence level of about 800 mJ/cm^2.

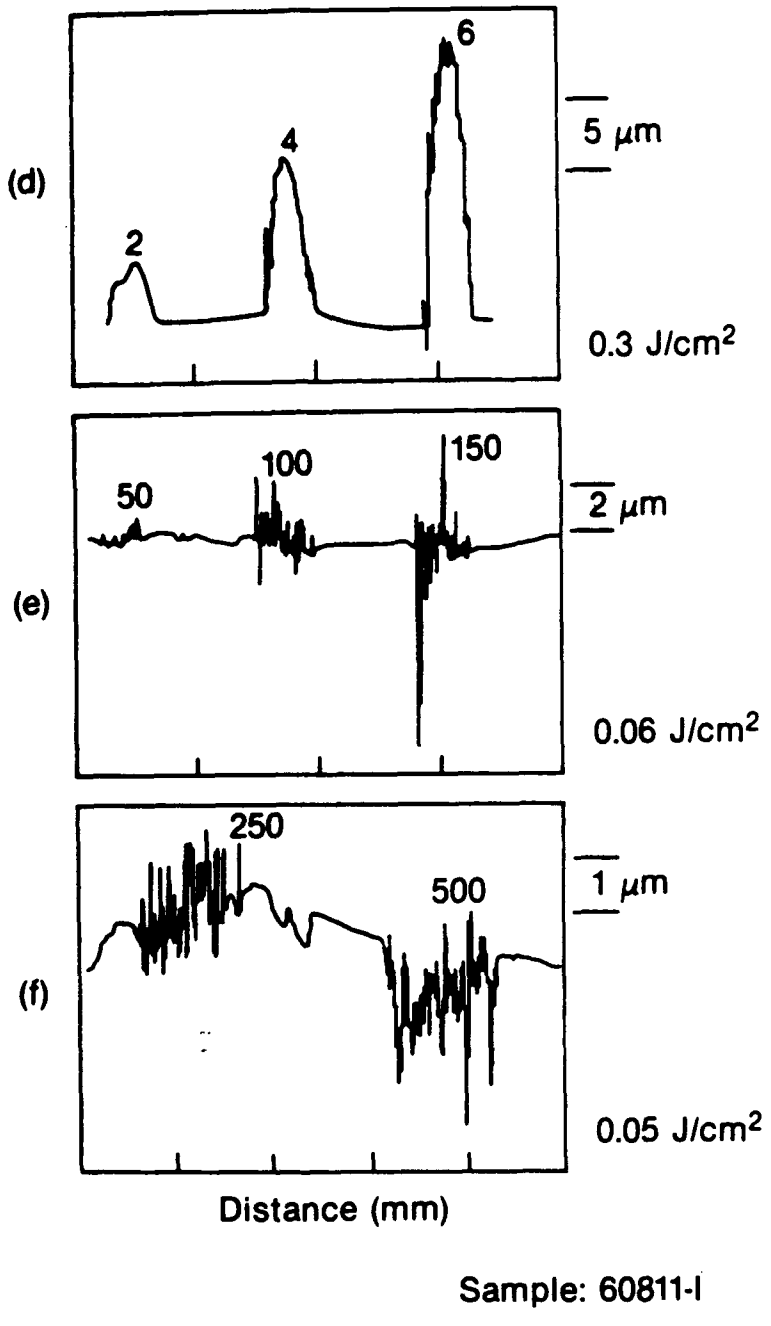

Figure 3.1-11. Surface profiles measured with a Sloan Dektek surface profilometer of a PMMA film irradiated at various fluence levels and pulses.

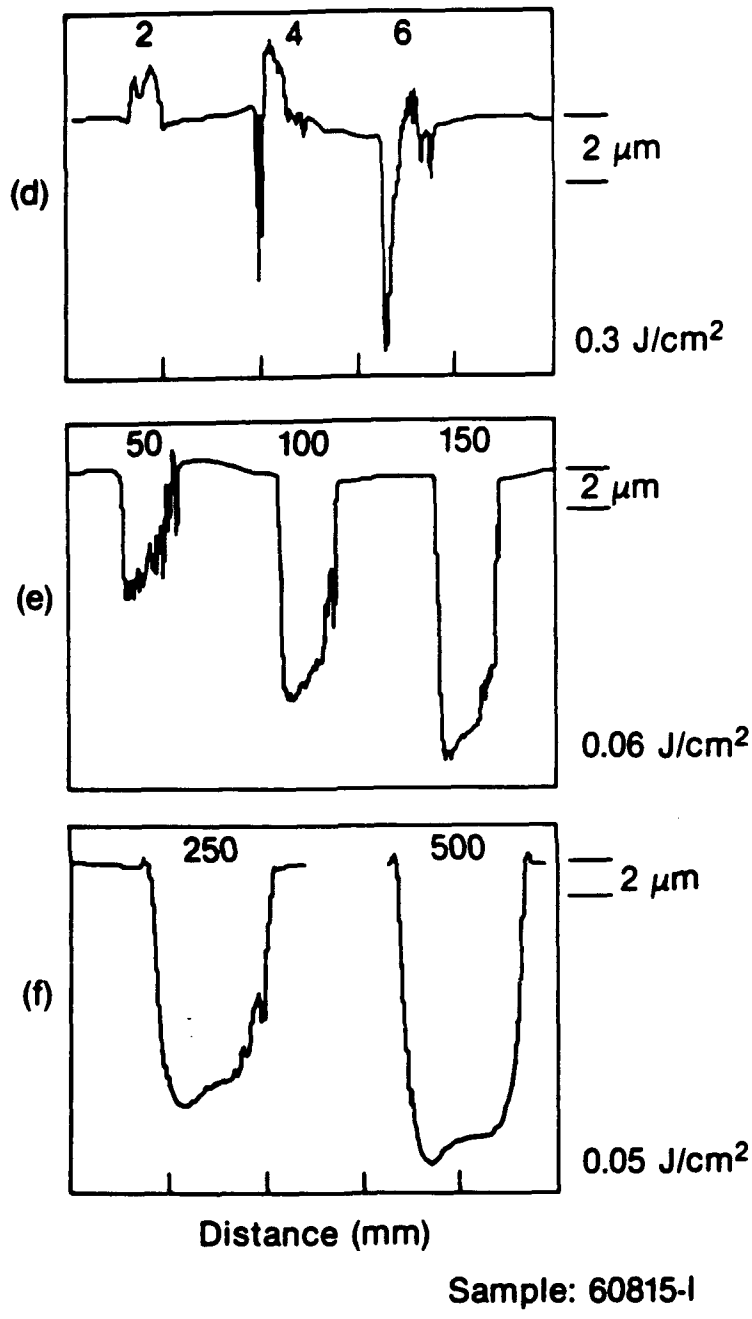

Figure 3.1-12. Surface profiles measured with a Sloan Dektek surface profilometer of a PMMA film irradiated at various fluence levels and pulses, then immersed in a MIBK solvent for 30 s.

This is consistent with the real-time transmission measurement discussed in the last section. For PMMA, we found that the transmitted probe beam, after an incubation period, was completely blocked because of the deformation during the ablation process until the PMMA film was completely removed. There was no modulation of the transmitted signal observed in PMMA during ablation.

For the polyimide sample, the modulation of the transmitted signal was clearly observed illustrating layer-by-layer removal of the polymer by each of the laser pulses. Depending on the laser fluence, the etched depth per pulse ranges from one-tenth to several hundredths of a micron, which is substantially larger than the optical absorption depth of the polyimide at the irradiation laser wavelength. Laser ablation in the highly absorptive region, photoetching is taking place continuously during the period in which the material is exposed to radiation within the entire pulse duration. Since the thermal diffusion length in a polymer is less than 0.01 μm over a period of 1 ns, rapid temperature rise takes place in, and is confined to, a very thin surface layer within the irradiated volume. Rapid volumetric expansion caused by localized heating can therefore be considered quasi-adiabatic and leads to rapid ruptures of materials, and the ablated materials are directly ejected from the sample surface. A model for the laser ablation was developed and discussed in the following section.

3.1.2.5 Theory of Polymer Ablation

Experiments have shown that the ablation process is due to a combination of local heating and bond breaking. If we define n(x,t) as the number of broken bonds per unit volume at a distance x from the surface at the time t, we follow previous theories in assuming that ablation occurs whenever this bond breaking density exceeds some threshold value n_T.

The first laser pulse produces a damage profile given by Beer's law of $n = (\alpha F/h\nu) \exp(-\alpha x)$, where α is the absorption coefficient, hv is the photon energy, and f is the fraction of absorbed photons which break bonds.

$$l = (1/\alpha) ln[F / F_T] G(F - F_T)$$
$$F_T = h\nu n_T / \alpha f, \qquad (1)$$

Where G is the step function, this formula has been widely used to interpret ablation data. The initial experiments seemed to show that l is proportional to ln (F), although the range of values for F was small. Recent experimental plots for large ranges of F show that Eq. (1) is not obeyed.

Experimental data are usually taken by averaging over many laser pulses. A key aspect of our theory is that broken bonds remain in the unetched portion of the polymer. The exponential nature of Beer's law guarantees that substantial bond-breaking density remains in that part of the polymer that is not etched away. The next laser pulse builds on this residual bondbreaking density. Equation (1) is only valid for the first laser pulse, but is invalid for subsequent pulses. This model distinguishes bond breaking from purely thermal effects. The low repetition rate of the pulses, on the order of several pulses per second, means that heating effects will dissipate between pulses. However, bond breaking that turns a polymer into a monomer seems to have a much longer relaxation time. Since the density of broken bonds is low, we can assume that their presence does not change physical parameters such as absorption coefficient.

Ample evidence exists for the concept of residual bond-breaking density. For polymers of low absorption coefficient, numerous laser pulses must be absorbed before any ablation occurs. This makes sense if the polymer is accumulating residual broken bonds from each pulse. We now introduce the concept of incremental ablation depth—the etch depth per laser pulse l after many pulses, that is, after the threshold processes are over and actual ablation occurs. We show below that incremental ablation has l proportional to F rather than to ln(F).

Our theory also employs the concept of a moving ablation front as introduced by Keyes et al. Typical laser pulses have a duration of 10 to 20 ns, during which time the ablated monomer can travel many microns away from the surface. We assume that the ablated materials leave the light path of the laser and no longer cause absorption.

Let s(t) be the position of the polymer surface during a single laser pulse. If the period of the laser repetition is 2 t , then we consider a single pulse during the duration from - t_r to + t_r where the pulse is a maximum at the surface at the time t = 0. The distance from the actual surface is (x-s),. the rate at which bond breaking offers is

$$\frac{dn(x,t)}{dt} = \frac{f\alpha I(t)}{h\nu}\exp\{-\alpha [x-s(t)]\} \qquad (2)$$

where the laser intensity I(J/cm^2-sec) is defined in terms of the fluence F(J/cm^2) and the normalized pulse shape i(t):

$$I(t) = Fi(t)$$
$$1 = \int_{t_r}^{t_r} dt' i(t') \qquad (3)$$

Equation (2) is solved by direct integration. The residual density of broken bonds n_T exp (- α x) is taken as the initial condition

$$n(x,t) = \frac{f\alpha F}{h\nu} e^{-\alpha x} \int_{t_r}^{t} dt_1 i(t_1) e^{\alpha s(t_1)} + n_T e^{-\alpha x} \qquad (4)$$

The position of the ablation surface s(t) is defined by setting n(s,t) = n_T in Eq (4). Then multiplying each term by the factor of exp(αs)/n_T gives the equation for s(t):

$$J(t) \equiv e^{\alpha s} = 1 + \lambda \int_{-t_r}^{t} dt_1 i(t_1) J(t_1)$$

$$\lambda = f\alpha F / h\nu n_T$$

We differentiate this equation with respect to time, which immediately brings us to the equation:

$$\frac{\partial T(t)}{\partial t} = \lambda i(t) J(t)$$

or

$$\frac{\partial}{\partial t}(\ln J) = \alpha \frac{ds}{dt} = \lambda i(t)$$

which has the solution

$$S(t) = \frac{\lambda}{\alpha} \int_{t_r}^{t} dt_1 i(t_1)$$

The incremental etch depth l is defined as the position of the surface at the end the laser pulse where eq (3) is used for the integral over the pulse shape i(t):

$$l = S(t_r) = \lambda / \alpha = fF / h\nu n_T \qquad (5)$$

This simple formula is the main result of this calculation. It shows that the incremental etch rate is proportional to the laser fluence and is not directly dependent upon the absorption coefficient: f and n may depend upon a. This dependence is quite different from the formula given by Beer's law in eq (1). The fact that l does not depend upon α is reasonable. A fraction f of the absorbed photons break bonds. In steady state, each pulse breaks a certain number of bonds which causes the proportional amount of etching. Eq. (5) agrees with our experimental data for incremental etch depth. Figure 3.1-5 in which different polymers with large variation of absorption coefficient show a difference of etch rate only by a factor of about 2. These results show that the incremental etch depth is relatively independent of absorption coefficient [12].

3.1.2.6 Applications of Laser Etching

Laser etching has been used for many electronic applications including micro-via fabrication, large area ablation, and large area patterning among others. Several novel techniques using laser etching for electronic packaging applications are described in this section.

Surface Patterning Using Excimer Laser Ablation

A negative large area patterning technique has been developed in which an excimer laser is used to desensitize the polyimide surface that has been spin-coated with a thin layer of Pd-containing compound. After the sample surface is exposed to the excimer laser using a contact mask or projection method, the laser radiation desensitizes the surface once the irradiation fluence exceeds a certain threshold level, a value depending on the wavelength of the excimer laser used. The threshold fluence for polyimide at 193 nm or 248 nm, for example, is about as low as 20 to 30 mJ/cm^2. This threshold laser fluence is equivalent to the laser ablation threshold for removing the polymer surface layer. After irradiation, a copper pattern is formed on the sample surface that was not exposed to laser radiation once the is immersed in an electroless copper plating solution. We will discuss this process further in Section 3.2.3.

Fabrication of Micro-vias

Fabrication of vias in polymers has been successfully demonstrated using various lasers sources and is a critical technology for the high-density interconnect application. The use of excimer lasers for via drilling in polyimide has attracted particular attention and has been extensively studied for IC's applications such as micro-vias drilling in HDI

[13]. Etch rates are typically on the order of a fraction of a micron per pulse at a fluence level of several hundred millijoules per square centimeter. The fabrication of blind micro-via holes using KrF excimer lasers for IC printed circuit board with high process throughput has also been recently reported [14].

Although excimer lasers produce high quality micro-via holes, the drilling speed, and thus the process throughput, are limited by the pulse repetition rate. We have overcome this problem by developing a high repetition rate Q-switched frequency-quadrupled YAG laser at 266 nm. We have demonstrated high-speed drilling of micro-vias at several milliseconds per via hole. Figure 3.1-13 is an optical micrograph showing micro-vias fabricated using a frequency-quadrupled UV YAG laser in 25 μm thick polyimide film and Figure 3.1-14 shows the corresponding SEM micrograph. Specific physical properties of the polymer, such as absorption coefficients and thermal stability, and match to the appropriate laser wavelength, must be taken into account [11].

REFERENCES

[1] C.A. Neugebauer, R.O. Carlson, R.A. Fillion, and T.R. Haller, Solid State Tech. p. 93 (June 1988), and the cited references.

[2] C.W. Eichelberger, R.J. Wojnarowski, R.O. Carlson, and L.M. Levinson, SPIE Symposium on Innovative Science and Tech. Paper 877-15 (January 1988).

[3] D.W. Tuckerman, IEEE Elec. Dev. Lett. EDL-8, 11, pp. 540-543 (November 1987).

[4] D.V. Smart and D.M. Stewart, Lasers in Microlithography, edited by D.J. Ehrlich, J.S. Gatehelder, and J.Y. Tsao, SPIE 774, p. 88 (1988).

[5] D.J. Ehrlich and J.Y. Tsao (ed.), Laser Microfabrication and Thin Film Processing (Academic Press, to be published, 1989).

[6] H.S. Cole, Y.S. Liu, R. Guida, and J. Rose, SPIE 877, p. 92 (1988).

[7] H.S. Cole, Y.S. Liu, H.R. Phillip, and R. Guida, Mat. Res. Soc. Symp. Proc. 72, p. 241 (1956).

[8] H.R. Philipp, D.G. Le Grand, H.S. Cole and Y.S. Liu, Polymer eng. Sci. 27,, 1148 (1987).

[9] H.R. Philipp, D.G. Le Grand, H.S. Cole and Y.S. Liu, Polymer eng. Sci. 29,, 15754 (1989)

[10] M.C. Burrel, Y.S. Liu and H.S. Cole, J. Vac. Sci. Technolo., Vol. 4,l No. 6, Nov/Dec (1986).

[11] F.W. Billmeyer, Textbook of Polymer Science, 2nd Edition (Wiley, New York, 1971).

[12] G.D. Mahan, H.S. Cole, Y.S. Liu and H.R. Philipp,l App. Phys. Letts. Vol. 53, No. 24, p. 2377 (1988).

[13] Y.S. Liu and H.S. Cole in Symposium Abstract, 4, "Laser Ablation of Dielectrics for IC Applications," 4th Electronic Materials and Processing Congress, ASM International, Aug 1991, Montreal.

[14] F. Bachmann, Chemtronics, Vol. 4, No. 3 (1989).

UV YAG LASER FABRICATED MICRO-VIAS IN POLYIMIDE

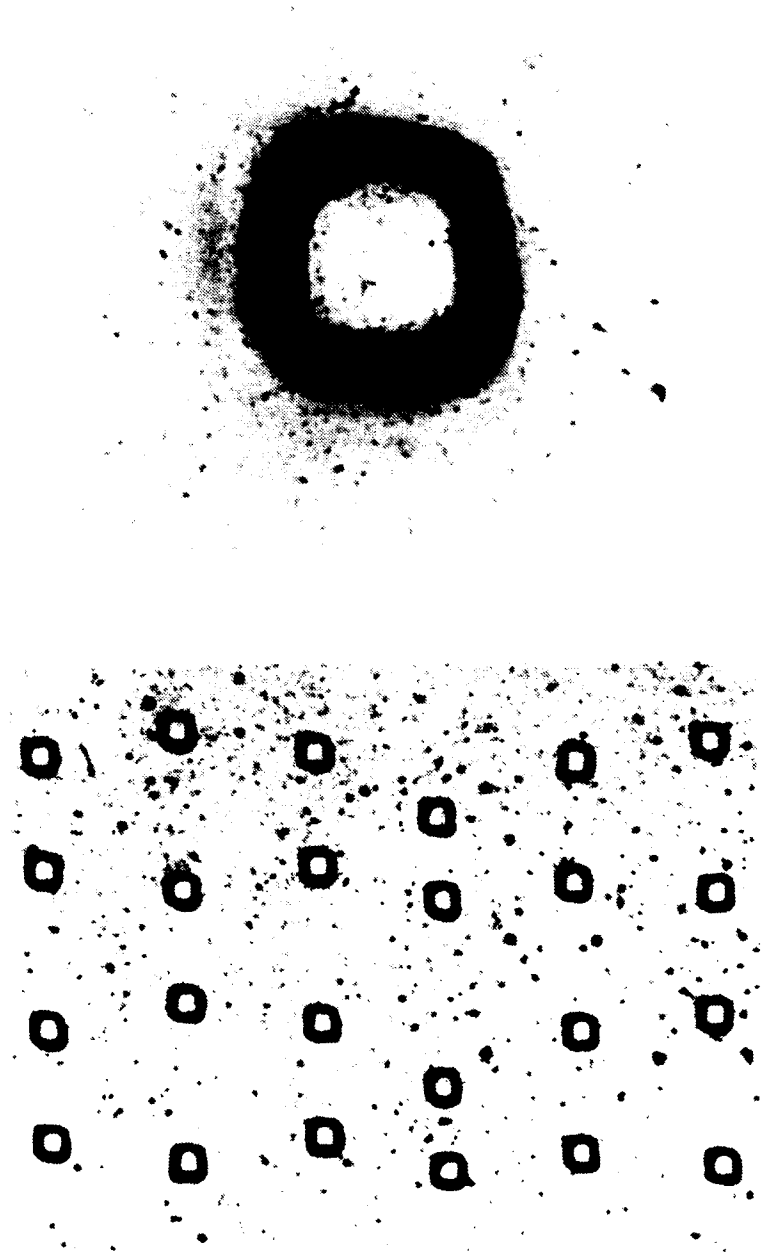

Figure 3.1-13. An optaical micrograph of micro-via fabricated using a frequency-quadrupled YAG laser at 266 nm (via diameter = 25 μm).

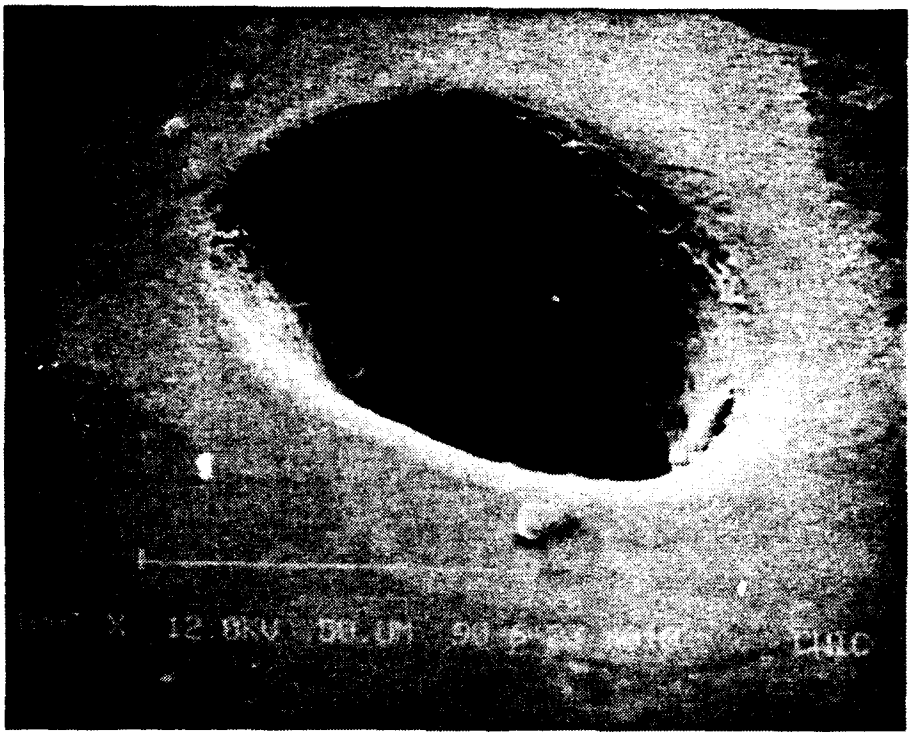

Figure 3.1-14. SEM micrograph of a UV YAG laser drilled microvia in polyimide..

3.2 Direct Patterning Technology

3.2.1 Introduction

The increasing complexity in VLSI design and fabrication has increased the demand for discretionary processing techniques for application specific designs, circuitry restructuring, yield enhancement, and localized masking and coating. Among various laser processing techniques, laser direct patterning for circuit interconnecting in VLSI and packaging applications is the most likely technology to have a major impact on next generation circuit and device fabrication. In this section we will discuss several laser direct patterning techniques developed during this program.

The writing speed in a laser direct writing process is dictated by the beam size, growth speed, and the final film thickness required for a specific application. The ultimate writing speed can be calculated using a simple model shown in Figure 3.2-1 in which D is the beam diameter, d the film thickness, V_g the film growth velocity, and V_s is the lateral writing speed. The values D and d are dictated by the resolution and resistivity required. The growth velocity V_g further depends upon the type of reaction, pressure, temperature, and the mass transport discussed earlier. For example, a writing speed of 1 mm/s is required for writing a 1-μm-thick and 10-μm-wide line at a film growth rate of 100 μm/s [1]. At this writing speed, a 1-m-long interconnect requires 16.6 min to complete. For packaging applications, a total of 1,000 to 2,000 interconnects are required with an average length of a few centimeters which suggest processes with a minimum writing speed of a few mm/s are required. Slower direct writing processes are useful only for short run interconnects such as circuit alterations, local restructuring, and repairs.

For practical consideration in the gas phase photolysis, growth rates are limited by the transport of reactants and products to and away from the reaction zone. The proper laser wavelength must be used in order to couple the spectral properties of gaseous phase compounds or adsorbates for photodissociation with efficient quantum yields. Thus these processes tend to be a few orders of magnitude slower than required. In the case of pyrolytic processes, reactants of higher concentration can be used to enhance writing speed. As a result, higher growth rates are possible with pyrolytic processes. Although these have been demonstrated [2], issues such as purity, adhesion, and appropriate metal selectivity make this an unattractive approach for interconnect metallization.

The approach taken in the present study was to develop a two-step process to achieve fast writing speed. The first step involves the use of catalysis or modification of the surface such that in a later step the metal can be selectively plated to the desired thickness using electroless or electrolytic deposition techniques. Since electrical conductivity is an issue, copper or gold were the metals of choice. In this section, we review our earlier work on direct-write copper deposition on polyimide, excimer laser projection patterning, and recent results on selective electrolytic deposition processes. Other developmental studies treated in this section include copper electro-deposition studies and process development of direct write schemes.

3.2.2 Laser-Activated Copper Deposition on Polyimide

In this process [3,4], shown in Figure 3.2-2, palladium acetate (PdAc) dissolved in chloroform was spun on a polyimide substrate. An argon laser at 351 nm was then used to selectively expose the surface to decompose the organometallic compound. The surface concentration of Pd was controlled by varying the initial amounts of PdAc dissolved in the solvent. After irradiation, the sample was immersed in an electroless copper plating solution to deposit copper on the surface areas that were exposed. Fast writing speeds of several cm/sec were achieved because only a few monolayers of palladium are required to catalyze electroless

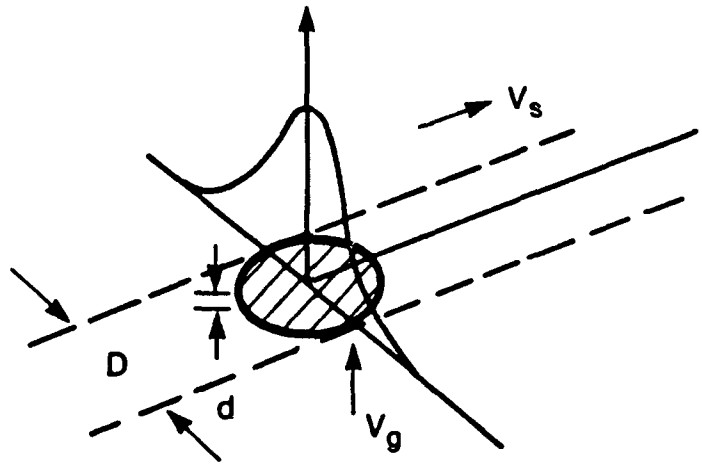

where:

$$V_s = \frac{D}{d} V_g$$

V_s = Scanning speed
V_g = Growth velocity
D = Beam diameter
d = Film thickness

Figure 3.2-1. A simple model for relating writing speed, film growth, thickness and width.

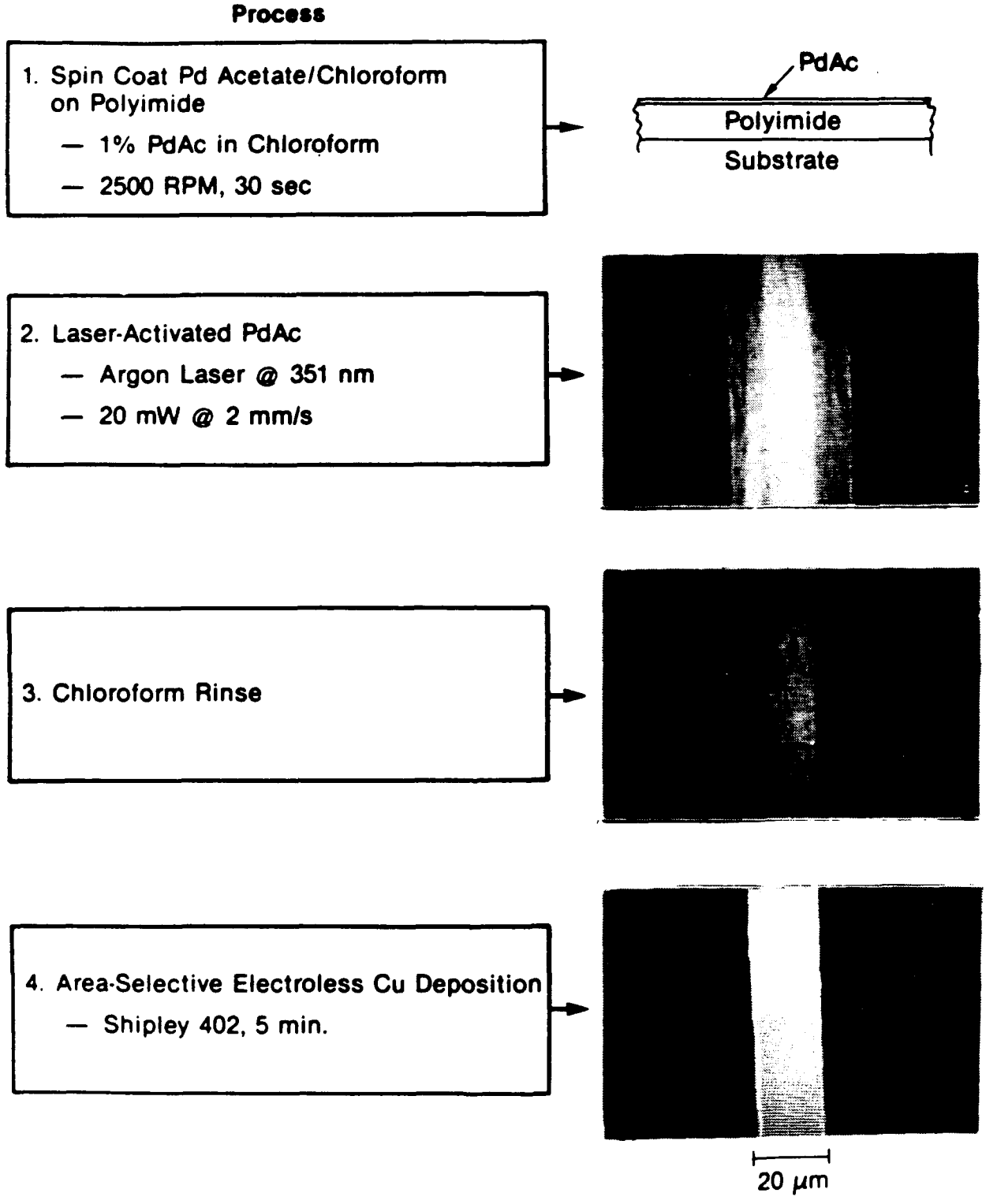

Figure 3.2-2 Laser-activated copper deposition process.

copper deposition.

Because of the strong absorption of polyimide at 351 nm, laser irradiation induces local heating of polyimide and results in thermal decomposition of PdAc at a temperature of about 225 °C to give a few monolayers of Pd metal. Figure 3.2-2 shows optical micrographs taken at each of the process steps.

The quality of copper from electroless copper deposition was observed to depend critically upon the surface concentration of Pd used as the catalyzing agent. RBS (Rutherford Back-scattering Spectroscopy) experiments were carried out to determine the optimum Pd surface concentration,.

Chloroform solutions containing various amounts of PdAc were prepared and spin-coated on polyimide substrates. The samples were all spun at the same spin speed, baked 250 °C for 15 min, followed by a dip and rinse in chloroform. A set of these samples was used for RBS analysis to determine the Pd surface density as a function of initial PdAc concentration. Figure 3.2-3 shows the data plotted as surface density as a function of PdAc concentration. The Pd surface densities were determined to be between 3.2.2 and $23.3 \times 10^{(15)}$ atoms/cm^2 for concentrations between 0.1 and 1.0 % PdAc. As seen in the figure, the surface density varied linearly with concentration.

Another set of samples prepared in a similiar manner was evaluated for copper plating quality. It was found that best results were obtained with the solution containing 1.0 % by wt. PdAc in chloroform. This concentration gave uniform copper films which were characterized by good adhesion and low bulk resistivity. This concentration was used as the standard for subsequent experiments. Typical resistivities were on the order of 3.0 μ Ω-cm and depending on power and scan speed, copper lines of about 7 to 50 μm with a thickness of 1.5 μm were achieved.

A plot of power/scan speed relationships is shown in Figure 3.2-4. The process window was determined by evaluating various power/scan combinations for quality of deposit before and after electroless copper deposition. As shown, at high power levels, enough energy is deposited to cause thermal decomposition of the polyimide. This is characterized by a darkening in the laser traced areas and in some instances actual carbonization. Copper, which is plated under these conditions, has been shown to have rough surface morphology and poor adhesion. Conversely, if laser power is too low, insufficient decomposition of PdAc is observed, and the Pd surface concentration is below the critical value for quality copper deposition.

In summary, the two-step laser catalyzed copper depostion process on polyimide has been demonstrated with fast writing speeds and good quality copper. The process is ideally suited for repair of opens and offers the potential for higher resolution interconnect structures than currently is available using thick film photoresist technology.

3.2.3 Excimer Laser Projection Patterning

Large area metal patterns have been grown on polyimide using an excimer laser as light source. The process is shown schematically in Figure 3.2-5 [5,6]. In this case, a Pd-containing compound is first spun on the poloyimide surface. The sample surface was then exposed to an excimer laser through a mask or by using a projection method. The exposed surface area becomes totally desensitized once the laser fluence is above a threshold level, which depends upon the wavelength of the excimer laser used. After immersing the sample in an electroless copper plating solution, a copper pattern is formed and is shown in Figure 3.2-6. Because of strong absorption of polyimide at both 193 nm and 248 nm, a threshold fluence less than 20

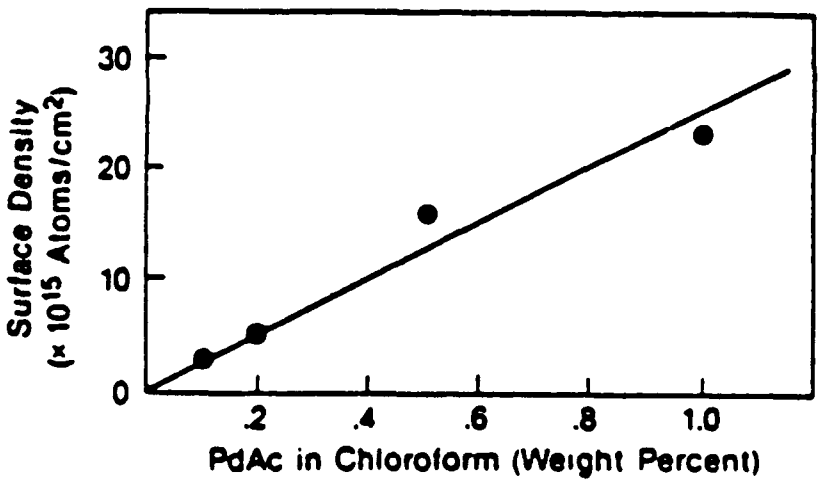

Figure 3.2-3 Pd surface density as a function of PdAc concentration.

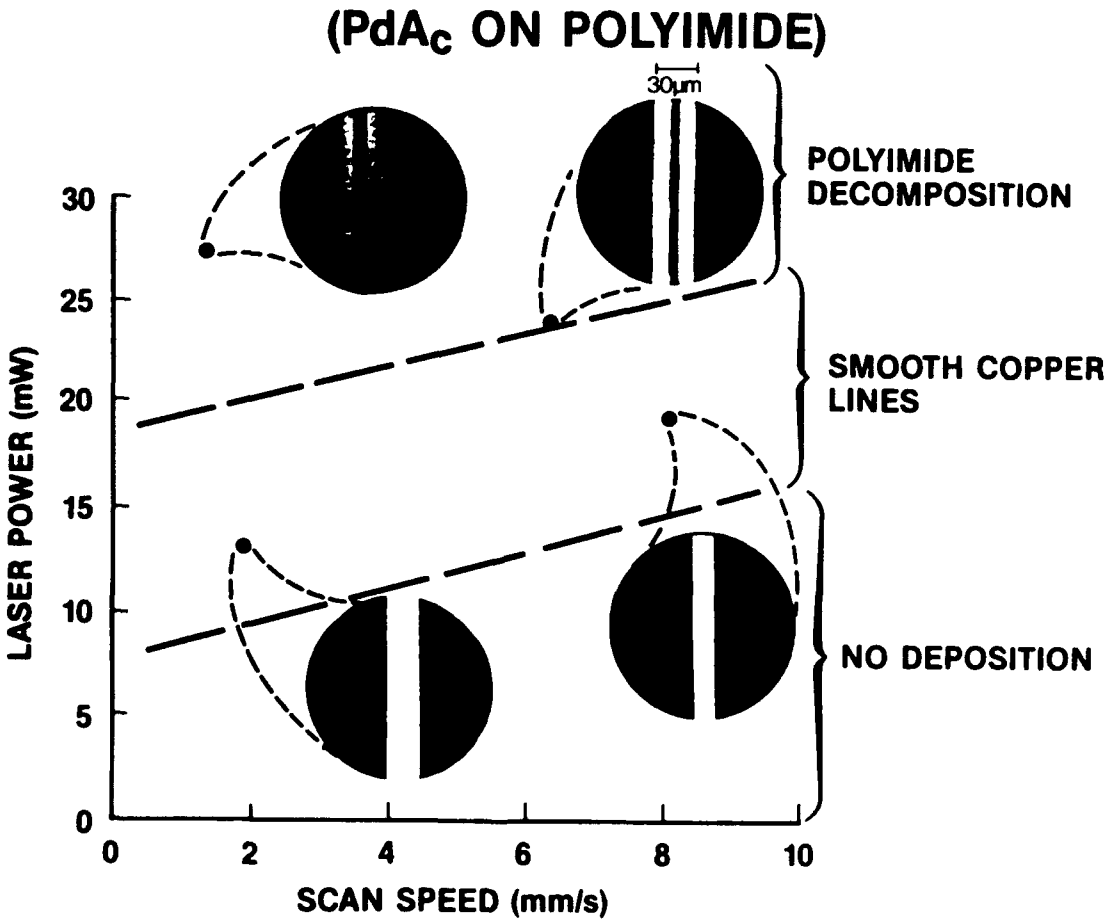

Figure 3.2-4. Power/scan speed relationships.

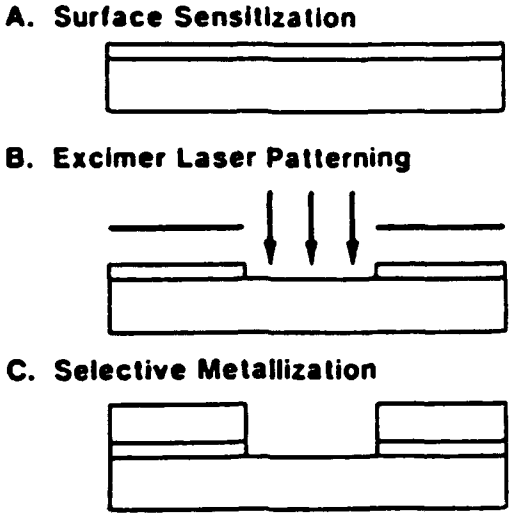

Figure 3.2-5. Excimer laser selective metallization.

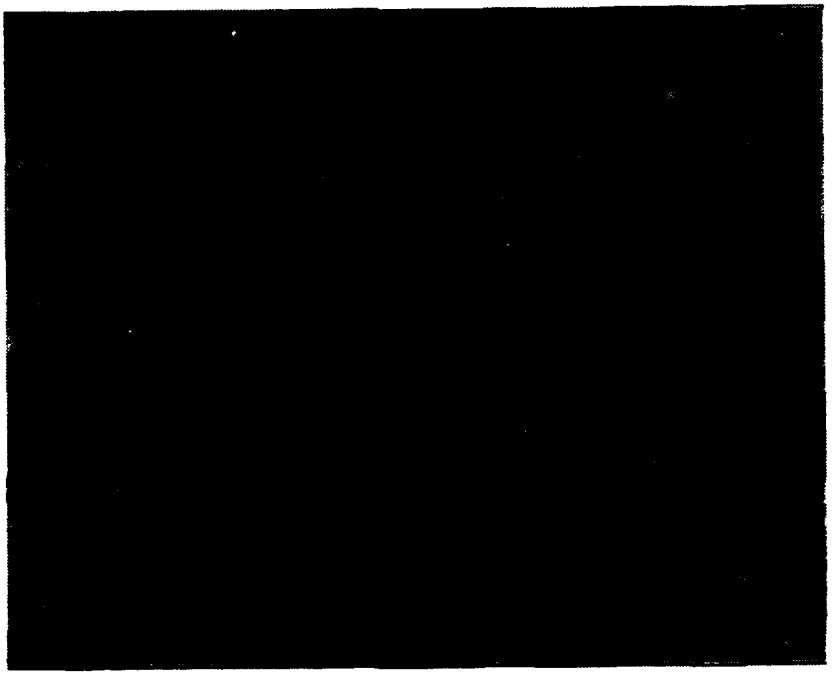

Figure 3.2-6. Metal pattern fabricated on Ultem surface using an excimer laser.

mJ/cm ^{2} was found to be sufficient to cause total desensitization. Once the irradiating fluence exceeds the threshold level, identical copper patterns were formed regardless of the number of irradiating pulses. Figure 3.2-7 shows x-ray photoluminescence spectra (XPS) of a sample sensitized with a Pd-containing precurser and irradiated with an excimer laser at a fluence level above the threshold. Figure 3.2-7(a) is the XPS spectrum of a sample after sensitization with the Pd-containing precurser. Figure 3.2-7(b) shows the surface area exposed to excimer laser irradiation for one single pulse, and Figure 3.2-7(c) shows that exposed to 10 excimer laser pulses at the same fluence level. As we see, a factor of 10 in exposure gives the same XPS spectra with no indication of Pd peaks. Both samples resulted in identical copper patterns after electroless copper deposition. This negative working copper deposition process results in equivalent copper quality as obtainable with commercially available electroless copper plating baths.

3.2.4 Selective Electrolytic Deposition (SED) Processes

Although the above mentioned direct write copper deposition processes demonstrated the capability of fast writing speeds and low resistance copper on polyimide, additional challenges must be addressed for practical direct-write interconnect metallization in MCM applications. In these systems, we are not only dealing with copper/polyimide interface issues, but adhesion to aluminum bonding pads and compatibility with metal primer/barrier layers used in polyimide/copper interconnect technology. It is well known that two problems that must be overcome in these systems are the adhesion of copper to polyimide and also the problem of electrimigration of copper in polyimide [7,8]. The solution to these problems has been to use thin barrier metal layers between the Cu and polyimide. Metals such as chromium, titanium, and nickel have been shown to prevent copper diffusion into polyimide and at the same time chemically bond to polyimide to act as an adhesion promoter for bonding copper to polyimide [9,10]. Typically, a thin layer of these metals is sputtered on polyimide prior to deposition of copper. The primer metal chemically bonds to polyimide to form new compounds at the interface such as carbides or nitrides. Evidence for this compound formation is shown in Figure 3.2-8 where XPS depth profiles for a sample containing 400 A of titanium sputtered on Kapton is shown. In (a), we see the C 1s spectra and note at the Ti/polyimide interface a shift in the binding energy to lower energy which is attributed to Ti carbide formation. The strong anchoring attributed to this chemical bonding manifests itself in significantly higher peel strength values. In addition, these metals adhere well to Al bonding pads on chips and provide a mechanism to obtain good adhesion of Cu in interconnect metallization applications.

The requirements of useful direct write metal deposition processes must therefore include compatibility with adhesion primer metals such as Cr and Ti. In addition to fast writing rate, the process must provide low resistance contacts to aluminum pads on chips, adhesion to aluminum, polyimide, and barrier metals, and must be able to accommodate large differences in thermal conductivity and optical reflectivity between polymer surface areas and via holes. In addition, metals such as Ti and Cr form native oxides which must be taken into account in designing a direct-write process. This is demonstrated in Figure 3.2-8(b) where we see the composition vs depth of a Ti/polyimide system. The high oxygen content at the surface combined with low Ti content are indicative of oxide formation at the surface. This tenacious layer propagates into the film to a thickness of about 50 to 100 A.

Our approach was to take advantage of this oxide layer to provide surface selective electrical properties which could again be used in a two-stage process referred to as selective electrolytic deposition (SED). In its simplest form, the process is shown in Figure 3.2-9 In this approach, a thin layer of Cu (i. e., 1,000 A) is sputtered on to a substrate followed by a thin layer of Ti (1,000 A). As shown in step 1 of Figure 3.2-9, the Ti is patterned using any number of approaches; in

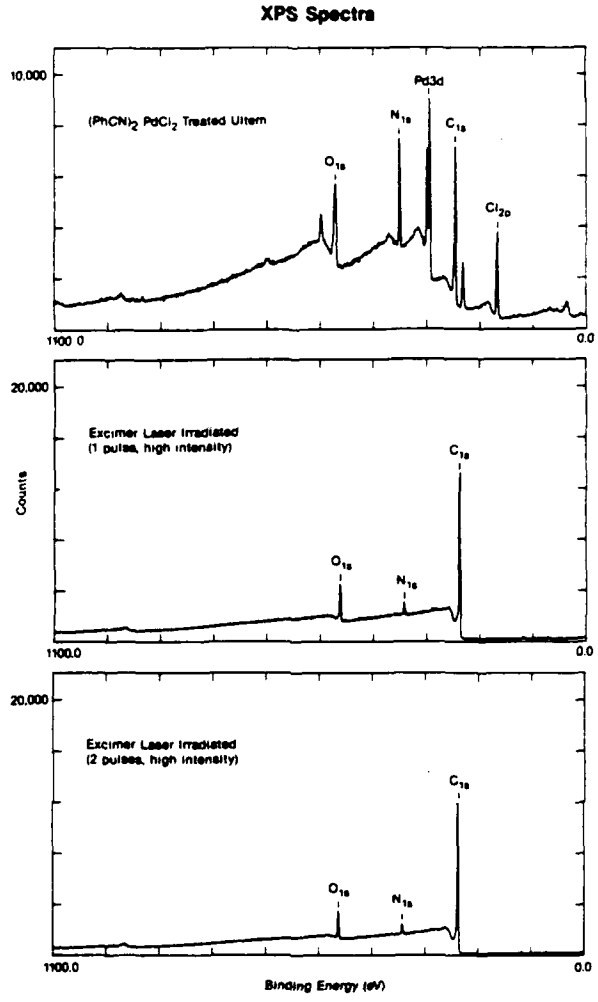

Figure 3.2-7 XPS spectra of Ultem before and after excimer laser exposure.

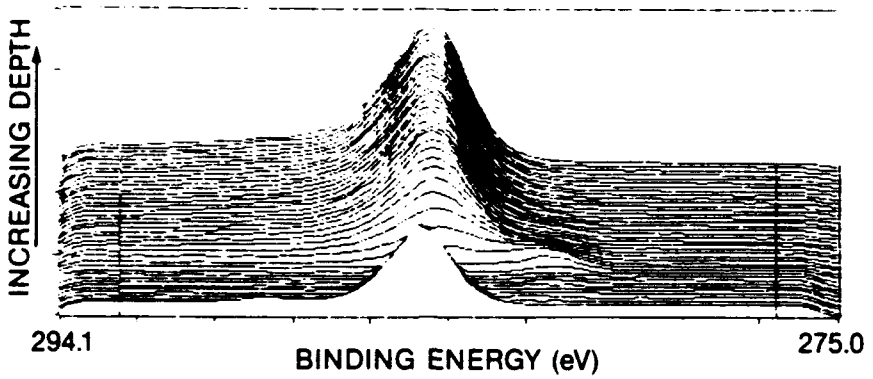

A.

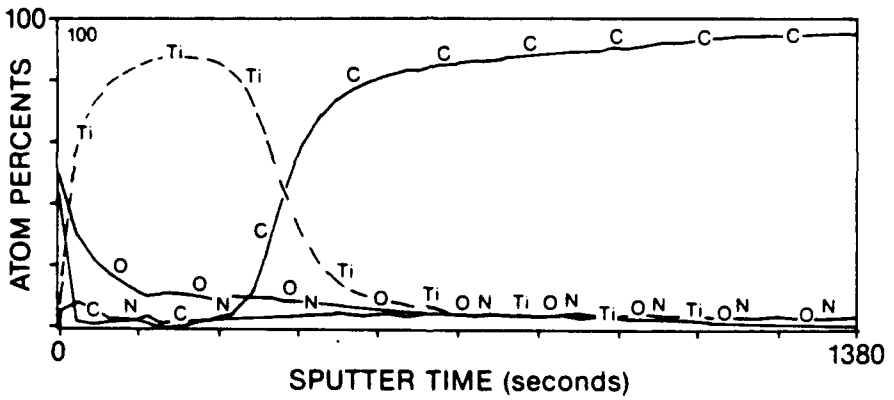

B.

Figure 3.2-8. XPS depth profile for sample containing 400 A Ti sputtered on Kapton.

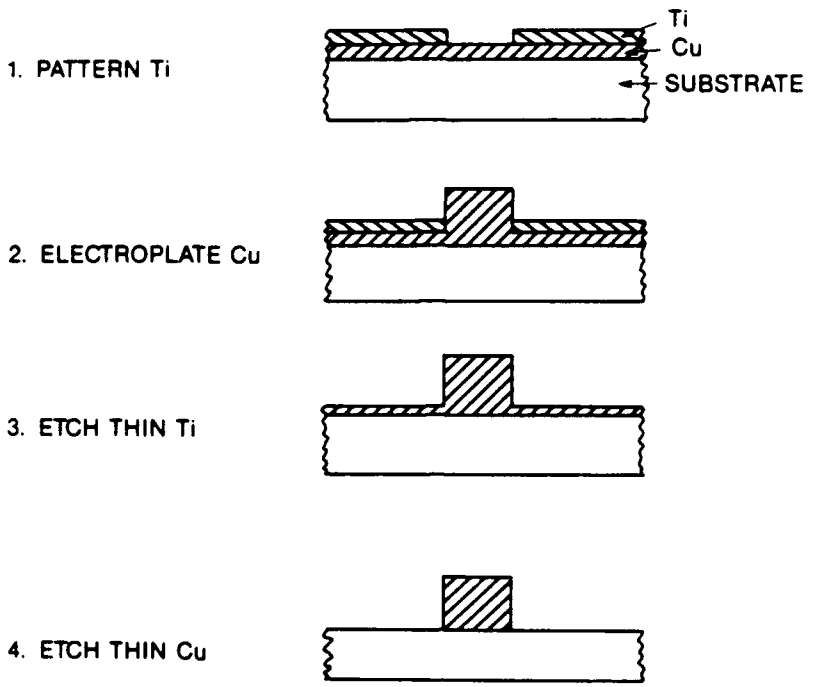

Figure 3.2-9. Selective electrolytic deposition (patterned Ti on Cu).

this instance, we used photoresist and Ti etch. After removal of resist, the part was immersed in an electroplating solution and thick Cu plated in the Cu regions which were not protected from Cu. The reason that only Cu is plated in the unprotected regions is that although Ti is conductive, the thin native surface oxide is highly resistive and inhibits current flow and hence deposition of Cu in these regions. After electroplating, the thin Ti and underlying thin Cu is etched away to give the desired patterned Cu layer as shown in step 4. Reversal of these layers gave similiar results, that is, thin deposition of Ti followed by a layer of thin Cu on a glass substrate was coated with resist and the Cu layer patterned. This process is shown schematically in Figure 3.2-10. Immersion in a Cu electroplating bath resulted in plating of thick Cu only in the regions containing Cu. In this instance, the current was carried by the Ti layer to give uniform plating thickness across the surface of a 2×2 substrate, but the surface oxide on the exposed Ti prevented Cu plating in those regions. In this instance, only the thin Ti layer needed to be etched to give the desired Cu patterned layer. It is also interesting to note that in this instance, a thin barrier/adhesion primer layer of Ti is present underneath the Cu. This unique feature provides a potential process compatible with the need previously mentioned for barrier layers in practical interconnect structures. The resistivity of metals and oxides of interest is summarized in the following table, and this data is used to understand the selective electrolytic depostion concept.

Resistivities of Metals and Oxides

Metal	Resistivity ($\mu\Omega$-cm)	Oxide	Resistivity ($\mu\Omega$-cm)
Al	2.7	Al_2O_3	1.0×10^{22}
Cr	12.9	Cr_2O_3	1.3×10^{10}
Ti	42.0	TiO_2	1.2×10^{9}

Metals such as Ti, Cr, and Al which form native oxides can be used in combination with metals that do not form oxides such as Cu, Au, and Ni to provide metal combinations useful for this SED concept. We have successfully plated selective layers of Cu, Au, and Ni on Al, Cr and Ti. In Figure 3.2-11 a photomicrograph of copper lines on Ti is shown These lines were formed by patterning 1,000 A sputtered Cu on Ti followed by a 2.5-min immersion in an electroplating Cu bath.

The SED process offers unique capability to provide patterned copper layers which are compatible with barrier layers needed in this technology. The key to successful implementation of this concept depends on developing a method to pattern thin metals that can be selectively plated and also provide sufficient aspect ratios during electroplating to give high resolution interconnect structures. These topics, treated below, formed the basis for detailed electroplating studies and laser selective metal patterning techniques.

3.2.5 Electrodeposition of Copper

Electroplating of Cu is a known commercial process that has been used in the printed circuit board industry for many years. Commercially available baths are available and much has been written about the process itself. The key requirement for our application is the aspect ratio, that is, the need to plate thick layers (up to 4 μm of Cu) with minimal change in line width. The plating process in general is isotropic and the growth in height is commensurate with a similiar growth in width. For example, a 10-μm-wide Cu line which is plated to a thickness of 5 μm could result in a final width of 20 μm. This phenomenon is demonstrated in Figure 3.2-12. In

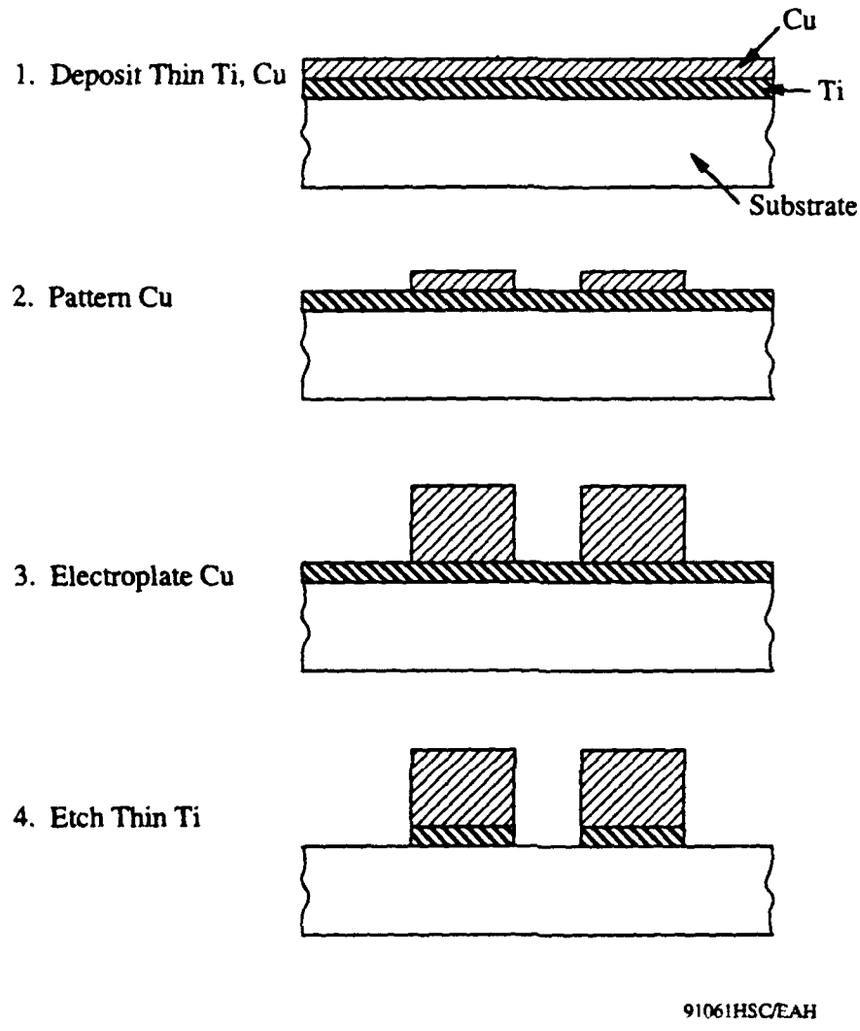

Figure 3.2-10. Selective electrolytic deposition (patterned Cu on Ti).

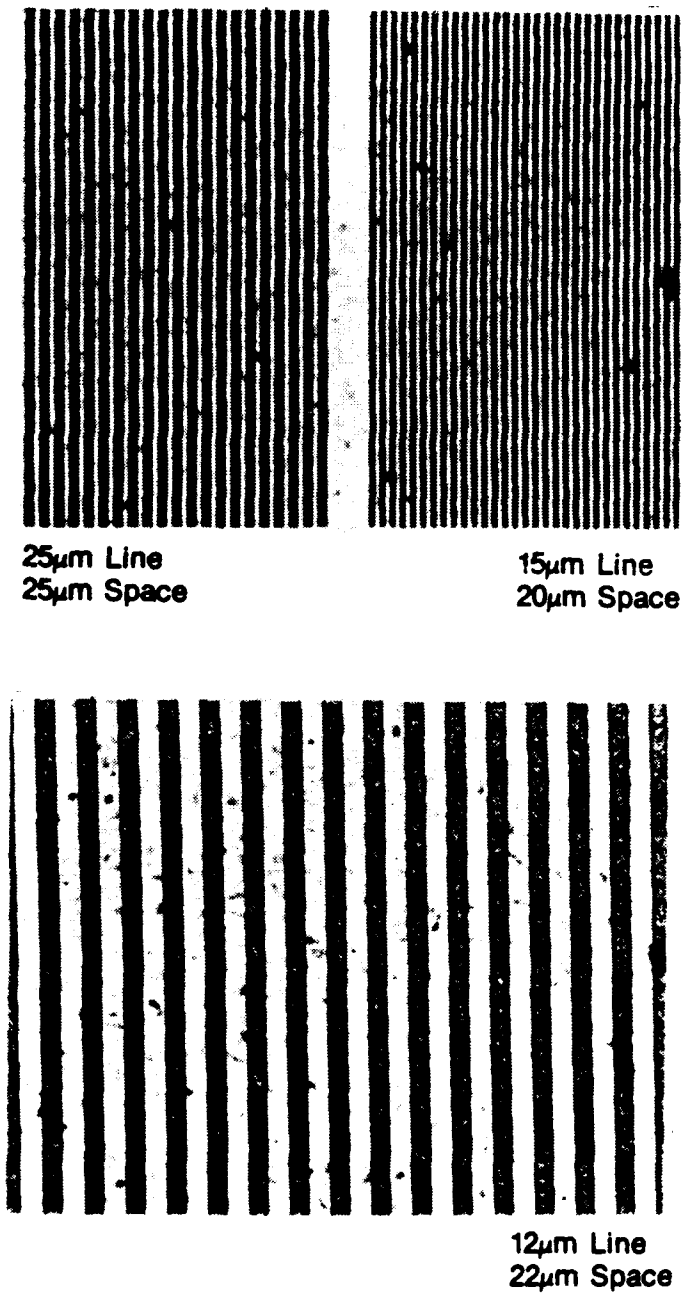

Figure 3.2-11. Selective electrolytic deposition of Cu.

this instance, Cu was patterned on Ti and electroplated for 2.5, 5.0, 7.5, and 10 min on similiar structures and then cleaved for SEM cross sections. As the time in the plating bath is increased, we see a dramatic sideways growth of Cu equivalent to that found for the increase in height. To alleviate this problem and to provide anisotropic metal deposition, electrochemists have used organic additives to improve the leveling power, brightness, and throwing power. The mechanism of these additives is that the organic compounds locally reduce high current density regions such as edges and high spots, thus providing a more uniform electrode upon which Cu is deposited.

For our studies, we chose a matte and bright Cu bath. The matte bath contained 50 g/l sulfuric acid, 140 g/l copper sulfate, and 175 ppm hydrochloric acid. The bright bath was made by adding 3% by volume of Electrobrite PC-667 (Electrochemicals Inc., Youngstown, Ohio) to the above composition. Patterned Cu on Ti samples were prepared and plating studies carried out as a function of current density and time for both the matte bath and bright bath. Using a surface profilometer and optical microscopy, the height and width of plated Cu were measured as a function of plating time and current. The matte bath is characterized by good electrical resistivity and ductility. The experimental bright bath was characterized and found to have identical resistivity and ductility. The appearance of coatings from the bright bath was specular and from the matte bath was diffuse.

The data is plotted in Figures 3.2-13 through 3.2-15. In Figure 3.2-13, the electrolytic Cu growth height is plotted as a function of plating time for various bright and matte bath conditions. The data shows an absolute growth rate of about a factor of two, with the higher current densities showing the highest growth rate. Current packaging design rules require Cu thicknesses of 3 to 4 μm, which is achieved with either of these baths in between 8 to 14 min. In Figure 3.2-14, the Cu growth width is plotted as a function of time for various conditions. In this case, there is a significant difference in width of Cu after electroplating. At low current density for both the matte bath and bright bath, the growth rate is much lower suggesting a reduction in fringing fields at the edges of the patterned Cu lines. There appears to be a knee in the plot and a change in slope after a plating time of about 5 min. At this point, the thickness is about 2.5 μm, which may result in a spike in the current density at the edge of the Cu line. The significance of this is shown in Figure 3.2-15 where the aspect ratio, defined as the ratio of the Cu height to the increase in Cu width on one side of the Cu line, is plotted as a function of time. By appropriately choosing the current density, it is possible to provide anisotropic electroplating which is necessary for high resolution interconnect structures. In Figure 3.2-16, an SEM photo is shown of 8 μm wide Cu lines which were plated using this approach. With a bright bath, it is possible to plate Cu to a thickness of 4 μm with only a 1-μm sideways growth on each side of the Cu line.

3.2.6 Selective Metal Patterning

Several metal patterning approaches were evaluated for use with SED processing to achieve a useful interconnect metallization process. A summary of these approaches include

1. Direct laser ablation of Cu on Ti.
2. Thin conformal resist on Ti/Cu.
3. Gas phase laser etch of Cu on Ti.
4. Selective laser ablation of thin inorganic oxide as mask on Ti/Cu.
5. Laser-selective interdiffusion of Au.

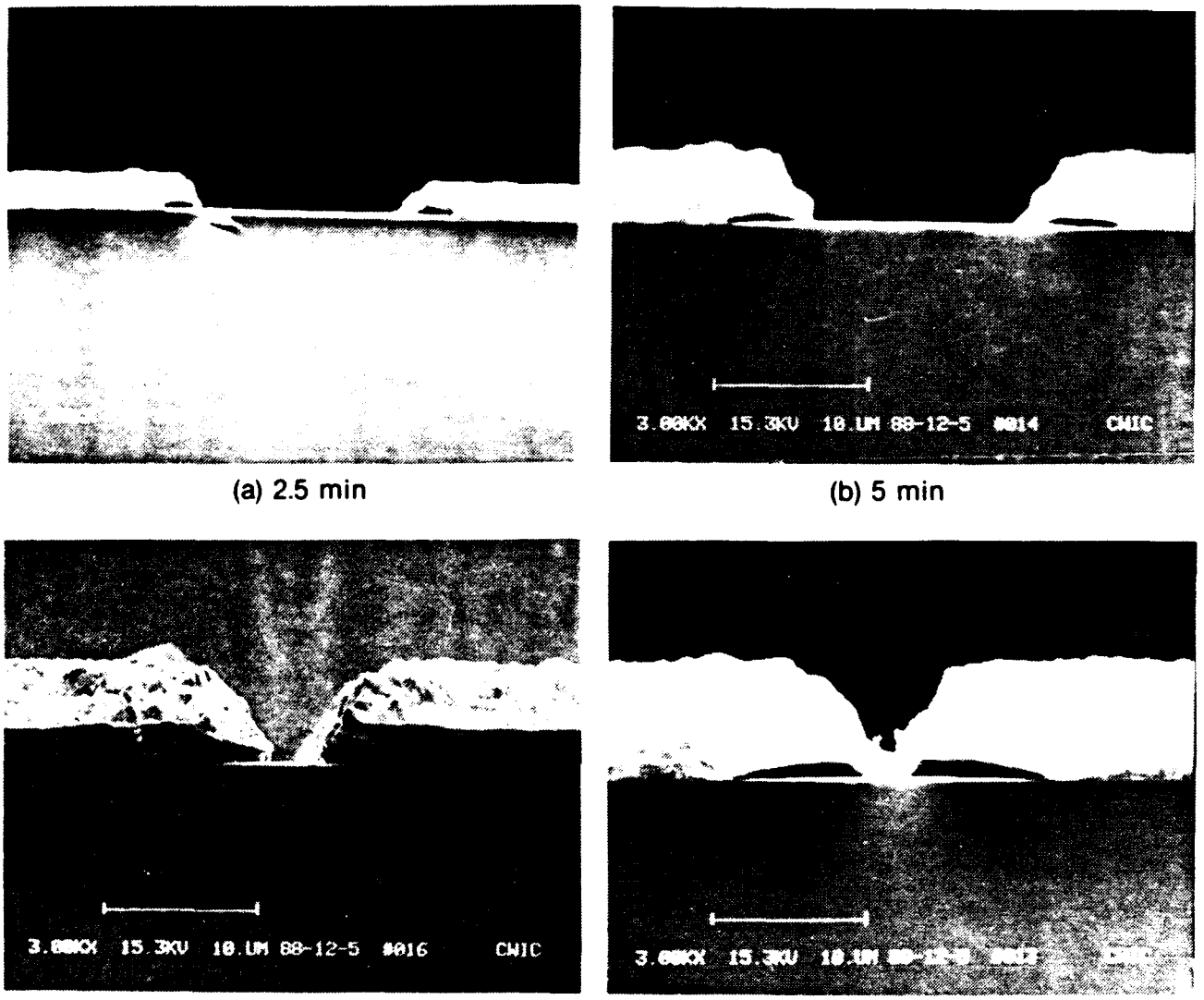

(a) 2.5 min

(b) 5 min

(c) 7.5 min

(d) 10 min

Figure 3.2-12. Effect of plating time on edge profile during electrodeposition of Cu.

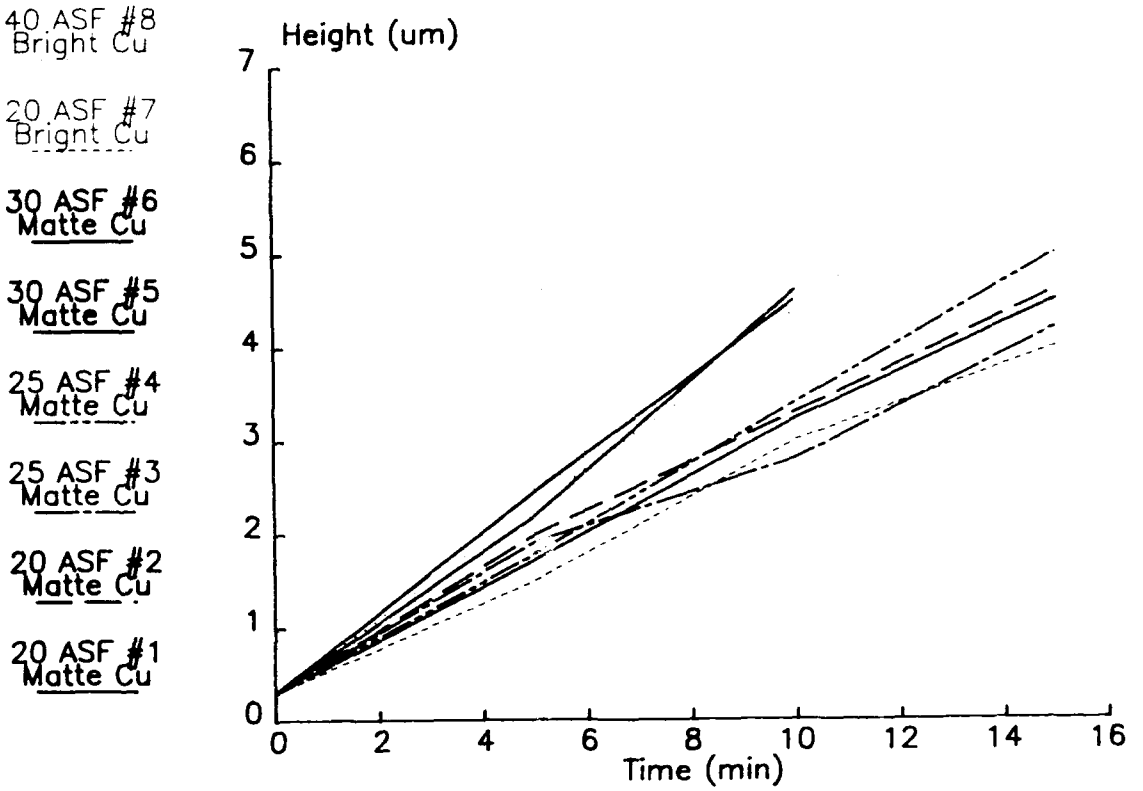

Figure 3.2-13. Electrolytic Cu growth (height vs. time).

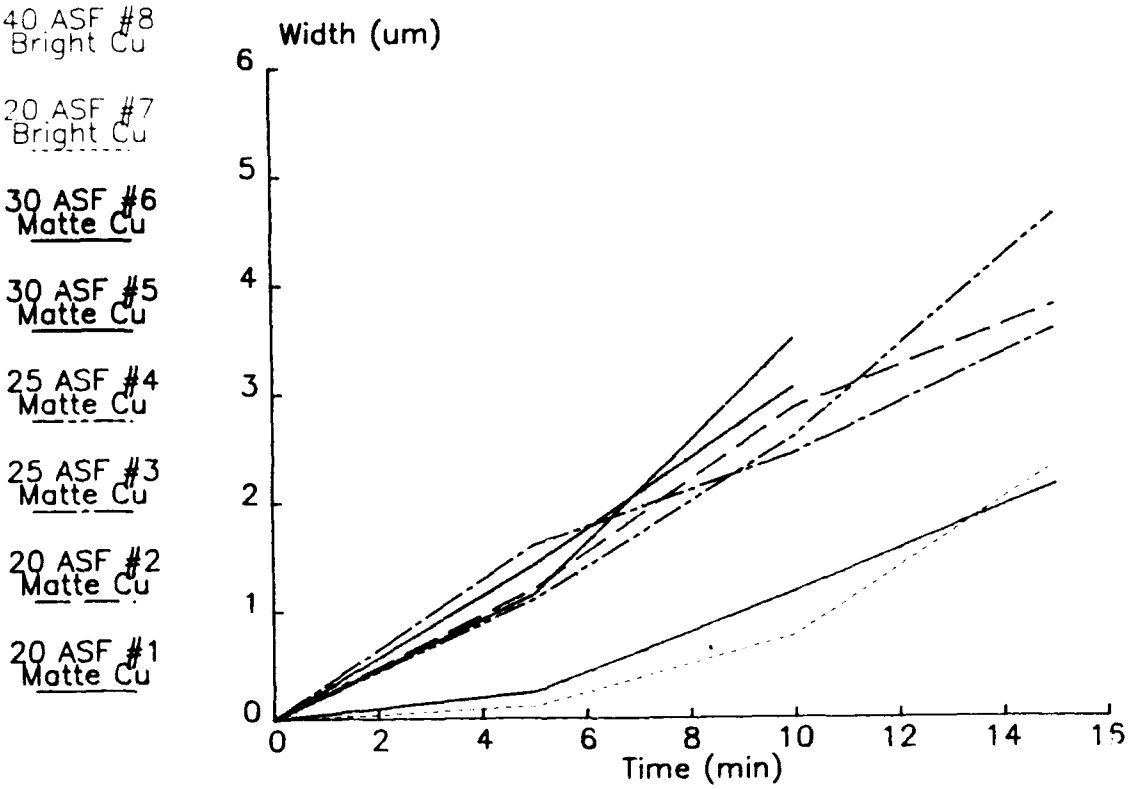

Figure 3.2-14. Electrolytic Cu growth (width vs. time).

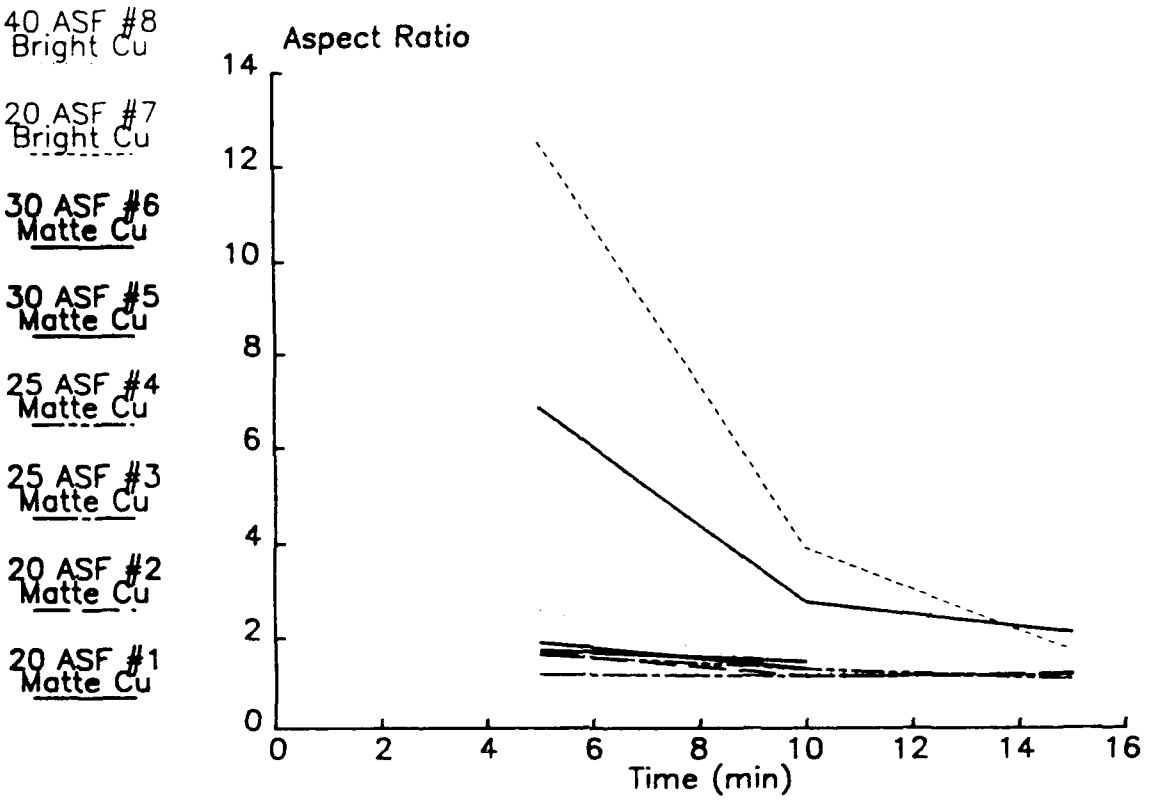

Figure 3.2-15. Electrolytic Cu growth (aspect ratio vs. time).

In approach 1 above, we take advantage of the high absorption coefficient of Cu (> $10^4 cm^{-1}$ at 351 nm. With sufficient power levels, the laser locally heats the Cu causing vaporization without affecting the underlying Ti layer. Various thicknesses of Ti and Cu were evaluated to optize the process sequence. Best results were obtained using 3,000 A Ti and 500 A of Cu with laser power levels of between 1.2 and 1.8 W and laser scan speeds similiar to those used for photoresist exposure. Although patterns were generated and electroplated, this approach was abandoned because of the narrow process window found for this process. It was found that to get complete removal of Cu uniformly across the surface required a power level and beam overlay spacing that in some instances removed the underlying Ti. Approaches 2 to 4 above all gave similiar results with varying degrees of success, although the requirements of fast scan, selectivity, and high resolution were not met by any of these approaches. However, in approach 5, an interesting observation led to the discovery of a patterning process which does meet the requirements of direct-write metallization.

Previous studies showed that Au patterns on Ti, Al, and Cr could also be selectively electroplated. In understanding the mechanism of plating, samples were prepared for RBS analysis which showed the presence of Au in Ti layers that had been immersed in Au etchant to remove a thin Au layer (Figure 3.2-17). In Figure 3.2-18, the RBS depth profile for a Au/Ti/glass sample after Au etch shows the Au to be interdiffused in the Ti layer at a concentration of about 1 % by atomic wt. In reviewing the history of sample preparation, it was noted that the Au was sputtered on the surface of the Ti without breaking vacuum and that the Au sputtering generated sufficient heat to presumably cause interdiffusion between the Ti and Au interface. This phenomenon is consistent with literature studies of these and similar metallization systems [11]. It was further observed that Ti/Au surfaces which had the Au etched away were capable of substaining electroplating of Au and Cu contrary to earlier observations of pure Ti samples with native oxides. The presence of 1 % atomic Au at the surface was sufficient to lower the resistivity and allow electroplating. This concept was used to develop the laser selective Au interdiffusion process shown in Figure 3.2-19. In this approach, the substrate is sputtered with a thin layer of Ti followed by a thin layer of Au. The key to this step is to sputter the Au under conditions which do not allow heating of the substrate. Under these conditions, there is no interdiffusion of Ti/Au at this time. The part is then selectively exposed to the argon ion laser at 351 nm. The absorption coefficient of Au is high at this wavelength resulting is efficient energy coupling and local heating of the thin Au. This step is sufficient to create interdiffusion of Ti/Au selectively. The part is then etched in Au etchant and immersed in a Cu or Au electroplating bath. The regions of the surface which were laser-exposed have much lower resistivity and can substain current for selective electroplating. The laser scan process can be done at scan rates of several cm/sec and plated linewidths were on the order of 25 μm.

REFERENCES

[1] Y.S. Liu, "Microfabrication: Thin Film Processing and Lithography," Chapter 1, Academy)Press (1989).

[2] Y.S. Liu, "Tungsten and Other Refractory Metals Deposition for VLSI Applications," edited by R.I. Blewer, Materials Research Society, p. 43 (1985).

[3] H.S. Cole, Y.S. Liu, J.W. Rose, R. Guida, L.M. Levinson, and H.R. Philipp, Conf. Proc. for Microelectronic Applications, Honolulu, Hawaii (1987).

[4] H.S. Cole, Y.S. Liu, J.W. Rose, and R. Guida, Appl. Phys. Lett. 53, 2111 (1988).

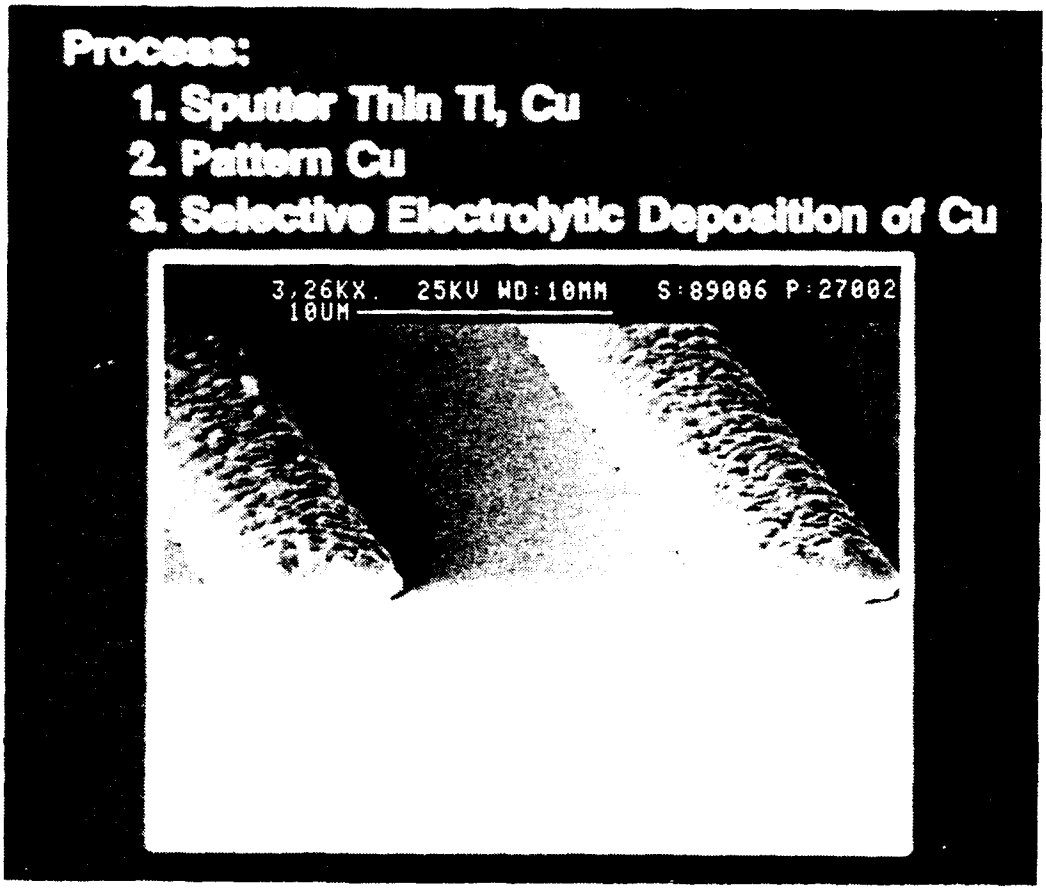

Figure 3.2-16. SEM of Cu lines fabricated by SED.

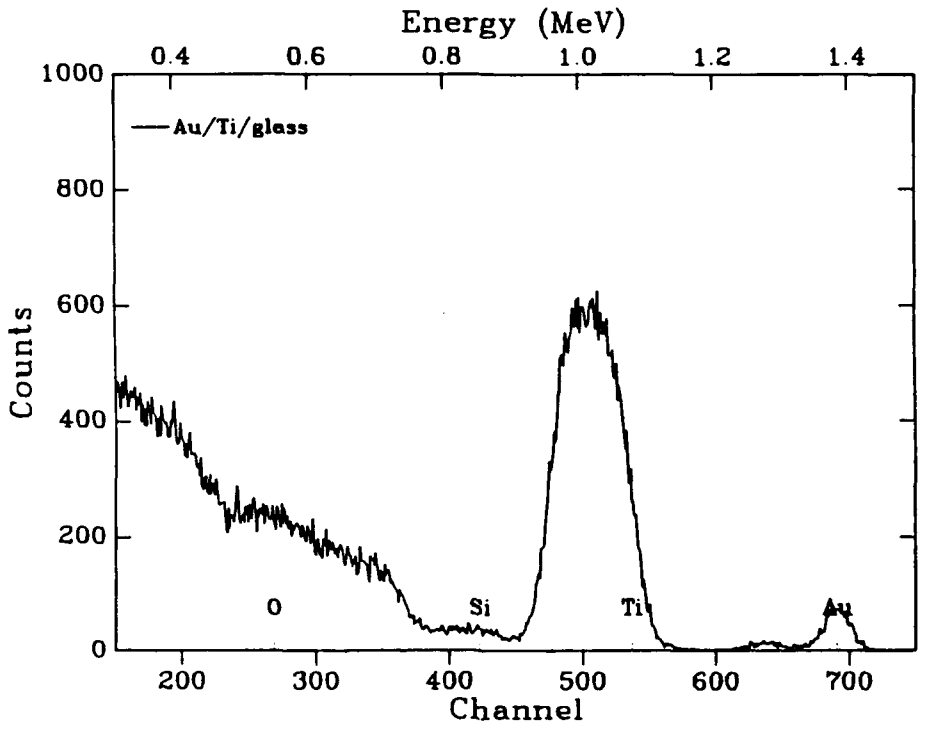

Figure 3.2-17. RBS data for Au/Ti/glass layer after Au etch.

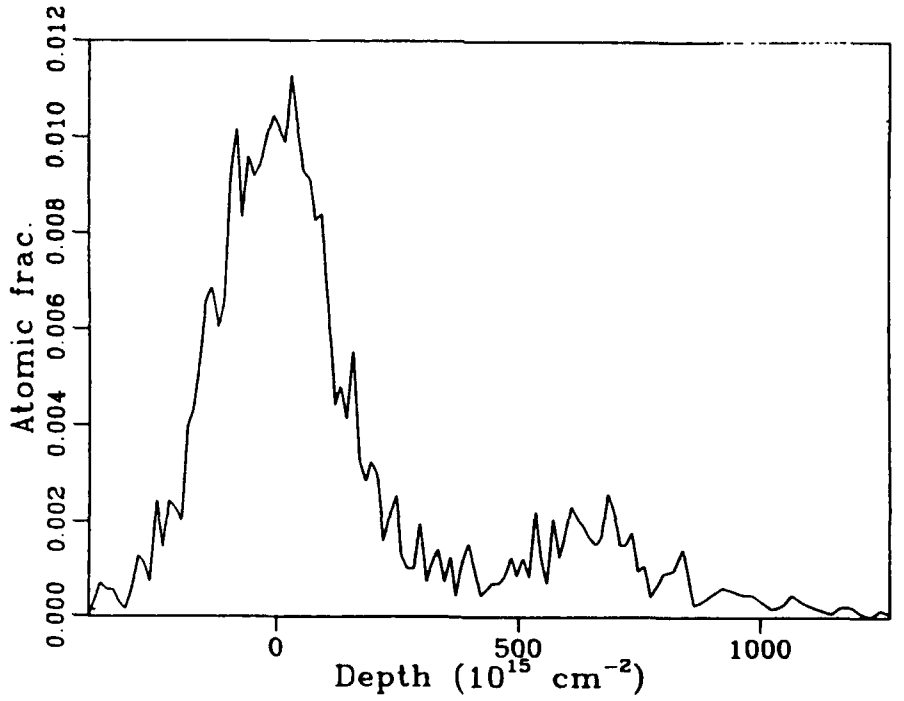

Figure 3.2-18. RBS depth profile of Au/Ti/glass layer after Au etch.

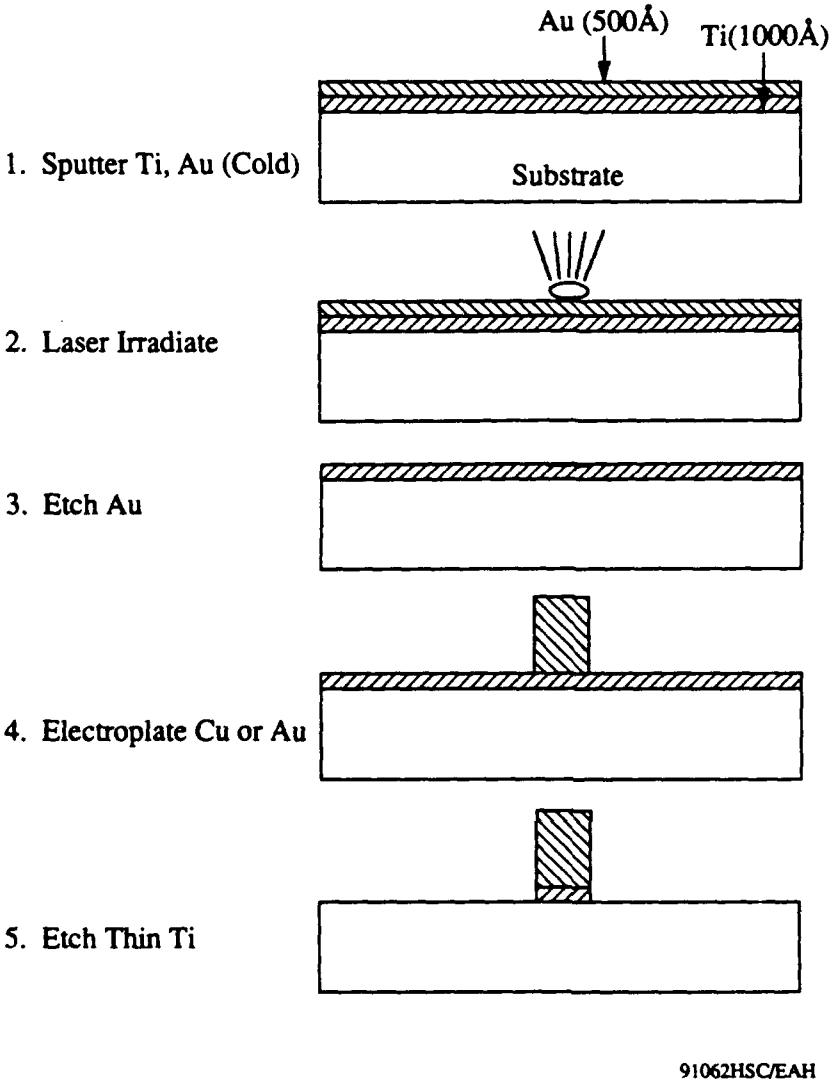

Figure 3.2-19. Laser seclective Au interdiffusion process.

[5] Y.S. Liu, W.T. Grubb, and H.S. Cole, Tech. Digest of Conf. on Lasers and Electo-Optics, WX-5, p. 286 (1988).

[6] Y.S. Liu and H.S. Cole, Chemtronics, Vol. 4, No. 3, 197 (1989).

[7] P.S. Ho, P.O. Hahn, J.W Bartha, G.W. Rubloff, F. K. Legoues, and B.D. Silverman, J. Vac. Sci. Technol. A3, 739-745 (1985).

[8] Y.H. Kim, G.F. Walker, J. Kim, and J. Park, J. Adhesion Sci. Tech., Vol. 1, 331-339 (1987).

[9] B.K. Furman, S. Puroshothaman, E. Castellani, and S. Remick, Proc. Electrochem Soc., Vol. 87-4, p. 142-151 (1987).

[10] M.J. Goldberg, J.G. Clabes, and C.A. Kovac, J. Vac. Sci. Technol. A, Vol. 6, p. 991 (1988).

[11] C. Chang, J. Mater. Res., 2, 697 (1987).

3.3 Polymer Interface Studies

3.3.1 Introduction

To obtain reliable adhesion between metal and polymer, adhesion mechanism, adhesion measurement, interface analysis, and adhesion enhancement techniques have to be understood. Precise measurement of true interface adhesion is very important for understanding the adhesion mechanism. Unfortunately, it is difficult to measure the true adhesion between metal and polymer using current-measuring techniques. In addition, the adhesion depends on the interface reaction, such as compound formation and diffusion. Therefore, interface characterization techniques such as SEM, cross-sectional TEM, XPS, AES, SIMS, and RBS are widely used to understand the interface reaction. For adhesion enhancement, adhesion promoters such as Cr and Ti, combined with surface modification techniques (surface cleaning by inert gas ion milling or surface etching by reactive ion plasma), are widely used.

In this study, the previous results on Cu, Cr, Ti and Ni on PMDA-ODA polyimide will be reviewed in the next section. In the experimental results, the adhesion strengths of Cu and Ti on Kapton ^{TM}, and siloxane-polyimide (SPI), with various surface treatments techniques, such as plasma-etching, backsputtering, and HF treatment, are measured. In order to understand the adhesion mechanism, the surface chemical structure and the surface morphology of polymers after various treatments were investigated by x-ray photoemission spectrometry (XPS) and scanning electronicmicroscopy (SEM), respectively. In addition, the diffusion of Cu into SPI was also examined using Auger depth profile. A new two-step dry etching process, which prevents the formation of SiOF compound formed after O_2 +CF_4 ashing on SPI, will be discussed

3.3.2 Background

3.3.2.1 Cu/Polyimide

An initial study by Chou, et al., using XPS [1] showed Cr and Ni react with the pendent oxygen of the polyimide while Cu and Ag do not. The C 1s signal from the substrate attenuates in intensity with increased thickness of Cu deposit, but the resolved peaks decreased proportionately as expected from the simple escape length effect. The author concluded that the metals, such as Al, Mg, Ti, and V, which have large heat of sublimation and heat of oxide formation, are expected to have good intrinsic adhesion strength.

Ho, et al. [2] observed by XPS that a weak interaction between Cu and polyimide affects mainly the bonding of the carbonyl but does not change the basic chemistry of the polyimide. With increasing coverage and reaction with Cu, the intensity of the carbonyl peak is reduced significantly faster than the two main peaks in C 1s spectra, indicating that most of the changes are seen to occur in the peaks associated with the carbonyl group. A cross section of TEM also showed enhanced copper intermixing at the interface as a result of annealing.

The diffusion of Cu into polyimide was investigated by Tromp [3] using medium energy ion spectrometry (MEIS) and TEM. In the temperature range of 293 to 593 K of specimen heating during deposition, Cu is found to diffuse into polyimide and to form small spherical particles. The size of these spheres and the depth at which they occur increase with increasing temperature.

Sanda, et al. [4] found that Cu evaporation has comparatively little effect on the PMDA-related features. However, Cr bonds with the PMDA part of the related mode compound, or fractures the carbonyl bonds and/or other bonds contained in the PMDA structure.

Ho [5] summarized that the chemical bond between Cu and polyimide is the weakest, thus Cu atoms can diffuse readily into polyimide to form clusters. The formation of metallic precipitate in the films was observed by LeGoues, et al. [6] using a cross section of TEM. A relationship between the microstructure of the polyimide/metal interface and the extent of chemical bonding at the interface was suggested. When the chemical bonding is weak, the metal is free to diffuse into the polyimide and form clusters. On the other hand, when the chemical reaction is strong, the diffusion into the polyimide surface is hindered.

The effect of annealing on Cu diffusion and the detailed information of diffusion were investigated by Paik, et al. [7] using Rutherford backscattering spectrometry (RBS). Diffusion of Cu in polyimide film was observed after Cu evaporation on PI at room temperature. Annealing treatment after deposition significantly enhanced the diffusion of Cu. The diffusion coefficient measured at 200 and 400 °C using the Fickikan error function (erfc) solution is 3×10^{-14} and 1×10^{-13} cm^2/s, respectively. Cu shows thermally activated Fickian diffusion behavior.

3.3.2.2 Cr/Polyimide

Cr shows different characteristics compared with Cu/polyimide. The first few monolayers of Cr appear to react with the pendent oxygen in the PI substrate, forming either Cr oxygen complexes or Cr oxides at the interface.

The carbonyl peak in C 1s spectra disappears as Cr coverage increases [8]. Other XPS studies by Jordan, et al. [9] showed that the Cr bonds with the PMDA part of the related model compound or fractures the carbonyl bonds and/or other bonds contained in the PMDA structure.

The detail XPS and UPS studies by Clabes, et al. [10] found that charge transfer occurs from metal atoms into the PMDA portion of the polymer at the initial stage of metal- polymer interaction. Hence, subsequent metal-polymer compound formation involving bond breaking and displacement of O, N, and C from the polymer chain is seen as a logical consequence of the polymer preactivation by reduction. The coordination of Cr^{+2} with two adjacent ligands belonging to different monomer units was suggested.

$$Cr + 2(PMDA - ODA) = 2(PMDA - ODA)- + Cr^{+2}$$

A multistep, coverage-dependent mechanism is proposed, which includes an initial electron transfer from Cr to PMDA-ODA, followed by formation of Cr-O and Cr-N polymer-bound intermediates. At high metal coverage, Cr-oxides and Cr-nitrides are formed that may activate the polymer for subsequent formation of Cr-carbide [11]. In general, there is a trend for initial electron transfer in the reaction of electropositive metals, such as Cr, Al, and Ni with electroactive polyimides.

3.3.2.3 Ti/Polyimide

The adhesion of electron beam evaporated Ti films onto polyethylene can be enhanced by Ar ion bombardment of the PE surface prior to film deposition. The strong film adhesion is related to a carbide-like Ti-C formation appearing at the film-substrate interface. The ion bombardment removes surface impurities mainly originating from the sample preparation process, and the optimal ion dose will thus depend on the surface condition of the samples [12]. Ti/polyimide interface studies were performed by Ohuchi, et al., using XPS and UPS. At low coverages, the polyimide surfaces react strongly with Ti, and strong charge transfer via the carbonyl group occurs. As the coverage increases, a Ti-C bond formation has been identified [13]. The most dramatic changes in the spectra are observed while monitoring the Ti(2p) peak. Electron density is transferred from Ti to polyimide via carbonyl group, followed by a second electron transfer from Ti to the imide. Ti-O followed by Ti-C formation is consistent with the

two-electron transfer model. Furthermore, it was found that the Ti interlayer effectively blocked the diffusion of copper to polyimide [14]-a monolayer of Ti blocks permeation of Cu to polyimide. This barrier effect is the result of a mixed Ti-O and Ti-C interface formed upon Ti deposition on polyimide.

Bodo, et al. [15] reported ion bombardment and Ti film growth on polyimide. A preferential bondbreaking of imide carbonyl groups and the formation of graphitelike carbons were observed as a consequence of the Ar ion bombardment. As Ti was deposited, a C 1s peak corresponding to Ti-C formation was observed for both as-prepared and ion-bombarded samples. The film growth is three dimensional in its character where islands of depositing atoms are formed in the initial stages. On ion-bombarded PI surfaces, the number of nucleation sites is so large that the Ti film growth is comparable with a calculated layer-by-layer growth.

3.3.2.4 Adhesion Mechanisms

Four adhesion mechanisms are proposed [16]:

1. Mechanical interlocking
2. Diffusion Theory
3. Electronic Theory
4. Adsorption Theory

Mechanical keying or interlocking of the adhesive into the irregularities of the substrate surface happens frequently in many cases, such as the metalplating of polymers. The surface of substrate is modified to have rough or textured surface to mechanically interlock subsequently deposited material. On the other hand, intrinsic adhesion of polymers to themselves and to each other because of mutual diffusion of polymer molecules across the interface is another adhesion mechanism that is involved in autohesion of elastomers and solvent welding of plastics. Electronic theory represents that some electronic transfer on contact to balance Fermi levels results in the formation of a double layer of electrical charge at the interface. Metal bonding on polymer is one of the examples of electronic theory. Finally, adsorption theory is applied when sufficiently intimate intermolecular contact is achieved at the interface. Then the materials will adhere because of weak van der Waals forces or stronger chemisorption-ionic, covalent, and metallic bonds.

Adhesion Measurement: There are several methods to measure the adhesion between two different materials: qualitatively or quantitatively [17].

1. Direct pulloff method
2. Scotch tape method
3. Peel method
4. Scratch method
5. Indentation method
6. Electromagnetic peel method
7. Pressure method

Among these methods, the peel method has been widely used to measure adhesion quantitatively. However, the measured peel strength value may represent a sum of true interface adhesion and other work expenditure rates primarily caused by the plastic deformation of the thin film. Major controlling factors of the measured strength are [18]

1. Thickness, Young's Modulus, yield strength, and strain-hardening of film
2. Compliance of the substrate
3. Interface adhesion strength
4. Peel conditions such as peel speed and temperature.

Even though the true interface adhesion strength is the same, a higher peel strength is obtained if the film is thinner or more ductile. The same effect can be obtained if the substrate is thinner. Therefore, specimen preparation has to be strictly controlled to have exactly the same dimension and material properties. Furthermore, the locus of failure is very important to evaluate the adhesion at interface. For cohesive debonding at the polymer, the measured peel force represents not the true adhesion between metal and polymer but a lower bound of the interfacial bonding energy per unit area.

3.3.3 Results and Discussion

Table 3.3-1 shows the adhesion strength of Cu or Ti on Kapton and SPI polymers at the various surface modification techniques. The data is reported for different apparatus and times and indicates in some instances the effect of specimen preparation on adhesion values. For example, in the case of Cu/Kapton adhesion after backsputtering, the high peel strength is attributed to the presence of Ti from the sputtering chamber.

3.3.3.1 Cu/SPI Interface

One interesting observation is that Cu sticks well on SPI even without surface treatment. It represents almost 80% of the Ti/Kapton adhesion. For an untreated SPI film, cohesive failure in SPI film occurs. About 40-A thickness of SPI film is observed at the backside of the Cu stripe using Auger depth profile as shown in Figure 3.3-1. Surface modification (plasma-ashing followed by backsputtering) decreases the adhesion strength significantly probably because of the change of surface chemistry. After O_2 + 20% CF_4 ashing, the C and N amounts decrease, and Si and O amounts increase at the surface as a result of SiOF compound formation by XPS analysis as illustrated in Table 3.3-2. A cross-sectional TEM picture of plasma-ashed SPI shows rough SPI surface. Probable Cu bonding with the Si part in SPI polymer, resulting in good adhesion, may be prevented by the presence of SiOF compound at the plasmaashed surface.

Annealing of SPI film ashed by O_2 +CF_4 plasma produces the partial removal of F. F and Si amounts decrease as annealing time increases. Annealing at 200 °C for 5 h restores the ashed surface to almost as-deposited, except for a little increase of oxygen amount. Therefore, for better adhesion, annealing after plasma-ashing or current HF treatment is recommended to remove surface SiOF compound on SPI.

Backsputtering on plasma-ashed SPI shows low adhesion strength because the surface SiOF compound still remains even after backsputtering on the plasma-ashed SPI surface. HF treatment to remove SiOF compound between ashing and backsputtering is necessary to increase the adhesion between Cu and SPI. Previous XPS studies showed that more than 3000-A thickness of SPI modified by current HDI process remains on the backside of peeled metal stripe. These results indicate that the weakest adhesion is located not at the modified SPI and Cu interface but at the modified SPI and bulk SPI interface.

Table 3.3-1

The Peel Strength of Metals and Polymers at the Various Surface Modification Conditions

Metals/ Polymers	Untreated	O_2/CF_4 Plasma Etch	Plasma Etch +Backspattering (No HF)	Plasma+HF +Backspattering
Cu/Kapton				
8/9,24/89*	1.92	0.1	9.3	
previous†	0.20	0.55	0.43	
Ti/Kapton				
8/9,24/89	1.04	0.2	9.5	
previous	0.45	0.47	11	
Cu/SPI				
9/26/89‡			5.3	10.0
8/9,24/89	7.7		4.5	
previous	7.7	7.7	10.4	
Ti/SPI				
9/26/89			4.0	10.5
8/9,24/89	4.0	0.1	4.7	
previous	5.1	5.1	10	

*tested on August 9, 1989 and August 24, 1989

†previous data measured by K-1 peel tester

‡tested on September 26, 1989

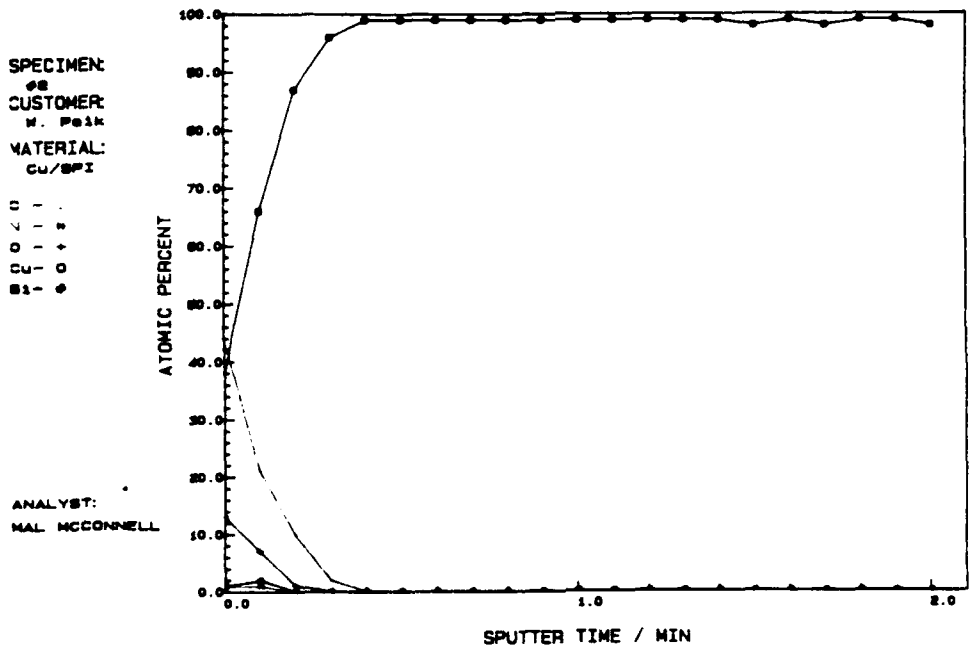

Figure 3.3-1. Auger depth profile of the backside of peeled Cu on SPI.

Table 3.3.-2

XPS Compositional Analysis of Polymers

Samples/Conditions	C	O	N	F	Si	Ti
SPI	66	17	3		14	
SPI/O_2+CF_4		14	51	0.5	1	34
SPI/O2+CF_4(2)	6	44	0.5	18	31(?)	—
SPI(O_2+CF_4/Anneal at 200 °C/1)	—	49.3	36.1	—	0.7	13.8
SPI(O_2+CF_4/Anneal at 200 °C/5h)	—	55.2	33.5	—	0.5	10.8
Cu stripe from SPI	67.9	22.1	2.7	—	2.7	Cu: 3.2, Cl: 1.4
SPI + Eximer	—	62.3	24.7	1.5	—	Si:11.5

3.3.3.2 Ti/SPI Interface

For untreated SPI, Ti/SPI shows poorer adhesion than the Cu/SPI. For modified SPI, Ti/SPI adhesion is still poor unless the surface SiOF compound is removed. HF treatment restores the peel strength to 10.5 lb/in. SEM with energy dispersed x-ray (EDX) on the backside of Ti/Cu stripe observes Si and O peaks from SPI film. The locus of the failure occurs at the modified SPI/bulk SPI interface as the previous Cu/SPI case. Since most failure happens at the modified SPI and bulk SPI, the effect of surface modification on the physical properties of polymer surface is very important not only to increase the peel strength, but also to understand the adhesion mechanism. If the mechanical strength of the surface polymer layer can be increased by surface modification methods, higher peel number can be obtained. However, higher peel strength does not alway represent better adhesion between metal and polymer.

3.3.3.3 Water Boiling Test on Ti/SPI

A water boiling test was performed in order to find the stability of Ti/SPI interface at the presence of humidity and temperature. Table 3.3-3 shows the peel strength at the various boiling times. For the Ti/SPI interface, about 80% of original peel strength is retained up to 20 h of boiling. After 20 h, the failure happens at SPI/Kapton interface, and the delamination of Kapton/alumina also occurs.

3.3.3.4 Cu Diffusion into SPI

Cu shows good adhesion on SPI without using a Ti inter- layer. However, Cu cannot be directly deposited on SPI unless the diffusion characteristics are fully understood.

Cu diffusion into SPI was observed for an as-deposited condition at room-temperature using Auger depth profile analysis. The Cu diffuses slightly less than 1000 A into SPI as seen in Figure 3.3-2(a). Annealing at 200 C for 3 h (Figure 3.3-2(b)) makes Cu diffuse about 2000 A. In addition, carbon also diffuses to the Cu side during annealing at 200 C for 3 h. Carbon is detected 1000 A below the surface of 2000-A-thick Cu. Further annealing makes Cu and C diffuse to the SPI and Cu side, respectively, and reduces the surface Cu concentration to 80% and 70% for 16-h and 64-h annealing (see Figure 3.3-2(c) and (d)). The diffusion of Cu in SPI seems to be approximately two orders of magnitude faster than that of Cu in Kapton PI.

As a result, Cu diffusion in SPI is so significant that a diffusion barrier layer, such as Ti or Cr, should be used between Cu and SPI. The Cu diffusion into SPI is even greater than Cu diffusion into Kapton polyimide. For reference, Cu can diffuse into Kapton polyimide up to 1000 A at 400 °C for 10-h annealing. However, Cu diffuses into SPI more than 1000 A, even at room temperature. Three explanations can be suggested. First, chemical reaction between Cu and uncured polymer and the remaining solvent can significantly enhance Cu diffusion into polymer. Second, usually the diffusion of Cu in polyimide is considered as a thermally activated process explained by the reptation mechanism. If the reptation diffusion model is also applied for SPI on diffusion, the free volume of SPI may be much larger than the Kapton polyimide. Third, 200 °C heating is over the glass transition temperature of SPI. Therefore, SPI softening may occur and activate Cu intermixing.

3.3.3.5 One- or Two-Step Etching Process

To have good metal adhesion on SPI, HF treatment has been recommended because the SiOF compound formed by O_2 + CF_4 plasma-ashing causes the low adhesion of metal. The SiOF compound is produced by the presence of oxygen gas in the ashing gas mixture. Therefore, the SiOF compound can be avoided or removed by using different gas mixture without oxygen. Three candidates are used such as CF_4 +H_2, CHF_3 +Ar, and pure CF_4. Reactive ion etching

Table 3.3-3

Water Boiling Effect on the Peel Strength of Ti/SPI

	Relative Peel Strength ($PS_{boiled}/PS_{as\text{-}received}$)
Specimens	Ti/SPI
2.5 h	0.95
5.0 h	0.95
9.0 h	0.96
15.0 h	0.73(SPI)
20.0 h	0.84
25.0 h	0.56*(SPI/Kap) (Kap/Al_2O_3 fail)

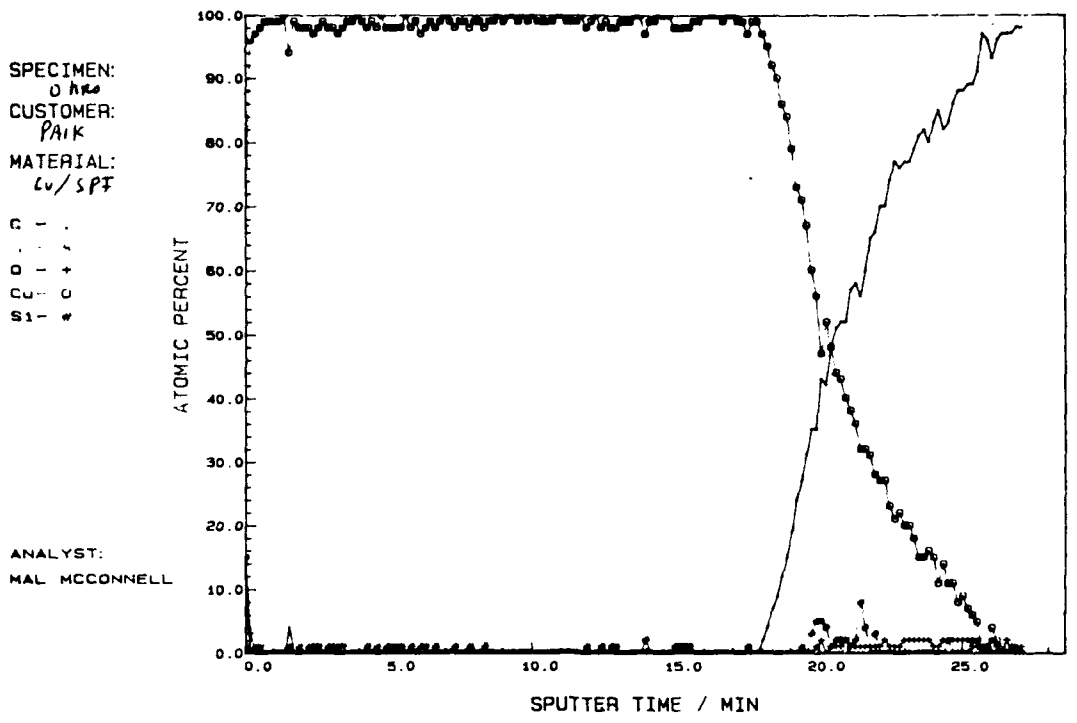

(a)

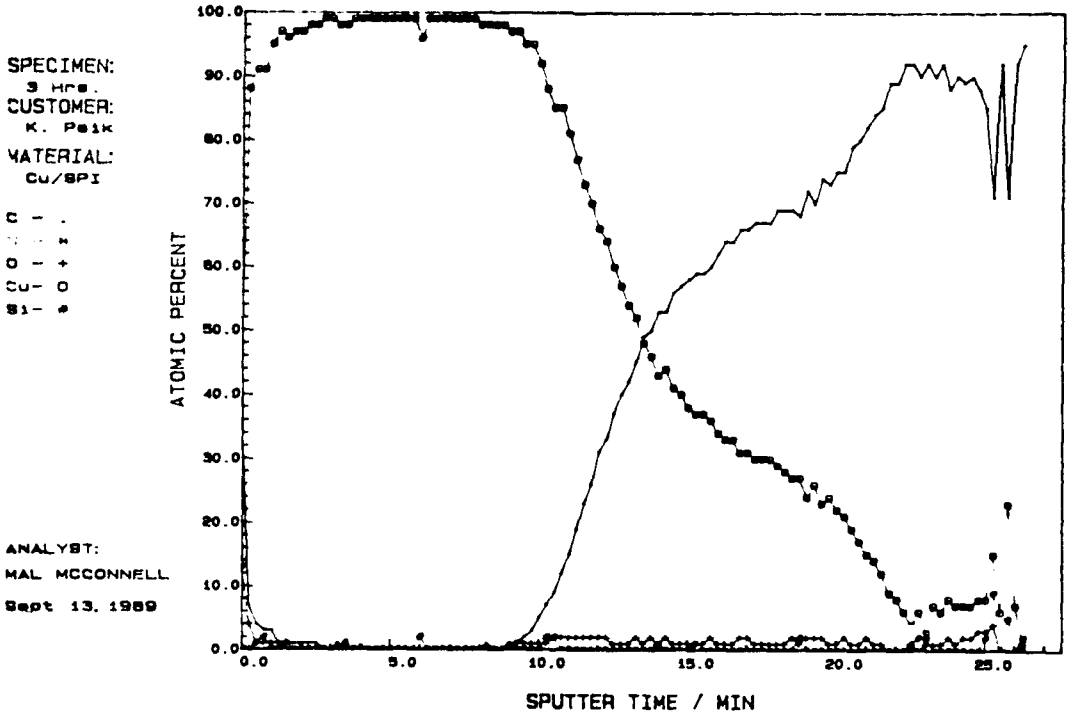

(b)

Figure 3.3-2. Auger depth profiles of Cu on SPI (a) as-deposited, and annealed at 200 C for (b) 3 hours;

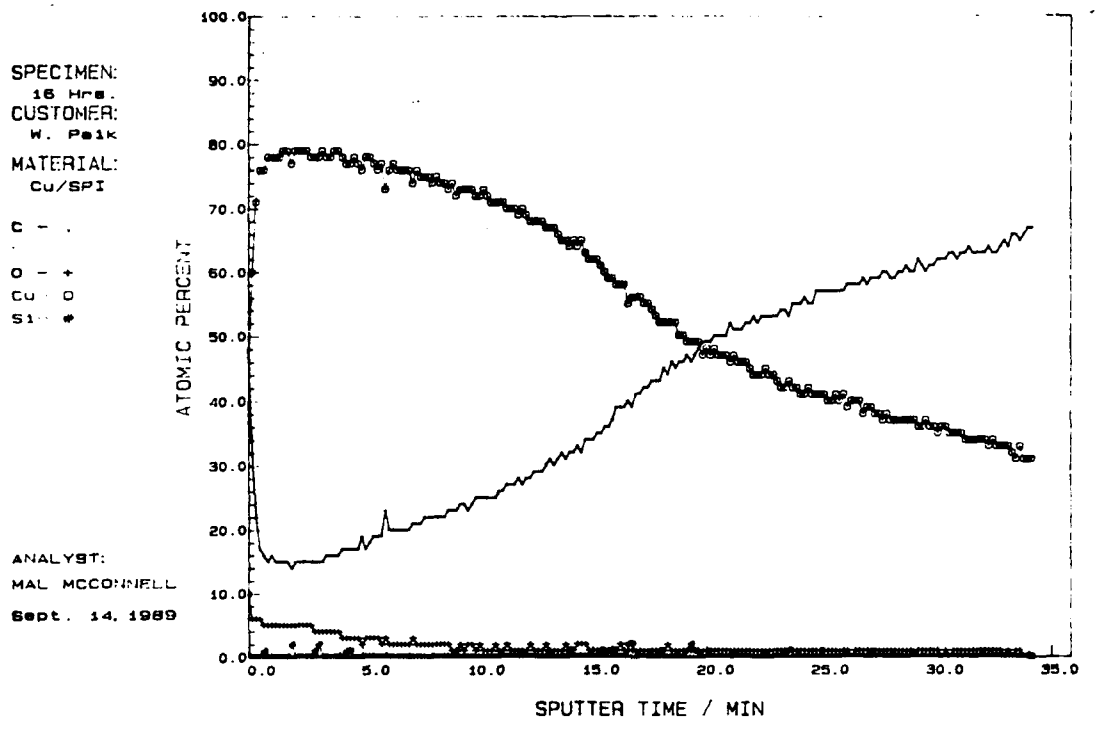

(c)

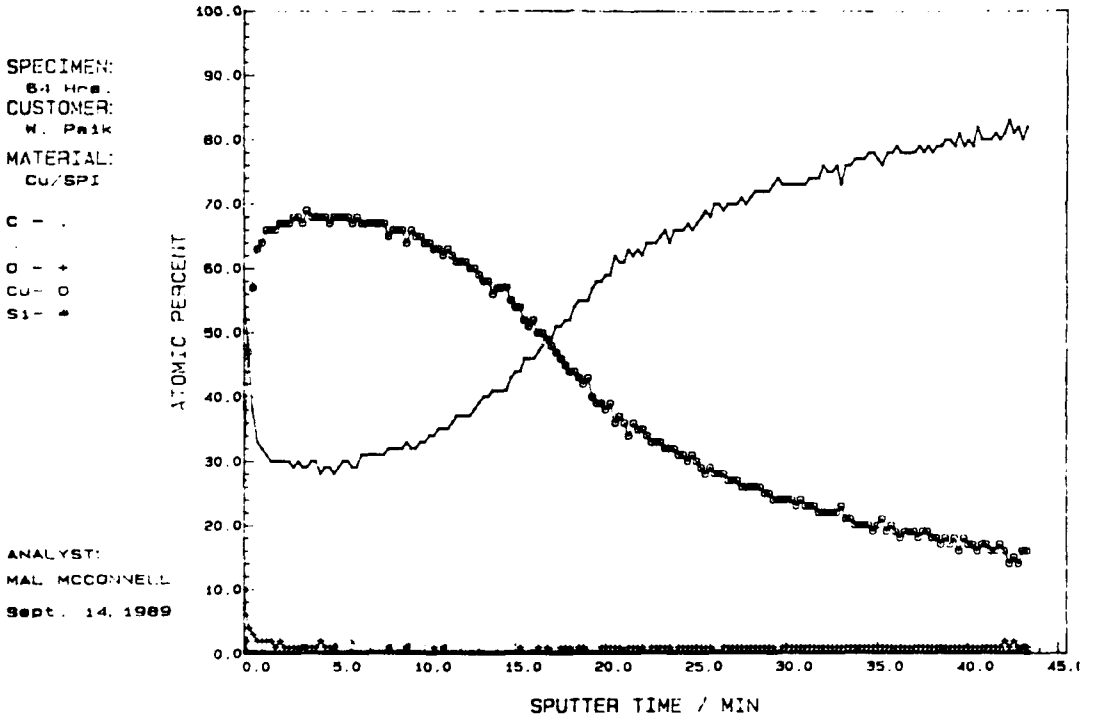

(d)

Figure 3.3-2 (continued): Auger depth profiles of Cu on SPI (c) 16 hours, and (d) 64 hours.

(RIE) has4been used in order to increase etch rate. Etching conditions and measured etch rate are shown in Table 3.3-4.

One-step etching on SPI with three different gas mixtures cannot remove surface residue around the via as shown in Figure 3.3-3 (a-f). Higher reactivity resulting in higher etch rate and rough surface morphology is observed with pure CF_4 RIE. A 25%CHF_3 +Ar mixture shows lowest etch rate and less rough surface morphology, since 75% of inert Argon gas was mixed with 25% of CHF_3 . For cleaning vias, a one-step etching process cannot be used because of its low etch rate.

A two-step etching process, O_2 + 20% CF_4 plasma-ashing followed by an RIE process using three different gases, produces a cleaner surface and via than the one-step etching process. Surface morphology is also rougher than the one- step because of additional plasma-ashing effects. These roughened surfaces may be used to increase the subsequent deposition of metal film by a mechanical interlocking effect. Surface-roughening of PI surface using oxygen reactive ion beam increases the peel strength of subsequently deposited copper film up to 25 times [7].

Table 3.3-4 illustrates the surface composition after each etching process. The amount of Si is small (ca. 1%) in all cases, and the Si 2p line was not characteristic of SiO_2. The formation of SiOF compound detected in previous CF_4 +O_2 plasma-etching can be avoided by these two-step etching techniques. However, each surface contains a considerable amount of fluorine. Under reactive ion beam etching conditions, with current density of 0.1 mA/cm^2, ion energy 1000 eV, a gas mixture of 80% CF_4 and 20% O_2, and etching time of 3 min, about 60-A depth of surface fluorination was observed [19]. In this case, the depth of surface fluorination will be less than 60 A because the physical ion energy of RIE is less than above 1000 eV. The high-resolution C 1s spectra indicates the presence of a complex mixture of fluorocarbon. A thin surface fluorination layer can be removed by either annealing or inert ion bombardment, as explained previously. Al and Mo contaminants from the chamber wall or previous uses are observed except with CHF_3 + Ar RIE.

3 3.3.6 Conclusions

Adhesion measurements were performed on Cu or Ti on SPI at the various surface-modification conditions. For SPI, removal of SiOF compound by HF treatment is necessary to have good peel strength. The measured peel strength represents the cohesive strength of modified polymer and bulk polymer and it only gives the lower bound of metal/polymer interface peel strength. In addition, the measured peel strength also includes the plastic deformation of metal stripe and substrate. Therefore, the adhesion strength between metal/polymer is far less that the measured peel strength.

Cu diffusion into SPI at 200 °C annealing is significant. The probable reasons are residual solvent in cured polymer, intrinsic free volume of polymer, or polymer softening by over Tg annealing.

A two-step etching process to avoid the formation of SiOF compound is promising. SiOF compound formation is removed as a result of nonoxygen-containing plasma-etching, such as CF_4 + H_2, CHF_3 + Ar, and CF_4.

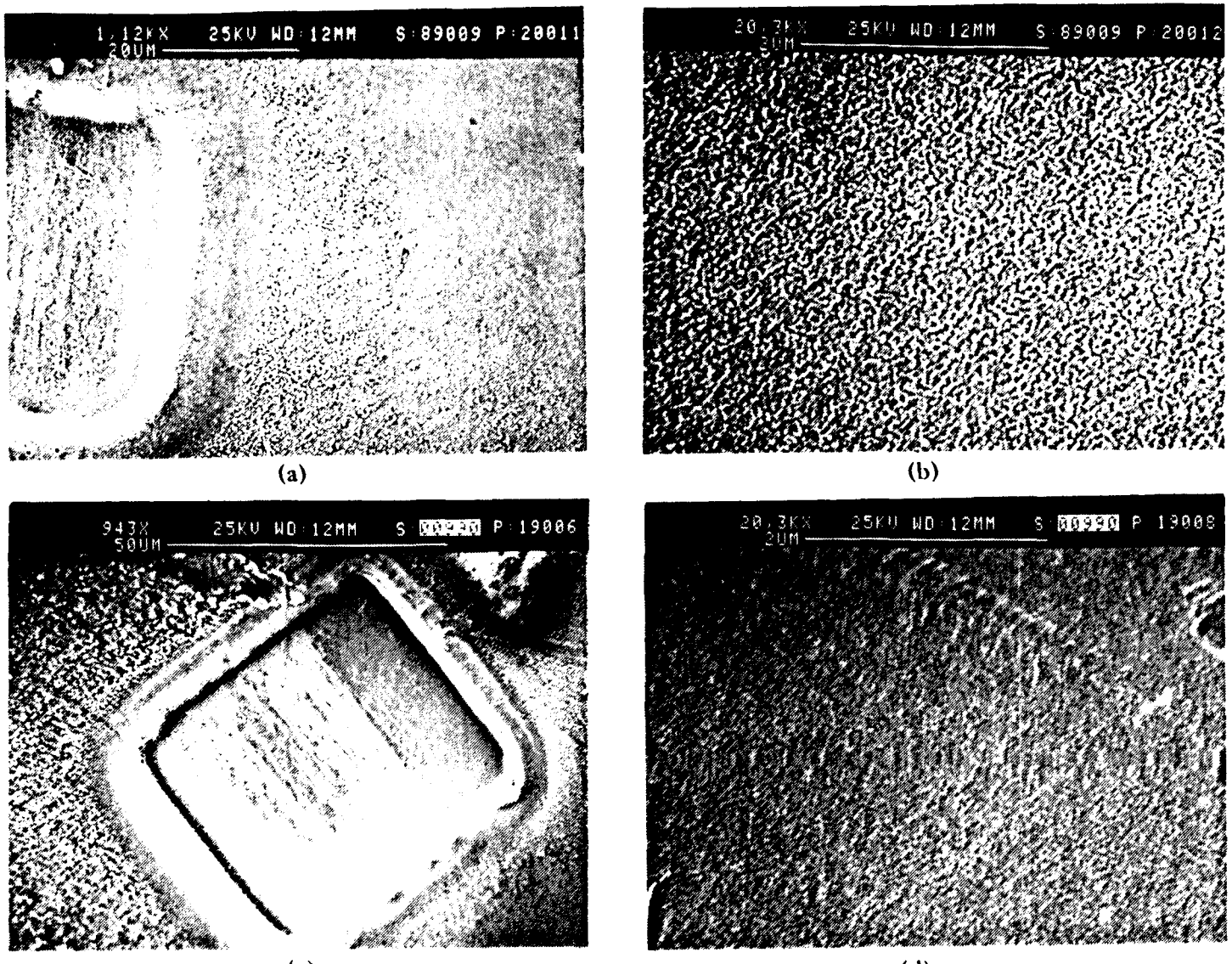

(a) (b)

(c) (d)

Figure 3.3-3. SEM photos of single step etched SPI film (a)(b) CF_4+15%H2 RIE, (c)(d) 25%CHF_3+Ar RIE;

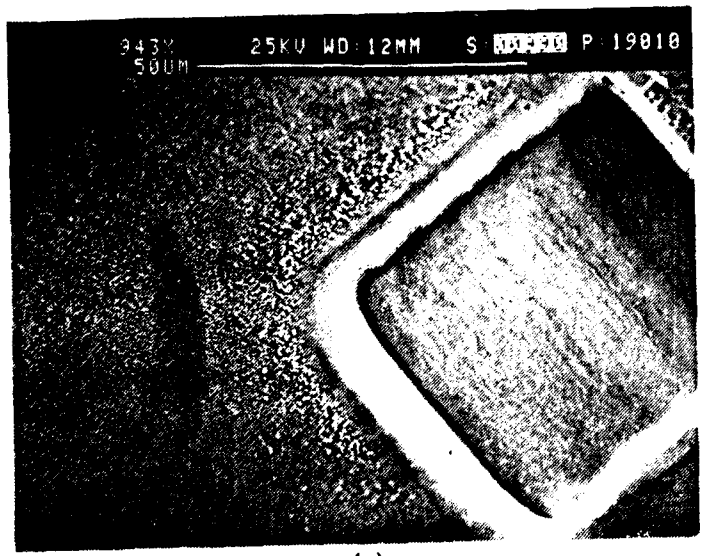

(e)

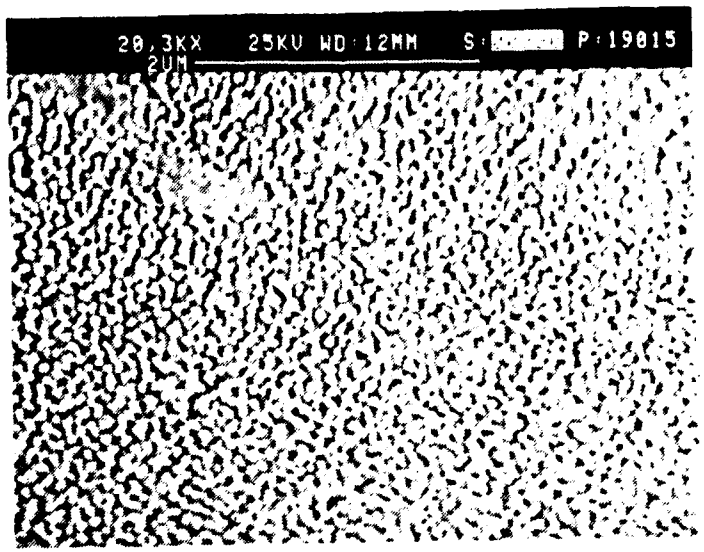

(f)

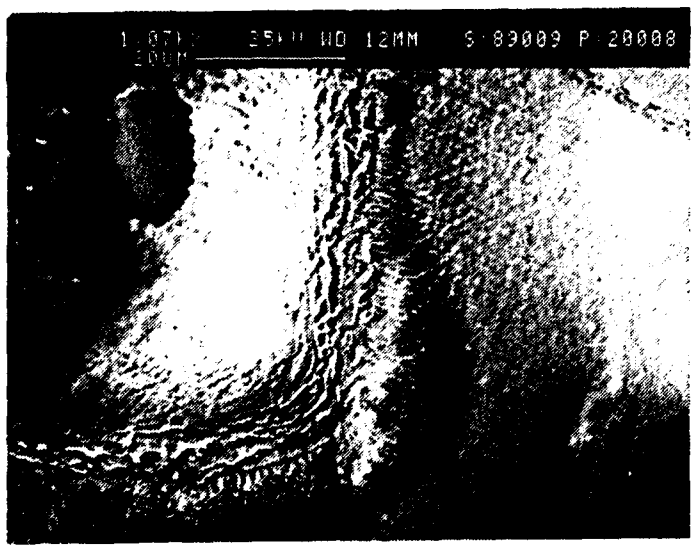

(g)

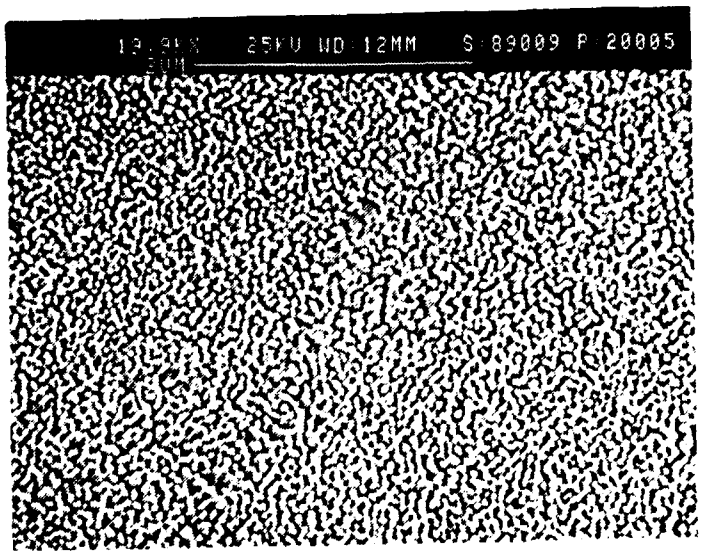

(h)

Figure 3.3-3 (continued): SEM photos of single step etched SPI film (e)(f) CF_4 RIE. SEM photos of double step etched SPI film O2+20%CF_4 plasma-ashing followed by (g)(h) CF_4+15%H2 RI;

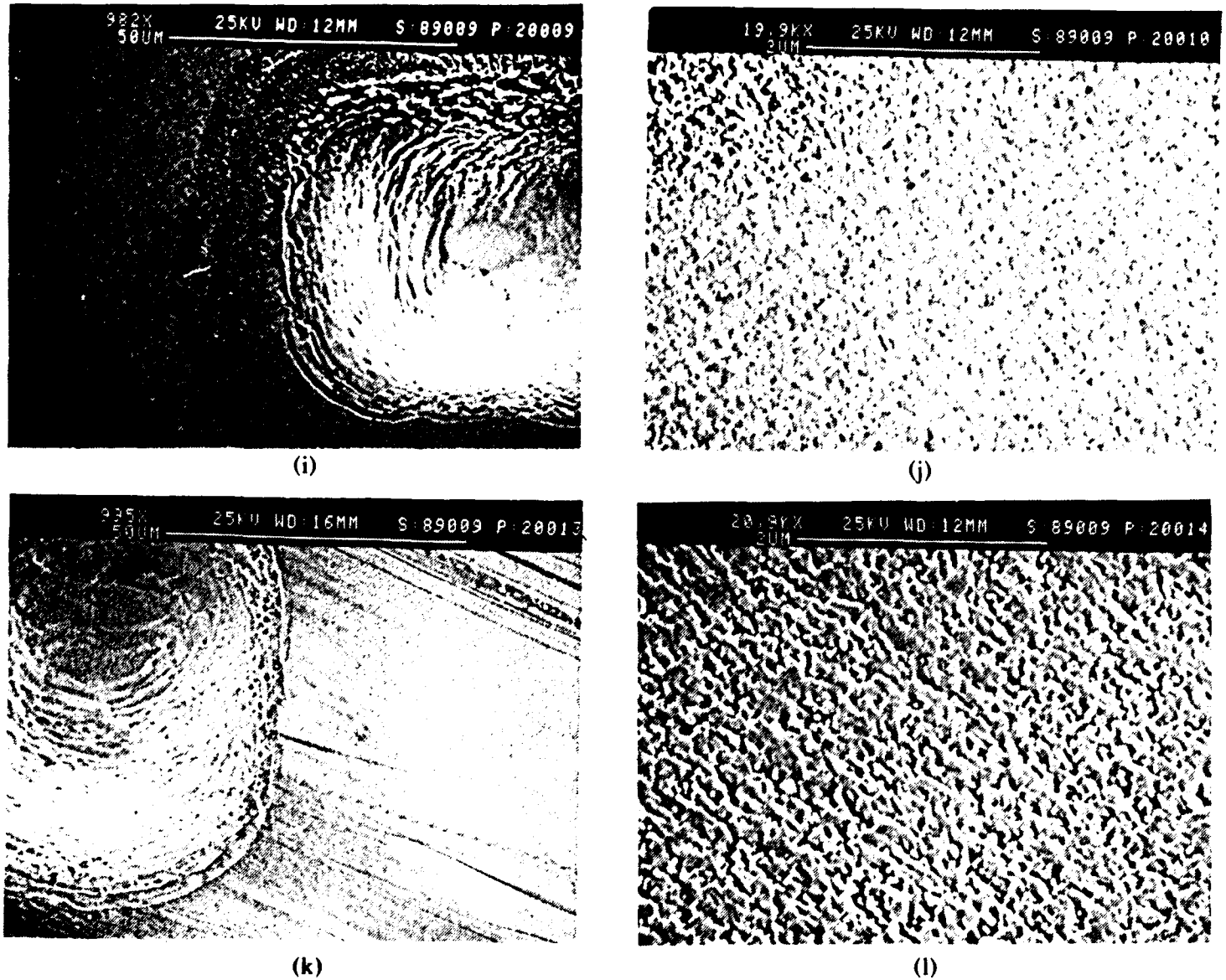

Figure 3.3-3 (continued): SEM photos of single step etched SPI film (i)(j) 25% CHF_3+Ar RIE, and (k)(l) CH_4 RIE.

Table 3.3-4

Surface Composition of One and Two Step Etched SPI Film

Etchant	C	O	N	Si	F	Other	Etch Rate (A/s)
Single-step etching							
CF_4/H_2	42.2	9.7	2.9	1.4	36.2	Al 7.6	3.6
CHF_3/Ar	56.7	6.6	1.1	0.6	35.1	—	2
CF_4	37.5	11.3	4.1	1.4	36.9	Al 8.8 Mo 0.7	6
Double-step etching							
CF_4/O_2 Plasma CF_4/H_2	42.3	9.5	3.3	1.4	36.6	Al 6.9	5.3
CF_4/O_2 Plasma CHF_3/Ar	57.2	9.3	1.3	1.4	30.8	—	4.3
CF_4/O_2 Plasma CF4	38.3	10.4	3.6	0.8	37.9	Al 8.8 Mo 0.3	9.1
SPI	70	15	3	12			
SPI/CF_4/O_2	6	44	0.5	31	18		

REFERENCES

[1] N.J. Chou and C.H. Tang, J. Vac. Sci. Technol., A2(2), 1984, 751-755

[2] P.S. Ho, P.O. Hahn, J.W. Bartha, G.W. Rubloff, F.K. LeGoues, and B.D. Silverman, J. Vac. Sci. Technol., A3(3), 1985, 739-744

[3] R.M. Tromp, F. Legoues, and P.S. Ho, J. Vac. Sci. Technol., A3(3), 1985, 78 785

[4] P.N. Sanda, J.W. Bartha, J.G. Clabes, J.L. Jordan, C. Feger, B.D. Silverman P.S. Ho, J. Vac. Sci. Technol., A4(3), 1986, 1035-1038

[5] Paul S. Ho, Presentation at Cornell University, 1987

[6] F.K. Legoues, B.D. Silverman, and P.S. Ho, J. Vac. Sci. Technol., A6(4), 19 2200-2204

[7] K.W. Paik and A.L. Ruoff, Ph.D. Thesis, Cornell University, 1989

[8] N.J. Chou, D.W. Dong, J. Kim, and A.C. Liu, J. Electrochem. Soc., 131, 1984 2335-2340

[9] J.L. Jordan, P.N. Sanda, J.F. Morar, C.A. Kovac, F.J. Himpsel, and R.A. Pol J. Vac. Sci. Technol., A4(3), 1986, 1046-1048

[10] J.G. Clabes, M.J. Goldberg, A. Viehbeck, and C.A. Kovac, J. Vac. Sci. Tech A6(3), 1988, 985-990

[11] M.J. Goldberg, J.G. Clabes, and C.A. Kovac, J. Vac. Sci. Technol., A6(3), 991-996

[12] P. Bodo and J.-E. Sundgren, J. Vac. Sci. Technol., A2(4), 1984, 1498-1502

[13] F.S. Ohuchi and S.C. Freilich, J. Vac. Sci. Technol., A4(3), 1986, 1039-10

[14] F.S. Ohuchi and S.C. Freilich, J. Vac. Sci. Technol., A6(3), 1988, 1004-10

[15] P. Bodo and J.-E. Sundgren, J. Vac. Sci. Technol., A6(4), 1988, 2396-2401

[16] A.J. Kinloch, J. Materials Science, 15, 1980, 2141-2166

[17] K.L. Mittal. Ed. Adhesion measurement of thin films, thick films, and bulk coatings, American Society for Testing and Materials, (Philadelphia, 1978)

[18] J. Kim, K.S. Kim, and Y.H. Kim, to published in J. Vac Sci. and Tech.,

[19] W. Vanderlinde, Ph.D. Thesis, Cornell University, 1988 Table content

3.4 Low Dielectric Constant Polymers

3.4.1 Introduction

Polyimides have been the material of choice for current polymer-based multichip module packaging approaches. These materials can be applied by solution coating or lamination processes, and when cured, give desirable properties such as relatively low dielectric constant and adhesion to metals used for interconnect. Because of the relative ease of application, multiple layers of polyimide and metal can be built up to produce the high density interconnect structure required. The electrical characteristics of polymers used in the current GE-HDI process and other commercial processes are more than adequate for devices operating at clock rates of up to several hundred megahertz. For high speed signal processing in the gigahertz regime, the dielectric constant and dissipation factor begin to limit performance, and the development of polymers with lower dielectric constant is thus required. Key requirements include

- low dielectric constant
- low dissipation factor
- low TCE (or TCE match to packaging components)
- metal/polymer adhesion
- laser processibility

Depending on the particular molecular structure, polyimides have dielectric constants in the range of 3.0 to 3.5. Because of the inherent polar nature of the molecule, however, the polymer is also hygroscopic, resulting in undesirable variations in dielectric constant with changing humidity. Other commercially available polyimides incorporate fluorinated molecules or siloxane groups in the molecular chain and thus have lower dielectric constants and less susceptibility to moisture. Polymers more aliphatic in nature, such as Teflon, have dielectric constants as low as 2.0. The ability to use polymers of this type as dielectric layers in high density interconnect structures would, theoretically, significantly improve performance.

An example of the performance impact of low dielectric constant polymers is shown in Figure 3.4-1 where the copper interconnect width needed for 50-Ω impedence is plotted as a function of dielectric thickness for two different dielectric constants. For equivalent dielectric thicknessses, the Cu interconnect linewidth with low dielectric constant can be 50 % wider thus improving signal quality by reducing noise. Furthermore, the skin effect in Cu starts to become an issue at GHz frequencies and wider lines will reduce this considerably. In addition, lower dielectric constant layers reduce crosstalk between signal lines and result in increased signal propagation velocity which is inversely proportional to the square root of the dielectric constant. For high speed, high density interconnects at gigahertz frequencies, a lower dielectric constant thus becomes a key prerequisite for improved device performance.

New low dielectric constant polymers are currently under development by various universities and commercial suppliers. In Table 3.4-1, a list of nonpolyimide, low dielectric constant polymers is shown. These materials are candidates for use in high frequency MCM structures and have been evaluated in various degrees under this program.

An alternative to low dielectric constant polymers is to provide composite structures or foams that use low dielectric constant ingredients to provide an overall lower dielectric constant film than is currently available with polyimides. This approach was also investigated and novel concepts were demonstrated. The results of these studies are also discussed in this section.

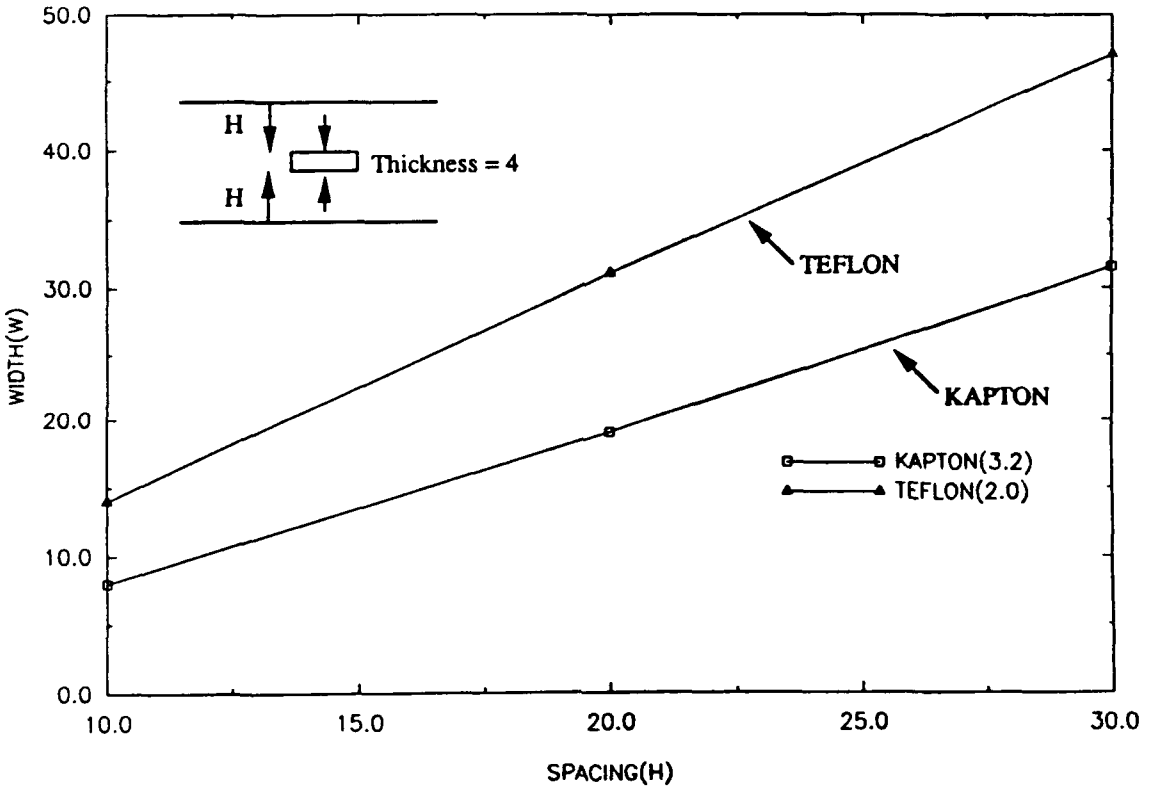

Figure 3.4-1. Width/spacing trade-offs for 50 ohm impedence.

Table 3.4-1

Candidate Dielectric Materials for High Frequency Interconnects

Polymer	Date	Source	Dielectric Conatant	Dissipation Factor	Remarks
BCB	Non-polar aromatic	DOW	2.6 (1MHz)	0.0004 (1KHz)	- metal/polymer adhesion issues - 250 °C bake req/d
parylene N	p-xylyne	Paratronix	2.65	0.0002	- applied by CVD - conformal
Polyquinoline	Rigid-rod polymer	Maxdem	2.5 (12 GHz)	0.0009 (12 GHz)	- experimental laminating film - potential Kapton replacement
Teflon	Fluorinated ethylene-propylene (FEP) Perfluoroalkoxy (PFA)	DuPont	2.1	0.0002	- available in film - insoluble
Teflon AF	Amorphous fluoropolymer	DuPont	1.9	0.0002	- soluble form of Teflon

3.4.2 Benzocyclobutene (BCB)

3.4.2.1 Introduction

Among various dielectric polymers shown in Table 3.4-1, benzocyclobutene (BCB), a thermosetting polymer, has desirable properties for use as an HDI dielectric [1]. Typical properties include high glass transition temperature (Tg) (>350 °C), low dielectric constant (2.7 at 1 MHz), low dissipation factor (0.0008 at 1 MHz), and low water absorption (0.25% in 24-h water boil) [2]. In addition, polymerization of the BCB functional monomer is a thermal process which does not require catalysts and does not generate volatile byproducts. Since the coating solution is in the form of low molecular weight oligomers, a high solid content can be spin- or spray-coated resulting in a high degree of planarization. Full polymerization/crosslinking does not occur until the dielectric film has been coated. Use of this material as a multilayer dielectric film in high density interconnect packages has recently been reported by DOW-Hughes Aircraft Co [2,3] and DOW-Apple Computer Inc. [4].

A key requirement of any multichip module packaging approach is the issue of metal/polymer interface characteristics such as adhesion, chemical reaction, and diffusion. In the case of polyimide, numerous studies have shown that to achieve good adhesion, one must use a metal primer layer such as Cr or Ti [5,6]. These metals have been shown to form chemical bonds at the polyimide interface resulting in strong bonding of the deposited metal layer. In addition, Cu which is used because of its excellent electrical conductivity, will diffuse in polyimide unless protected by a diffusion barrier such as Cr or Ti. It was found that the diffused Cu increases the dissipation factor and changes the electrical properties of the line structure [7]. Therefore, it seemed of interest to study the interfacial characteristics(adhesion, diffusion, and reaction) of Cu, Cr, and Ti when applied to a BCB surface.

For better metal adhesion on polymers, polymers are usually modified by plasma ions. It has been known that modification of polymer surface by plasma ions changes the surface chemistry and morphology of polymers [8,9]. Dry etching characteristics have been studied to open vias in the BCB film using plasmas containing pure O_2, or mixtures of SF_6/O_2 and CF_4/O_2 [2]. However, surface modification of the BCB film by various plasma ions has not been fully investigated. In addition, another important requirement for polymers used in GE HDI application, laser via drillability, and cleaning procedure, was also investigated.

3.4.2.2 Experimental

The BCB solution XU 13005.02 was spin-coated on Kapton or Si wafers at 3000 rpm for 30 s. The film was baked and cured at 100 °C for 10 min, 220 °C for 15 minutes, and then at 250 °C for 1 h in a nitrogen-purged oven. The amount of residual oxygen in the nitrogen-purged oven was controlled to be in the order of 10 ppm because of film oxidation during curing [6]. Metallization (Cu, Cr, and Ti) was performed using a sputtering technique after Ar gas pre-backsputtering. A typical Ar backsputtering condition was 5 W/in^2, 600 V, for 1 min. Metal-deposited samples were then annealed at 200 to 250 °C in a nitrogen atmosphere or vacuum in order to initiate diffusion and interfacial reactions.

Cross-sectional TEM specimens were prepared by ultramicrotomy. Specimens were embedded in Epon 812, cured overnight at 60 °C, and then cut into thin sections with a diamond knife. The thickness of sections varied from less than 500 A to 2000 A, depending on cutting parameters. Selected areas of the specimens were examined with energy disperse x-ray spectrometry (EDX) and electron diffraction. X-ray photoemission spectrometry (XPS) and Auger electron spectrometry(AES) with in situ Ar sputtering depth profiling was carried out to

investigate the formation of chemical compounds at the metal/BCB interface. The adhesion of metal film on a modified BCB was measured using a peel tester.

The etching of XU 13005.02 BCB films was performed in a Plasmatherm 2406 reactive ion etcher (RIE) and a barrel plasma etcher, using Ar, O_2, O_2+10%CF_4, and O_2+10%SF_6. A Sloan Dektak II profilometer was used to measure etch depths for the calculation of etch rates, and a PSS100 optical emission spectrometer was used to monitor the plasma through a quartz window in the RIE chamber. Surface morphological and compositional changes of the BCB film, after plasma modification were investigated using SEM and XPS, respectively.

Laser via drilling was performed using an Ar laser to investigate the laser drillability of BCB film and subsequent via cleaning methods.

3.4.2.3 Results and Discussion

Cu/CB Interface

Cu on BCB showed poor adhesion. No precipitates were observed after annealing in vacuum at 200 °C for 18 h (see in Figure 3.4-2(a)). However, precipitates were observed at 250 °C for 17 h annealing in nitrogen (see in Figure 3.4-2(b)). The diameter of the precipitates ranged from 20 to 120 A. Diffraction peaks from CuxSiy were observed (Figure 3.4-2(c)). The adhesion of Cu to unmodified or modified BCB was too low to be measured by a peel tester (<1 lb/in). Adhesion was lost at the Cu/BCB interface. Direct Cu metallization of BCB should be avoided because of poor adhesion and diffusion problems.

Cr/CB Interface

A typical cross section of the as-deposited Cr film is shown in Figure 3.4-3(a). The Cr/BCB polymer interface is irregular, with Cr spikes penetrating approximately 300 A into the BCB film. This roughening of the BCB film by Ar backsputtering enhances the adhesion of Cr to BCB by providing mechanical interlocking of the metal to the BCB surface. The lower two thirds of the Cr film from the Cr/BCB interface shows dendritic growth, while the upper third of the film is randomly oriented. In the TEM photo, the BCB film shows no visible structure. Cr was not detected in the BCB film with EDX analysis, and no diffusion of Cr into the BCB film was observed.

Annealing of the Cr/BCB interface at 200 °C for 18 h in vacuum and nitrogen atmosphere resulted in no visible change as can be seen in Figure 3.4-3(b). Cr was not detected in the BCB film with EDX analysis. However, annealing at 250 °C in vacuum and nitrogen atmosphere resulted in significant changes. After 3 h in a nitrogen atmosphere (250 °C), the presence of Cr was detected in the BCB film to a distance of approximately 2 mm from the Cr/BCB interface using EDX analysis. During this time, the presence of Cr precipitates was not detected (Figure 3.4-3(c)).

Further annealing up to 17 h in nitrogen atmosphere showed Cr-precipitates visible throughout the entire thickness of the BCB film (Figure 3.4-3(d)). The precipitates appear to be spherical in shape. Most of them range from 20 A to 80 A in diameter. Analysis of electron diffraction patterns shown in Figure 3.4-3(e), taken in areas with many precipitates as shown in Figure 3.4-3(d), indicate no match with Cr or the various Cr oxides. There was a good match, however, with $CrSi_2$. It is known that the BCB film used in this experiment contains Si, and the nominal composition measured by XPS consists of 9% O, 8% Si, and 83% C. The measured Cr concentration was considerably higher at distances close to the Cr film than at some distance away from the interface. The Cr concentration gradient across the interface indicates that the

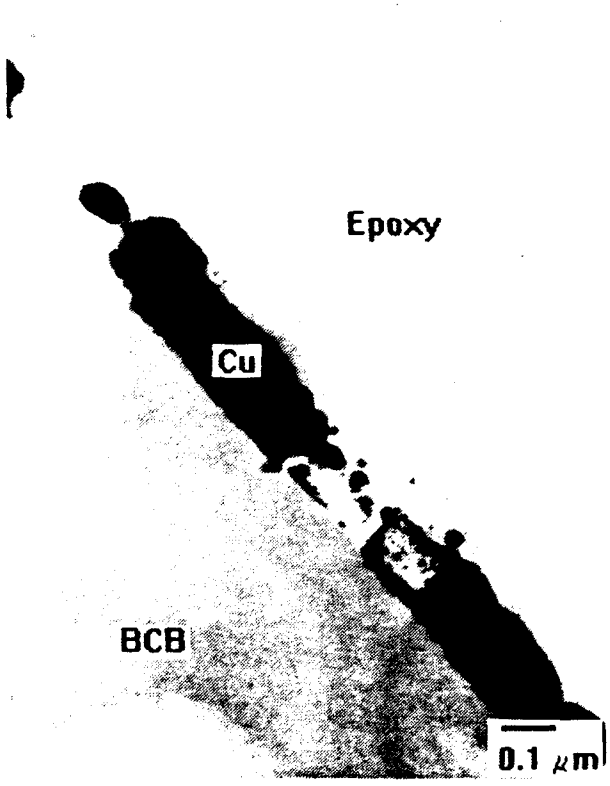

(a)

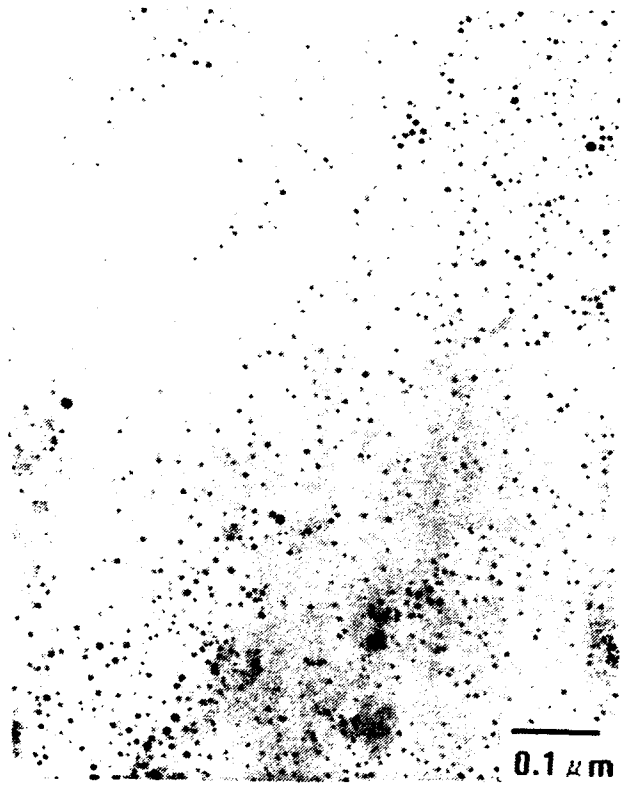

(b)

(c)

Figure 3.4-2. Cross-section TEM of Cu/BCB interface (a) annealed at 200 °C for 18-hrs in vacuum, (b) Cu-Si precipitates in the BCB film annealed at 250 °C for 17 hrs in N_2 gas, and (c) electron diffraction pattern from Cu-Si precipitates shown in Figure 3.4-2(b).

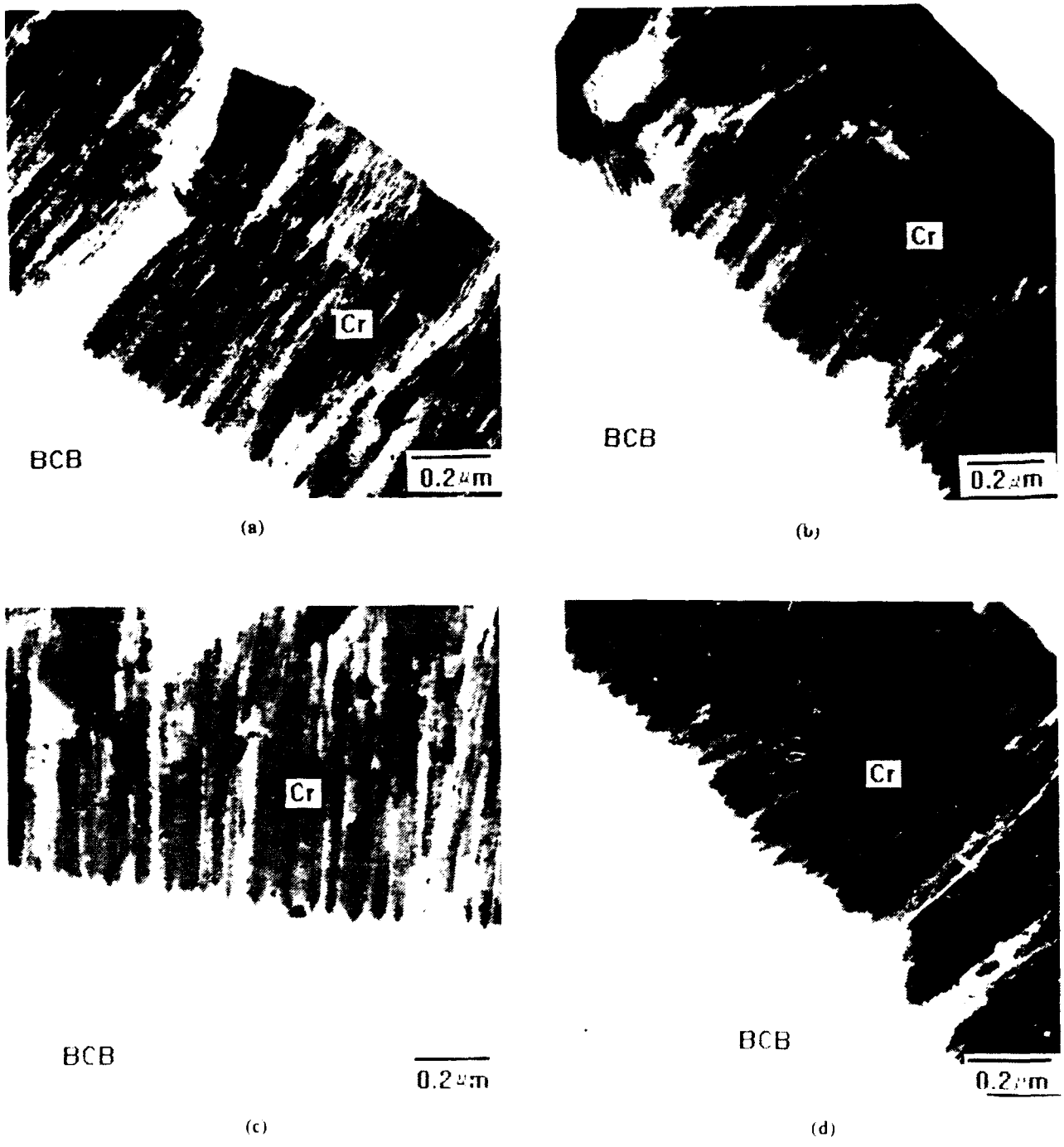

Figure 3.4-3. Cross-section TEM of Cr/BCB interface (a) as-deposited Cr film on BCB, (b) annealed Cr film on BCB polymer at 200 °C for 18 hrs., (c) annealed in nitrogen atmosphere at 250 °C for 3 hrs. and (d) annealed in nitrogen atmosphere at 250 °C for 17 hrs.

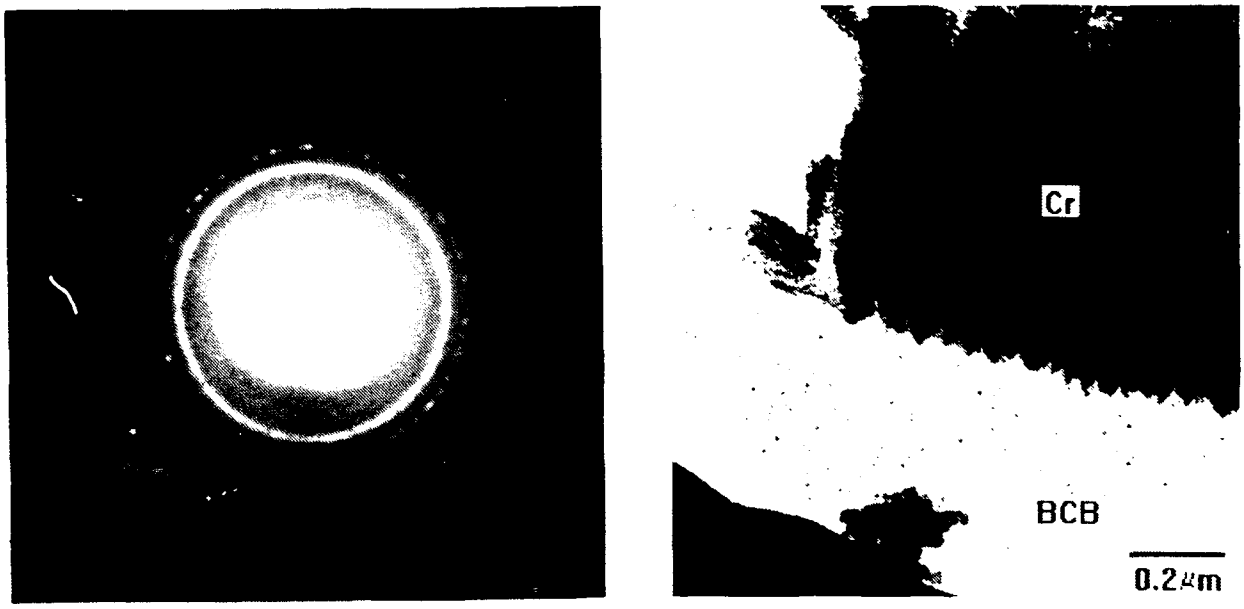

(e) (f)

Figure 3.4-3. Cross-section TEM of Cr/BCB interface (e) electron diffraction pattern of precipitates in Figure 3.4-3(d), and (f) annealed in vacuum at 250 °C for 17 hrs.

reaction at the Cr/BCB interface is determined by Cr diffusion into the BCB film. A sample annealed at 250 °C for 17 h in vacuum in Figure 3.4-3(f) contained small $CrSi_2$ precipitates similar to those observed in the previous sample annealed in nitrogen (Figure 3.4-3(d)).

Figure 3.4-4 shows the Auger depth profile of the asdeposited Cr/BCB film. The thickness of Cr was measured to be about 8500 A using Ar depth profiling. Near the Cr/BCBinterface, substantial increase of oxygen content was observed, suggesting the presence of Cr-oxide. A study on the mechanism for oxide formation at the interface is necessary.

The measured peel strength of the Cr/BCB interface was about 1 lb/in. And the cohesive failure occurred at the BCB film presumably caused by the brittleness of BCB film. The 1 lb/in. peel number therefore,only represents the lower bound of the Cr/BCB adhesion.

As a result, because Cr diffuses into the BCB film resulting in the formation of $CrSi_2$ precipitates and poor adhesion to the BCB film is observed, Cr cannot be deposited directly on the BCB film.

Ti/BCB Interface

Figure 3.4-5(a) shows the cross section TEM of an asdeposited Ti/BCB interface. Ti and BCB were identified by EDX analysis. No precipitates were found in the asdeposited BCB film, and a 200 °C anneal did not induce Ti diffusion into BCB.

However, 250 °C annealing for 10 h in vacuum caused precipitates as shown in Figure 3.4-5(b). The precipitates were similar to those seen with the Cr/BCB interface (Figure 3.4-5(c)), but their average size was smaller and there were fewer of them because of the shorter annealing time (10 h). A diffraction pattern of the precipitates could not be obtained because of the smaller size. The precipitates are presumably Ti-Si compounds as in the case of the $CrSi_2$.

Figure 3.4-6 shows the XPS depth profile of the BCB/Ti interface which was prepared after peel testing of the Ti on BCB. Some BCB was attached to the backside of Ti peel stripes. The carbon spectrum (1s), from the organic carbon (binding energy = 284.6 eV), was detected in the BCB film region (see Figure 3.4-6(a)). Further sputtering reveals another carbon peak from Ti carbide (BE = 281.8 eV) at the Ti/BCB interface. The organic carbon peak disappeared with additional sputtering upon entering into the Ti film region.

The formation of Ti carbide (or Ti oxide) was also confirmed by the Ti peak profile shown in Figure 3.4-6(b). In Figure 3.4-6(b), the Y-axis is opposite that of Figure 3.4-6(a). No Ti was detected in the BCB region during initial sputtering, but a Ti peak was observed (at binding energy of 454.6 eV) at the Ti/BCB interface which represents TiC (or TiO). The TiC (or TiO) peak (BE = 454.6 eV) gradually changed to the metal Ti peak of BE = 453.7 eV upon entering the Ti film region.

The Ti adhesion on modified BCB was 0.5 lb/in. after simple Ar backsupttering, and 1.2 lb/in. after the BCB was roughened by an excimer laser followed by plasma etching. The peel strength was very low compared to what would be observed with a polymide-type film. The failure mode of about 1 lb/in. peel strength was a cohesive failure at BCB material because of the brittleness of BCB. The actual Ti/BCB adhesion is therefore higher than 1 lb/in.

As a result, Ti cannot be directly deposited on the BCB because of diffusion and poor adhesion.

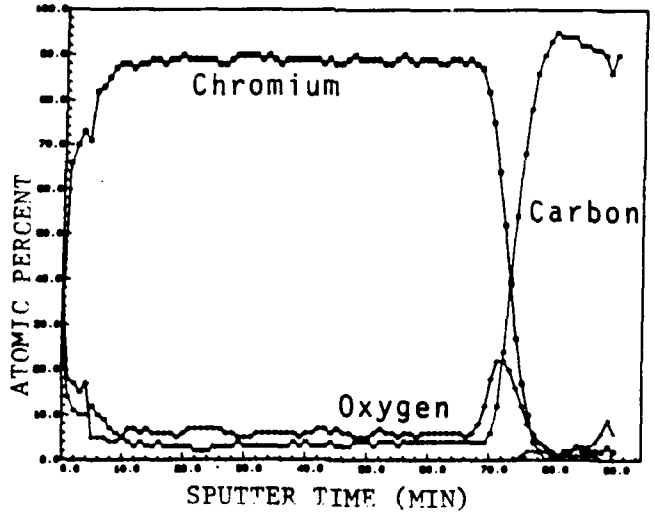

Figure 3.4-4. Auger depth profile of Cr/BCB film.

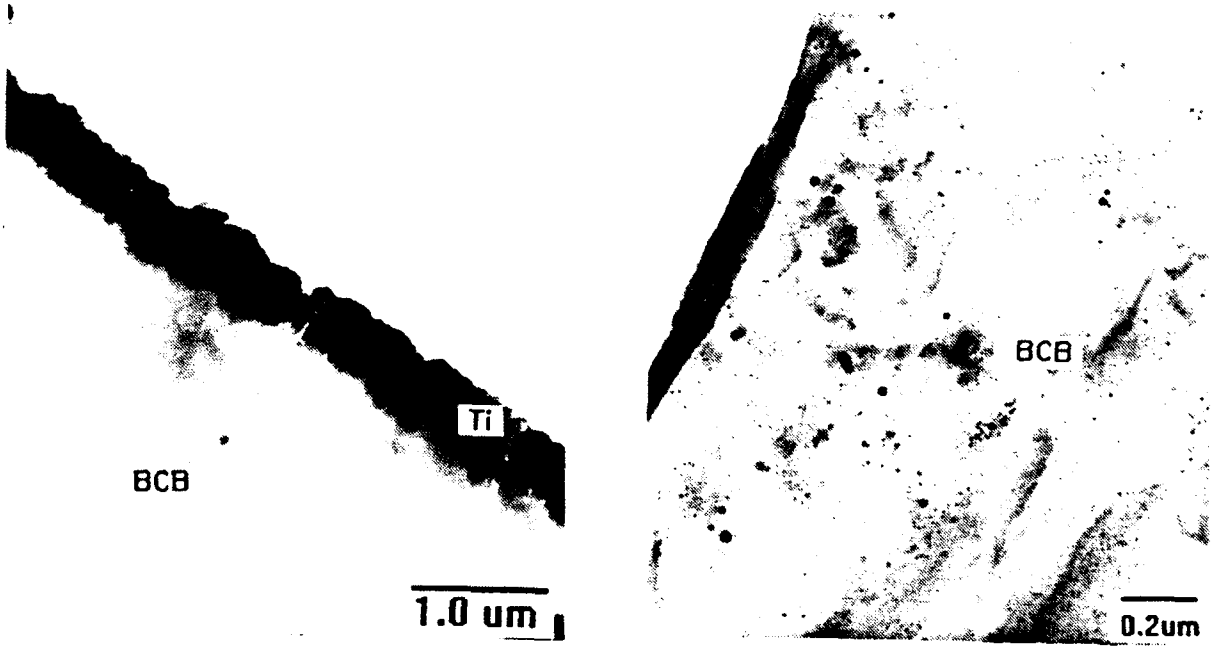

(a) (b)

Figure 3.4-5. (a) As deposited Ti/BCB interface, and (b) Ti/BCB interface annealed in vacuum at 250 °C for 10 hrs.

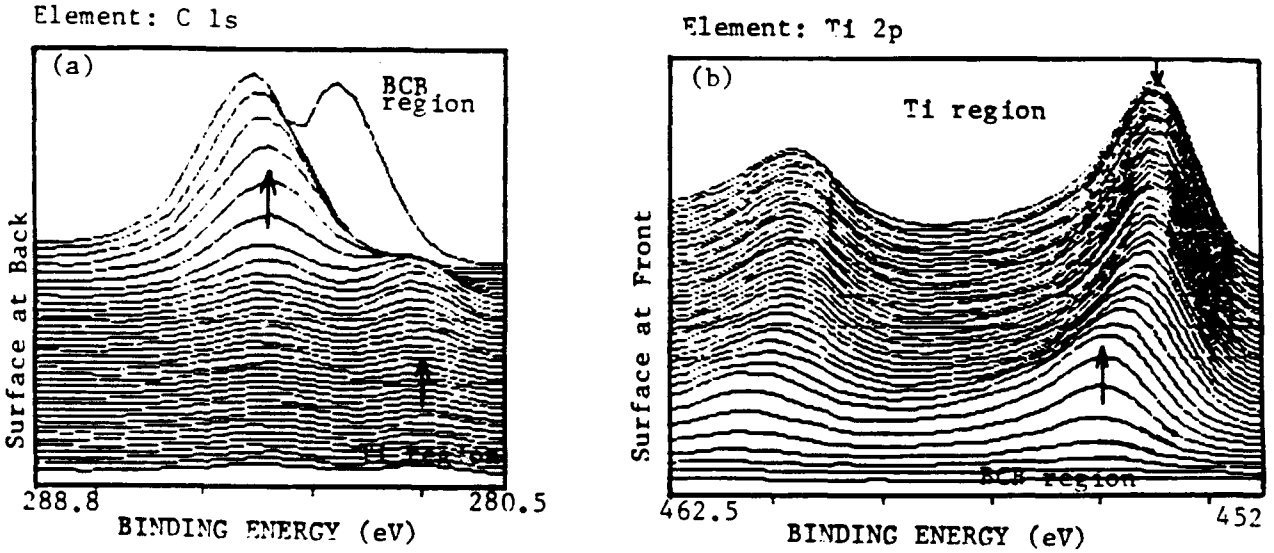

Figure 3.4-6. XPS depth profile of the BCB/Ti interface (a) C is spectrum and (b) Ti 2p spectrum.

3.4.2.4 Etch Rate and Surface Morphologies

Table 3.4-2 shows the etch rates of BCB film, Si, and SiO_2, and the relative intensity of atomic fluorine (704 nm) present for each of the gases used.

It can be seen that the etch rates of BCB are significantly higher when CF_4 or SF_6 is added to oxygen. It is well known that small fluorocarbon additions to oxygen can produce dramatic increases in the etch rate of organic films [10]. In addition, since BCB contains silicon, atomic fluorine present in the plasma can more effectively remove Si and SiO_2, a byproduct formed by exposure to oxygen containing plasma, so that they will not remain on the surface slowing down the organic etch rate. Note that at the etch conditions that were chosen, there was a larger amount ofatomic fluorine present with SF_6 in O_2, than with CF_4 in O_2. Correspondingly, the etch rates of BCB, Si, and SiO_2 are also higher. As will be shown from the results of the XPS analysis, surface SiO_2 was observed on BCB etched with $10\%CF_4/O_2$; however, almost no SiO_2 was observed on BCB etched with $10\%SF_6/O_2$, which may be explained by the relative amount of atomic fluorine present in each of the mixtures.

After RIE, a small surface asperity was observed on the BCB surfaces. Ar gas ion etching caused little changes in surface morphology, but only 500 A of BCB was removed during 5 min of etching. Oxygen RIE induced a rough surface with many small asperities (less than 1000 A size) presumably caused by the formation of surface SiO_2. Furthermore, O_2+CF_4 RIE created a rougher surface with surface impurities which are usually observed for O_2+CF_4 plasma etching [11]. In constrast to O_2 and O_2+CF_4 RIE, O_2+SF_6 RIE produced a smoother surface morphology (about several hundred A size) than O_2 and O_2+CF_4, probably because of faster Si and SiO_2 etch rates, as previously discussed. Table 3.4-3 illustrates the etch rate of BCB in a barrel plasma etcher. Etch rate reached a maximum at about 20% of CF_4. The etch rate also increased with higher power.

3.4.2.5 XPS Compositional Studies

Table 3.4-4 illustrates the binding energies and assignment of each elemental peak observed in XPS analysis on the BCB films modified at the various conditions. Three major peaks were observed: carbon 1s, oxygen 1s, and Si 2p, and some impurities (fluorine and metal atoms (Cu and Ti)).

The as-coated BCB film contains about 82% carbon, 9% oxygen, and 8% silicon by XPS analysis. The high resolution carbon region exhibits two types of carbon as shown in Figure 3.4-7(a). The major carbon peak is located at 284.6 eV, corresponding to C-C, C-H, and C-Si bonds. A second peak is located at 286.1 eV, which possibly corresponds to the C-O bond on the surface. Oxygen peaks at 532.1 eV, corresponding to the carbo-siloxane linkages (Si-O-Si), and at 533.6 eV, assigned to C-O are also observed (Figure 3.4-7(b)). The single Si 2p peak in Figure 3.4-7(c) at 101.4 eV corresponds to the carbo-siloxane linkage (C-Si-O-Si-C).

After oxygen ion etching, the surface composition of the BCB film changed. The percentage of carbon was significantly reduced from 82% to 21.6%, while that of oxygen and silicon increased. A new carbon peak at 288.6 eV, corresponding to C = O, was added to the previous C-Si, C-C, and C-O peaks as is shown in Figure 3.4-8(a). The presence of extra oxygen functionality after oxygen plasma etching is typically observed by polymers such as polyimide [12]. In addition, a significant change occurred to the Si 2p peak located at 103 eV, corresponding to the formation of SiO_2 from the initial carbo-siloxane C-Si-O peak at 101.4 eV (Figure 3.4-8(b)). The formation of SiO_2 was also proved by the O 1s peak at 532.4 eV, which also corresponds to SiO_2 (Figure 3.4-8(c)).

Table 3.4-2

Etch Rates of the BCB, Si, and SiO2 in RIE treatments (conditions: 40 scam, 250 mTorr, 0.47. W/cm2, 5 mins.)

Gas	Etch Rate (A/min) BCB	Si	SiO_2	Relative Intensity of Atomic F (704 nm)
Ar	100	3	2	0
O2	240	2	2	0
10% CF_4/O_2	1060	8	24	7.6
10% SF_6/O_2	1620	40	116	14.2

Table 3.4-3

Etch Rate of BCB Film by a Barrel Plasma Etcher

Gases	Pressure (Torr)	Power (W)	Etch rate (A/min)
O_2 + 10% CF_4	0.7	150	1290
O_2 + 20% CF_4	0.7	150	1900
	0.7	300	2020
O_2 + 32% CF_4	0.7	150	950
O_2 + 10% SF_6	2	150	1400
	2	300	2050

Table 3.4-4

XPS Analysis on BCB Film Modified by Various Plasmas
(Surface Composition (atomic %))

Samples	C 1s	O 1s	Si 2p	Other
Control	82%	9%	8%	
BCB	284.6 (91%*)	532.1 (77*)	101.4	
(B.E.eV)	286.1 (9%)	533.6 (23)		
O_2	21.6%	52.3%	24.3%	
ion	284.6 (63)	532.4	103.0	
etched	286.1 (25)			
	288.6 (11)			
$O_2 + CF_4$	14.8%	55.1%	28.4%	F: 1.2%
ion	284.5 (77)	532.4	103.0	N: 0.5%
etched	286.1 (23)			
$O_2 + CF_4$	66.8%	20.4%	1.3%	F: 1.8%
ion	284.6 (74)	530.7 (16)	101.7	Cu: 1..7%
etched	286.0 (14)	532.1 (71)		Ti: 0.8%
/Ar ion	287.3 (5.5)	533.4 (13)		Cl: 0.6%
sputter	288.7 (6.5)			
$O_2 + SF_6$	58.3%	23.9%	2.4%	F: 9.1%
ion	284.6 (61)	532.1 (70)	101.3	Al: 1.4%
etched	286.1 (16)	533.6 (30)		N: 2.9%
	286.6 (16)			
	290.0 (7)			
$O_2 + SF_6$	62.7%	24.9%	4.0%	Cu: 4.7%
ion	284.6 (65)	530.3 (4)	101.8	S: 0.9%
etched	285.9 (16)	531.9 (84)		
/Ar ion	287.2 (6)	533.5 (12)		
sputter	288.6 (13)			
Ar ion	27.5%	34.8%	10.8%	F: 14.7%
sputter	284.6 (84)	530.5 (18)	102.4	Al: 9.2%
	286.1 (7)	531.9 (66)		N: 2.8%
	287.7 (10)	533.1 (16)		

*: The numbers in parenthesis represent the area % of the peak

C 1s	O 1s	Si 2p
284.6 (C-C(H), C+C, Si-C)	530.3 (metal oxide)	99.4 (Si)
286.0 (C-O)	532.0 (C-Si-O)	101.4 (C-Si-O)
287.3 (C=O)	532.4 (siO_2)	101.8-102.2 (O-Si-O)
288.6 (O-C=O)	533.5 (O-C)	103.0 (SiO_2)

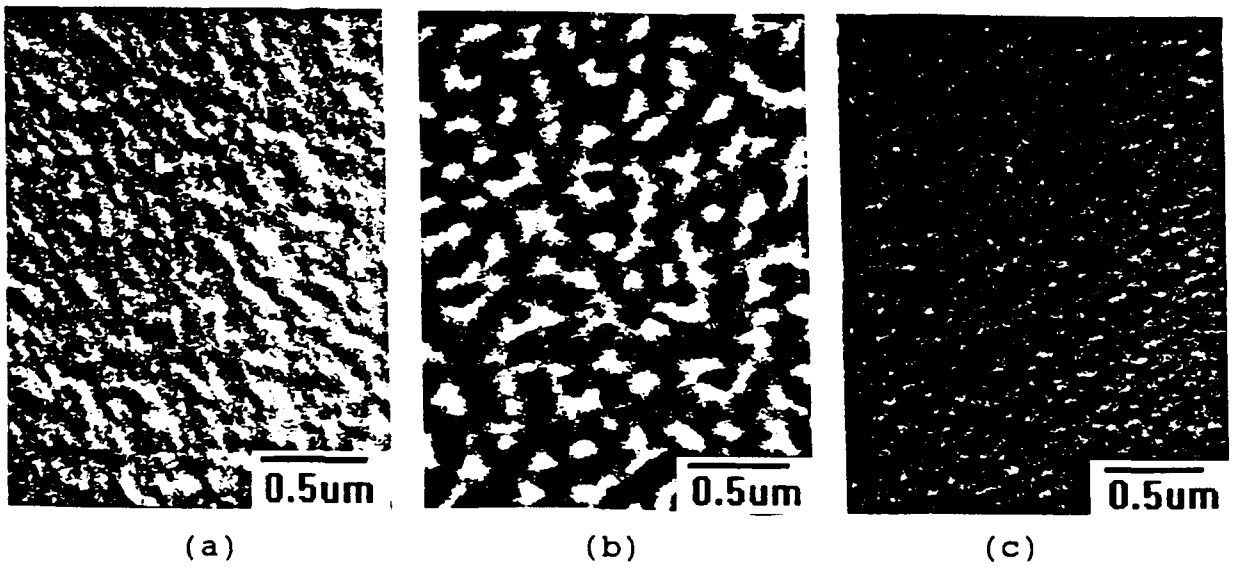

Figure 3.4-7. Surface morphology of the BCB film modified by RIE (a) O_2, (b) O_2 + 10 % CF_4, and (c) O_2 + 10 % SF_6 (conditions: 40 sccm, 250 m Torr, 0.47 W/cm^2, 5 min.).

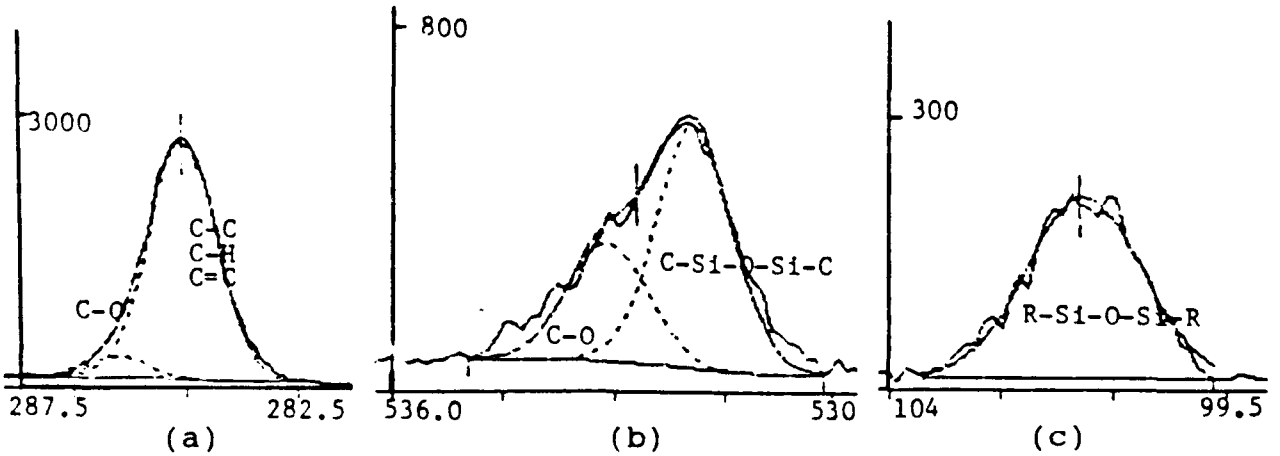

Figure 3.4-8. XPS elemental peaks of as-coated BCB film (a) C 1s, (b) O 1s, and (c) Si 2p.

The surface characteristics of the BCB film after O_2+10%CF_4 plasma etching are similar to those obtained using oxygen. The amount of C was reduced to an even lower value of 14.8% because the etch rate of BCB is faster with O_2+CF_4 than with pure oxygen. The formation of SiO_2 was also detected by the presence of the Si 2p peak at 103 eV, and O 1s peak at 532.4 eV. Fluorine was incorporated as a result of adding 10% CF_4 to oxygen.

The percentage of carbon was restored from 15% to 67% after Ar ion sputtering on O_2+10% CF_4 plasma-etched BCB. In addition, the carbo-siloxane Si peak at 101.7 eV was observed, and C-Si-O bonding was also proved by the presence of an oxygen peak at 532.1 eV. The Ar ion sputtering, which can be part of an in situ pre-metal sputter clean and metal deposition cycle, restores the chemical composition of the BCB surface that was etched using O_2+CF_4, to a state which is similar to the original unetched surface. In addition, impurities from exposure to O_2+CF_4 were also cleaned, but some metal impurities from the sputtering chamber were added.

O_2+SF_6 ion etching on the BCB film decreases the percentage of carbon and silicon, but increases oxygen. The majority of carbon peaks were from C-C, C-H, and C-Si bonds at 284.6 eV, C-O at 286.2 eV, and C = O at 288.6 eV. The oxygen increase was attributed to C-Si-O (532.1 eV) and O-C (533.2 eV). In addition, most Si peaks were from the carbo-siloxane peak (C-Si-O, at 101.3 eV). A significant amount of fluorine, about 9%, was incorporated. The etching behavior using O_2+SF_6 is somewhat different from that using O_2+CF_4. The O_2+CF_4 plasma oxidized the carbo-siloxane Si into SiO_2, while the O_2+SF_6 plasma did not. The observation of less Si is due to a faster etch rate of Si and SiO_2, which may be formed during the O_2+SF_6 etch. An Ar ion sputter etch after O_2+SF_6 plasma etching restored the BCB surface close to its original chemical composition, similar to the case described above with O_2+CF_4.

Ar ion sputtering reduced the amount of carbon on the BCB surface; however, it increased the amount of oxygen and silicon slightly. The decrease of carbon after Ar ion sputtering is opposite the usual observations for most polymers. Usually inert gas ion bombardment concentrates the amount of surface carbon [13]. However, for the BCB case, Si had a lower sputter rate than carbon and oxygen, and it was left on the surface during Ar sputtering. Most of the carbon peaks were from C-C, C-H, and C-Si bonds at 284.6 eV. Some C-O and C = O were also observed. However, Si binding energy was slightly shifted to higher energy resulting in 102.4 eV, which may correspond to the O-Si-O bond. Also, the oxygen binding energy of O-Si-O appeared to be shifted to lower energy at 531.9 eV.

3.4.2.6 Laser via Drilling

Vias were drilled through the BCB film coated on Si and Ti/Cu/Ti coated substrates using the standard laser drilling conditions. The BCB film was easily drilled, leaving residues around the vias as shown in Figure 3.4-9(a). Redeposition of the ablated BCB film around the via and flake type residues at the side walls of the via was observed. The O_2+10% SF_6 plasma etching cleaned the via reasonably as shown in Figure 3.4-9(b). However, the laser ablation combined with O_2+SF_6 plasma etching cleaned the via more efficiently (as shown in Figure 3.4-9(c)) than the plasma etching only.

3.4.2.7 Summary

Metal films of Cu, Cr, and Ti were deposited on BCB to evaluate their interfacial characteristics. Argon backsputtering treatment on BCB causes a rough surface morphology on BCB resulting in spike-like metal structures at the metal/BCB interface. The formation of Ti carbide and Cr oxide was observed at the metal/BCB interface using XPS and Auger depth profiling analysis, respectively. The reaction of Cu, Cr, and Ti with BCB at the interface appears

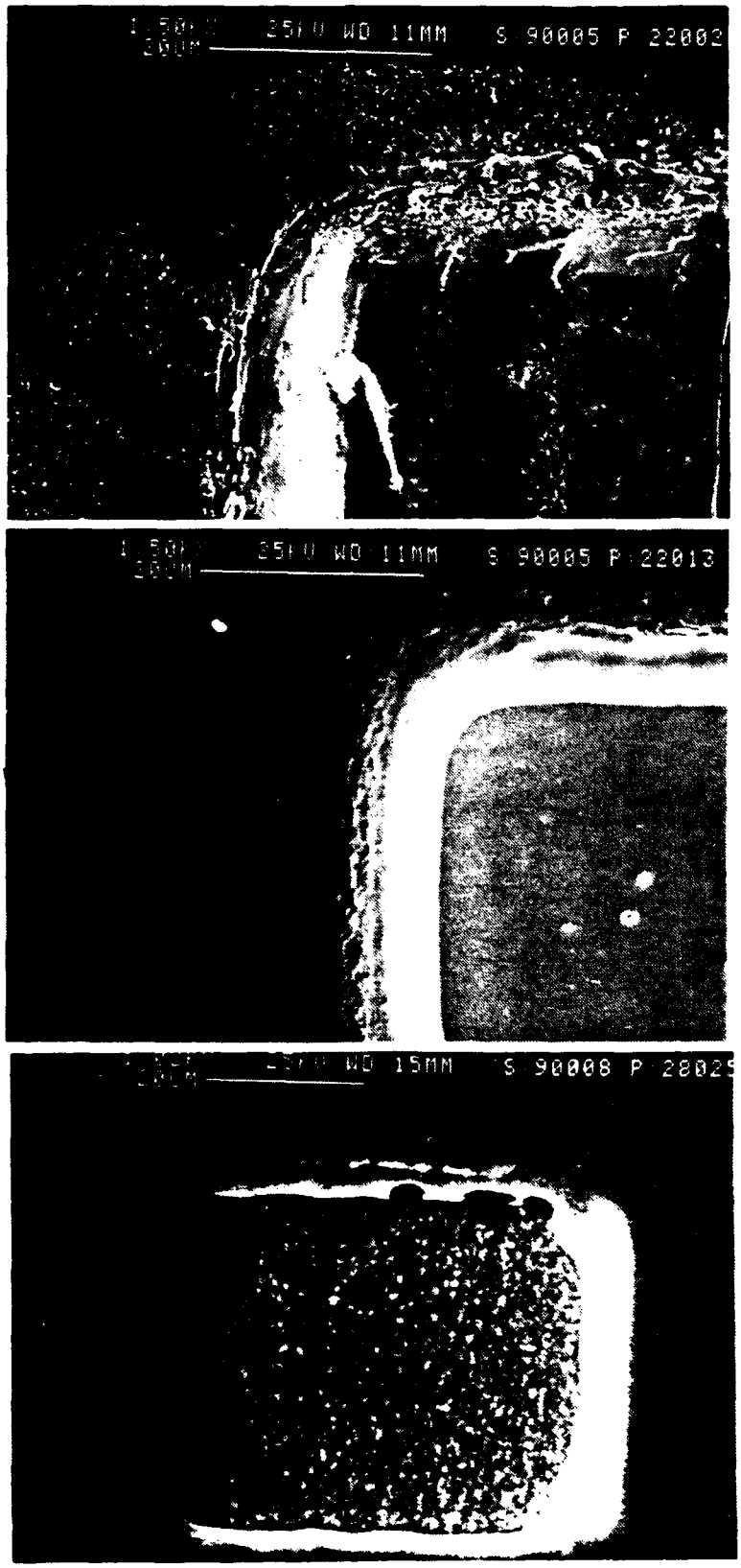

Figure 3.4-9. (a) As-drilled via, (b) O_2 + 10 % SF_6 plasma etched via (280 m Torr, 60W, and 5 mins.), and (c) excimer laser ablation followed by O_2 + SF_6 plasma etching.

to be threshold-dependent as well as temperature-dependent. At temperatures below 250 °C, little or no reaction was observed. On long-term annealing at 250 °C, Cu-Si, Cr-Si, and Ti-Si precipitates were observed. Cu, Cr, and Ti cannot be used directly on BCB film because of metal diffusion and poor adhesion. The etch rate of silicon containing BCB film was found to be faster when 10%CF_4 and 10%SF_6 were added to oxygen in a RIE and in a plasma etcher. Silicone was oxidized in a pure O_2 and O_2+CF_4 plasma, slowing down the etch rate. The surface compositional change of the carbo-siloxane linkage (C-Si-O) of the BCB film to SiO_2 was proved by the observation of an oxygen 1s peak at 532.4 eV (SiO_2) and a silicon 2p peak at 103 eV (SiO_2) during O_2 and O_2+CF_4 plasma etching. In contrast to the O_2+CF_4 plasma, the O_2+SF_6 plasma produced smoother surface morphology because of faster Si and SiO_2 etch rates. Laser via drilling through the BCB film and cleaning of via by the laser ablation and O_2+10% SF_6 plasma etching were demonstrated.

REFERENCES

[1] S.F. Hahn, P.H. Townsend, D.C. Burdeaux, and J.A. Gilpin, "The Fabrication and Properties of Thermoset Films Derived from Bisbenzocyclobutene for Multilayer Applications," Technical Report from Dow Chemical Co., 1988.

[2] P.H. Townsend, D.C. Burdeaux, S.F. Hahn, M. Thomsen, R. McGee, J.N. Carr, R.W. Johnson, and K. Weidner, "Multilayer interconnection structures using second generation polymers derived from Bisbenzocyclobutane," ISHM '89 Proceedings, Baltimore, MD, p. 447, 1989.

[3] S.O. Fong, F.Z. Keister and J.W. Peters, "Polybenzocyclobutene resins in multilayer thin films for electronic packaging," 22nd International SAMPE Technical conference November 6-8, 1990, p. 602.

[4] J.N. Carr, D.C. Burdeaux, P.H. Townsend, T.A. Manial, T. Tsao, T. Ritter, and R. Lester, "Migration from printed wiring board to multichip module technology," IEPS Multichip Modules Vol. 2, p. 103, 1990.

[5] J. Kim, S.P. Kowalczyk, Y.H. Kim, N.J. Chou and T.S. Oh, "Adhesion, reaction and stability of metal/polyimide interfaces," Mat. Res. Soc. Symp. Proc. Vol. 167, p. 137, 1990.

[6] F.S. Ohuchi and S.C. Freilich, "Ti as a diffusion barrier between Cu and polyimide," J. Vac. Sci. Technol., A 6(3), p. 1004, 1988.

[7] L.-T Hwang, D. Nayak, G.M. Adema, G.A. Rinne, and I. Turlik, "Measurement of high-speed signal propagation characteristics in thin-film interconnections," IEPS proceeding, p. 272, 1990.

[8] M. Braun, B. Emmoth, G.M. Mladenov, and H.E. Satherblom, "Erosion of polymer thin-films during ion bombardment," J.Vac. Sci. Technol., A1(3), p. 1383, 1983.

[9] P. Bodo and J. Sundgren, "The adhesion of evaporated metal films to polyethylene substrates," Surface and Interface Analysis, Vol. 9, p. 437, 1986.

[10] J.J. Hannon and J.M. Coole, "Oxidative removal of photoresist by oxygen/Freon 116 discharge products," J. Electrochem. Soc. Vol. 131, No. 5, p. 1164, (1984).

[11] M. Kogoma, G. Turbun, "Plasma Chemistry and Plasma processing," vol. 6, p. 349, 1986.

[12] K.W. Paik and A.L. Ruoff, "Adhesion enhancement of thin copper film on polyimide modified by oxygen reactive ion beam etching," J. Adhesion Sci. Technol., Vol. 4, p. 465, 1990.

[13] W. Vanderlinde, PhD Thesis, "Reactive ion beam etching of polyimide thin films," Cornell University, 1988.

3.4.3 Teflon and Amorphous Teflon

Saturated aliphatic polymers such as Teflon and the recently developed amorphous Teflon from Dow Chemical represent the class of polymers with the lowest reported dielectric constant for commercially available polymers to date. Teflon has a dielectric constant of 2.0 and the amorphous polymer has a dielectric constant of 1.9 and a dissipation factor less than 0.001. The extremely low dielectric constant and dissipation factor make these materials particularly attractive for high frequency MCM applications. Key issues to be addressed include metal/polymer adhesion and the laser processibility. The polymer does not absorb appreciably above 200 nm, thus making it difficult to couple the laser energy needed for polymer ablation and via formation. However, the amorphous Teflon (AF-1600 and AF-2400) derivatives were also soluble in fluorinated solvents thus providing a method of application where it might be possible to modify the absorption coefficient of the basic polymer. This approach was demonstrated using an ethylene-vinylacetate copolymer which had little absorption at 351 nm. By the addition of an absorbing dye, the absorption coefficient at this wavelength was sufficiently modified to allow efficient coupling of energy and to promote polymer ablation to form vias. The absorbance spectra of this polymer with and without the addition of dye are shown in Figure 3.4-10. This approach was investigated with the AF 1600 polymer, but because of the poor solubility of dyes in the solvent system, an appropriate blend was not found. Several classes of dyes were evaluated for solubility in the polymer/solvent system, but to date this search has not led to a useful dye additive.

Films of the AF-1600 were spin-coated on alumina and were subjected to various surface modification treatments in an attempt to improve the metal/polymer adhesion and polymer/polymer adhesion. The samples were then Ar backsputtered and thin Ti/Cu sputtered. In all instances, the films discolored and delaminated from the alumina surface. These results were attributed to substrate heating during the sputtering process which was not evident on other polymers processed under identical conditions. Another problem encountered with this material was the poor self-adhesion. When multiple layers were coated, the polymer film crazed, thus rendering the film unacceptable for interlayer dielectric applications. Thus, these problems must be overcome for utilization of these low dielectric constant materials.

In summary, Teflon has excellent electrical characteristics for MCM applications, but additional work is required to develop techniques to process and use the excellent characteristics this material offers.

3.4.4 Parylene

Parylene polymers are formed using a vapor phase polymerization process developed by the Paratronix Corporation. The materials have dielectric constants on the order of 2.6 depending on the exact molecular structure of the polymer. Parylene N, available from the Nova Tran Corp., Attleboro, MA, has a dielectric constant of 2.65, but values as low as 2.34 have been reported for the fluorinated derivative (Dr. J. Moore, Rensselaer Polytechnic Institute, Troy, NY). The exact nature of the process makes it ideal as a conformal coating. In addition, the moisture uptake is extremely low (< 0.01 %). The absorption coefficient is low at 351 nm, thus complicating laser processing for via formation; however, through appropriate masking techniques, the material can be selectively etched using dry plasma processing.

Since special equipment is required for coating these polymers, alumina substrates were shipped to the Nova Tran Corporation, where thin layers of parylene N were

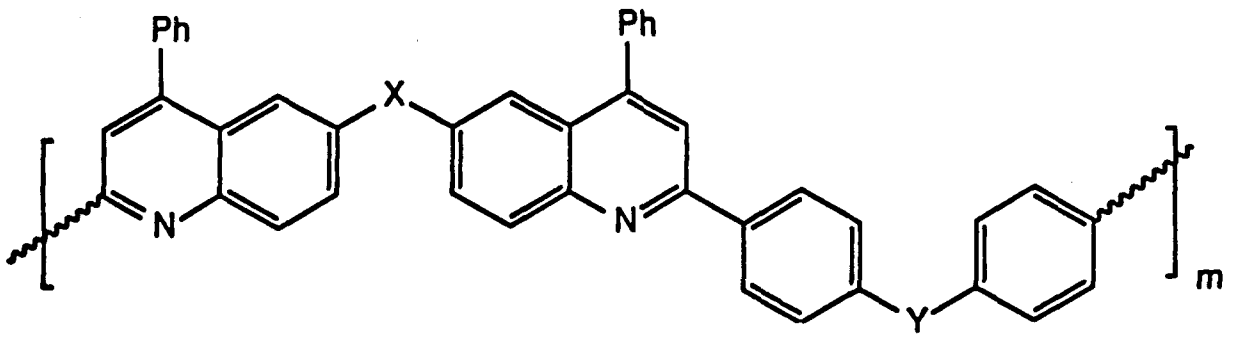

Figure 3.4-11. General structure of polyquinoline.

3.4.5.3 Results and Discussion

Dry Etching

Table 3.4-5 shows the etch rates of the PQ film at the various RIE conditions. Faster etch rates were observed with O_2 and O_2+CF_4 plasma etching than with non-oxygen containing plasmas such as Ar and CF_4/Ar. The PQ film contains basically O, C, N, and H atoms that can be easily etched away in the presence of fluorine atoms and ions. Figure 3.4-12 shows the surface morphology of PQ films after various RIE treatment. As we see, rougher surface morphology was observed after Ar ion etching. The surface morphology of CF_4/Ar mixed RIE appeared almost the same as that of the Ar RIE modified PQ; however, the surface morphology of the O_2 RIE modified PQ changed to a very rough surface presumably because of its faster etch rate than the Ar and CF_4/Ar RIE.

Table 3.4-5

Etch Rates of PQ Film at the Various RIE Conditions

Gases	RIE Conditions	Etch rates (A/min)
Ar	40 sccm, 250 mtorr, 60 W	1020
O_2	40 sccm, 250 mtorr, 60 W	2800
	75 sccm, 50 mtorr, 400 W	2000
O_2+10% CF_4	40 sccm, 250 mtorr, 60 W	2580
CF_4/Ar	20/20 sccm, 50 mtorr, 450 W	610

Metal/PQ Interfaces

Ti/PQ interface: An XPS depth profile of the Ti/PQ interface (Figure 3.4-13(a)) showed the presence of a Ti-O type of compound at the interface which results in strong chemical bonding at the interface. This type of bonding is also observed at the Ti/polyimide interface resulting in good adhesion [5]. The elemental depth profile of Ti2p in Fiure 3.4-13(b) showed the binding energy peak changes across the interface because of Ti-O compound formation at the interface. The Ti binding energy shifted from 454.1 eV of the pure Ti region to 454.8 eV at the interface, representing the formation of Ti-O compound. The formation of the Ti-O compound is also confirmed by elemental O1s peak change. An Auger depth profile of the same interface shows oxygen and nitrogen peaks located at the Ti/PQ interface similar to Figure 3.4-13(a). It confirmed not only the presence of Ti-O compound but also the Ti-N type of compound formation at the Ti/PQ interface as in the case of Ti/PI interface [5]. However, the XPS elemental N1s peak change is not noticeable because of such a small amount of nitrogen in the PQ. A fully cured PQ film should not contain oxygen atoms as shown in Figure 3.4-11. However, oxygen may be supplied from the residual solvent in the PQ film. In general, Ti at the PQ interface reacts with C, N, and O atoms of the PQ film to form chemical compounds such as Ti oxide, nitride, and carbide, which all provide chemical bonding and hence improved adhesion.

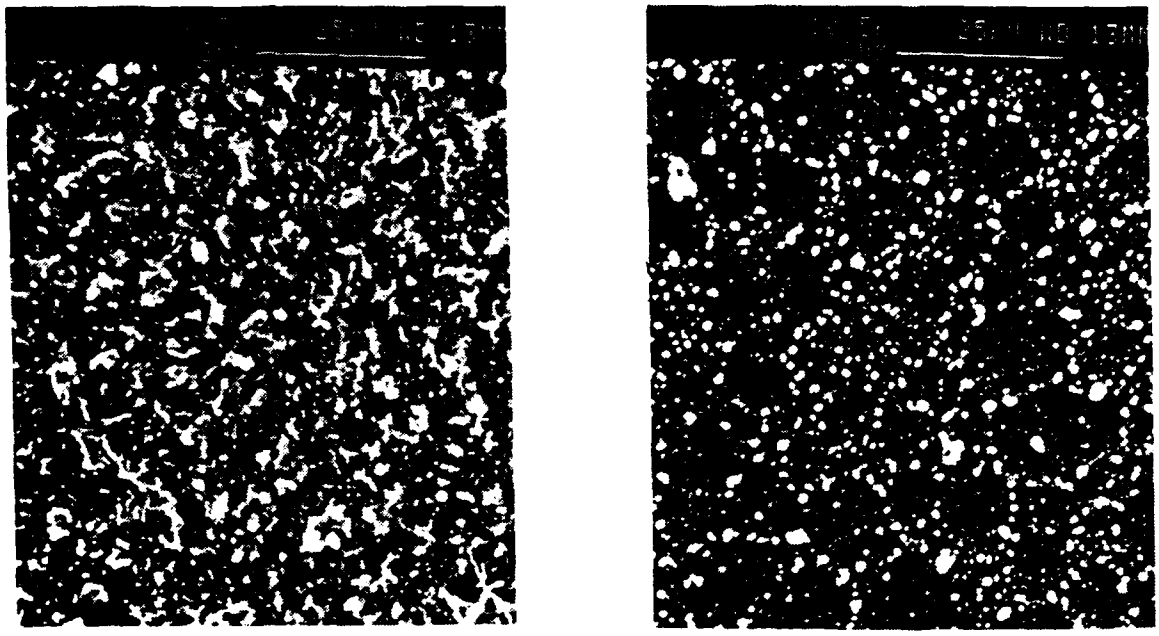

(a) (b)

Figure 3.4-12. Surface morphology of PQ-100 film after various RIE treatments (a) O_2 (b) O_2 + 20% CF_4.

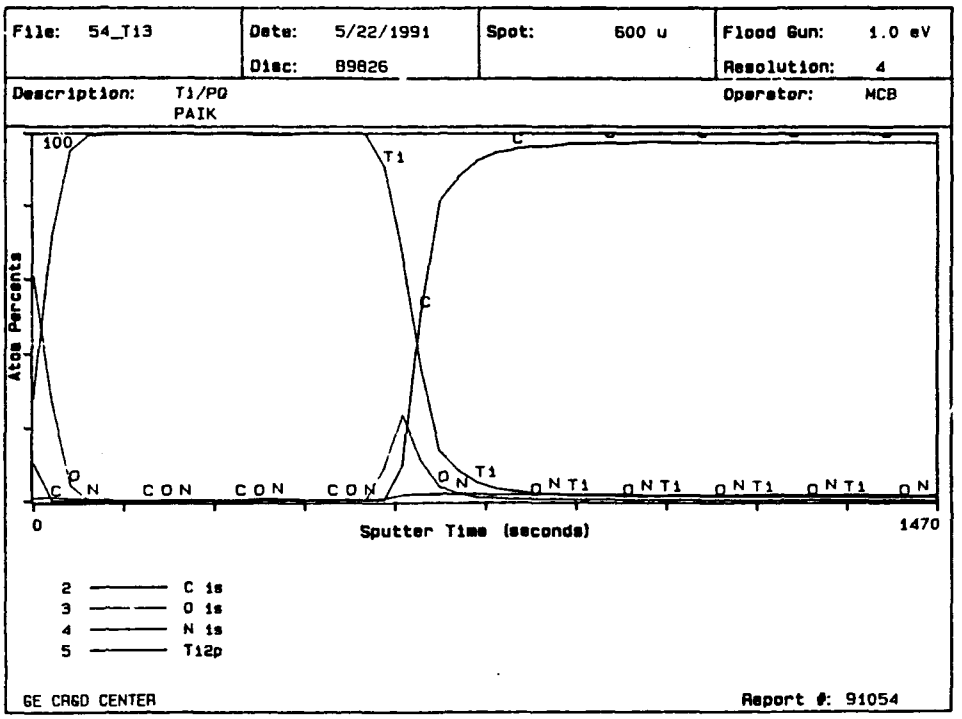

(a)

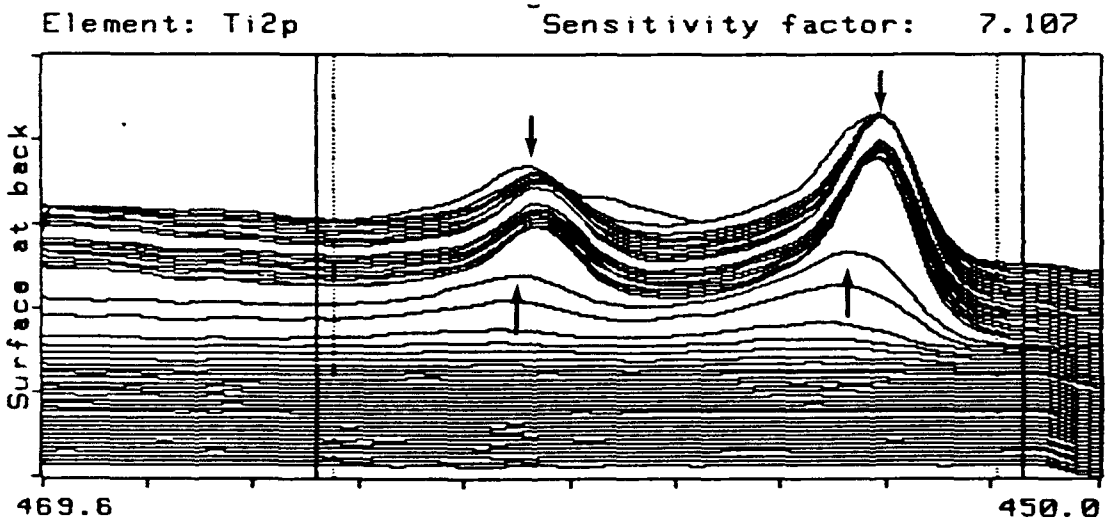

(b)

Figure 3.4-13. (a) XPS depth profile of the Ti/PQ-100 interface.
(b) Elemental depth profile of Ti_{2p} spectrum at the Ti/PQ-100 interface.

Cross-sectional TEM showed good Ti film integrity at the interface because of strong chemical bonding between Ti and PQ. The formation of Ti-O and probable Ti-N(Ti-C) compound at the interface restricts the diffusion of Ti atoms into the PQ film. The diffusion of Ti through a Ti-O compound layer was proved to be almost impossible at normal polymer processing temperature in polyimide systems [6]. For an as-control case (Figure 3.4-14(a)), an annealed one at 250 °C for 20 hrs (Figure 3.4-14(b)), and one for 45 hours, no Ti precipitates were observed in the PQ film region. Energy disperse x-ray (EDX) analysis of the Ti atom inside the PQ film showed no diffusion of Ti.

Cu/PQ interface: In contrast to Ti/PQ, Cu showed no chemical interaction at the Cu/PQ interface. Oxygen and nitrogen peak changes were not observed by the XPS depth profile shown in Figure 3.4-15(a). Elemental peak change of Cu2p (Figure 3.4-15(b)) across the interface showed no binding energy shift, which indicated no copper compound formation at the interface. This was also confirmed by the Auger depth profile. An oxygen peak was not observed at the Cu/PQ interface.

Because of weak chemical bonding at the Cu/PQ interface, the Cu film was easily peeled off during the preparation of cross-sectional TEM samples. Copper-rich precipitates were not observed in the PQ film for any specimen conditions. Cu was also not detected within the annealed PQ layers by EDX analysis. This observation is different from what has been reported for Cu/polyimide. In this instance, Cu diffuses into polyimide during 400 °C annealing treatment because there is no chemical reaction with polyimide and also be-cause of the presence of residual solvents in the polyimide. This mechanism of metal diffusion into a polymer was explained by the reptation model which is determined by the free volume in the polymer [6]. The fact that we do not observe Cu interdiffusion in PQ film may be related to this mechanism. It is speculated that the free volume in PQ film is less than that found in polyimide based on the much lower CTE found in the rigid-rod PQ structure.

Ti/PQ adhesion: Ti adhesion to the PQ film baked at 250 °C for 1 h showed 10 lb/in. peel strength which is almost equivalent to that found for Ti adhesion to Kapton polyimide film. In this case, the PQ film was roughened by excimer laser treatment followed by O_2+CF_4 plasma etching prior to Ti metallization. During peel test, the failure occurred at the PQ film itself. Table 3.4-6 shows the Ti adhesion to the PQ film modified by various RIE treatments followed by Ar backsputtering prior to Ti metallization.

Table 3.4-6

Peel Strength of Ti/PQ Film Modified by Various RIE Treatments

Conditions	Peel strength(lb/in)		
	As-RIE modified	Boiling water for 1 h	Annealed at 250°C/2.5h
Control	11.4	10.7	4.1
O_2	9.6	9.5	5.0
O_2+10%CF_4	10.5	10.4	5.5
Ar	10.0	9.8	4.9

* All the RIE conditions are 40 sccm, 50 mtorr, 400 W, and 10 min

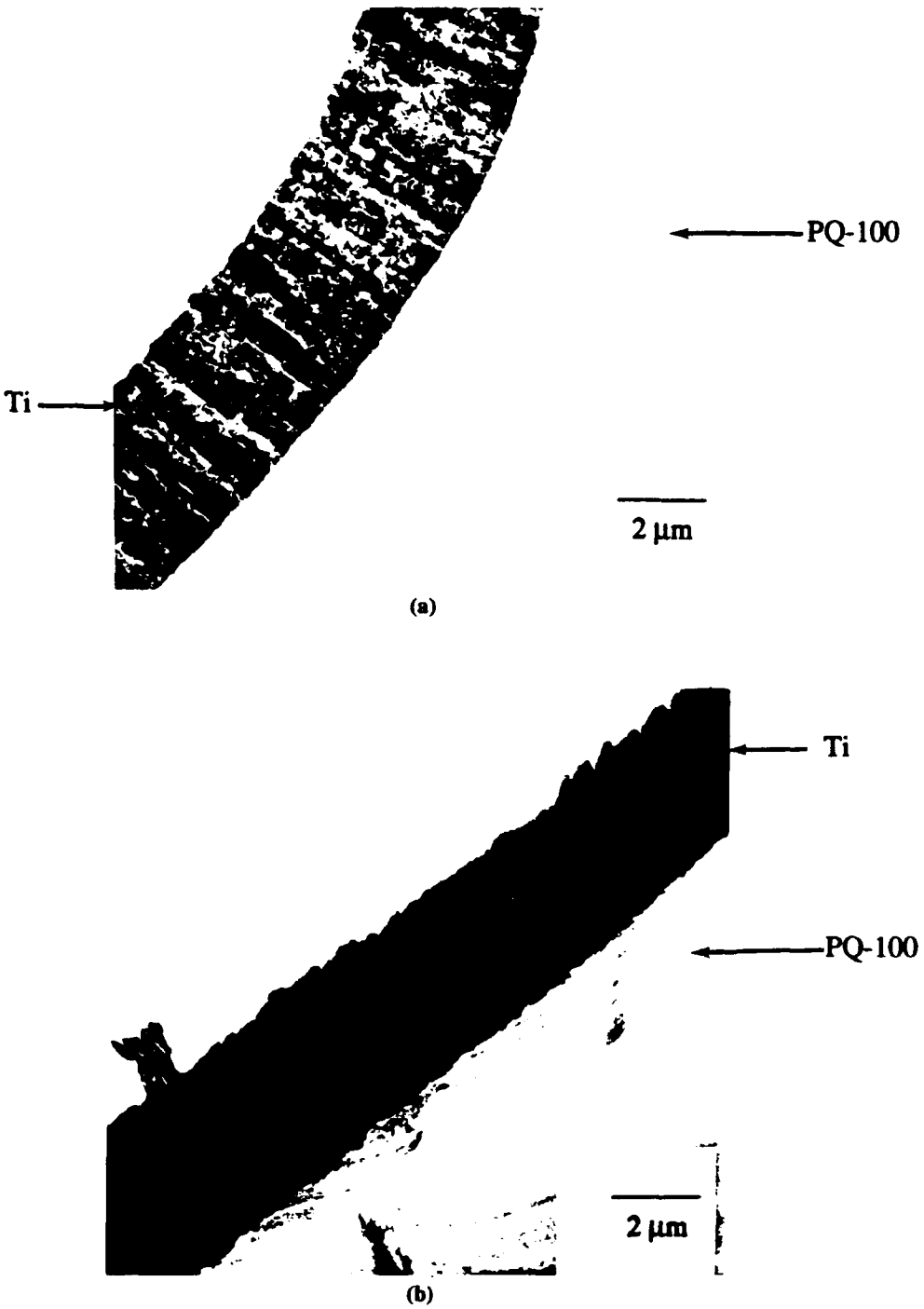

Figure 3.4-14. Cross-sectional TEM of Ti/PQ-100 interface (a) control, (b) annealed at 250 °C for 20 hrs.

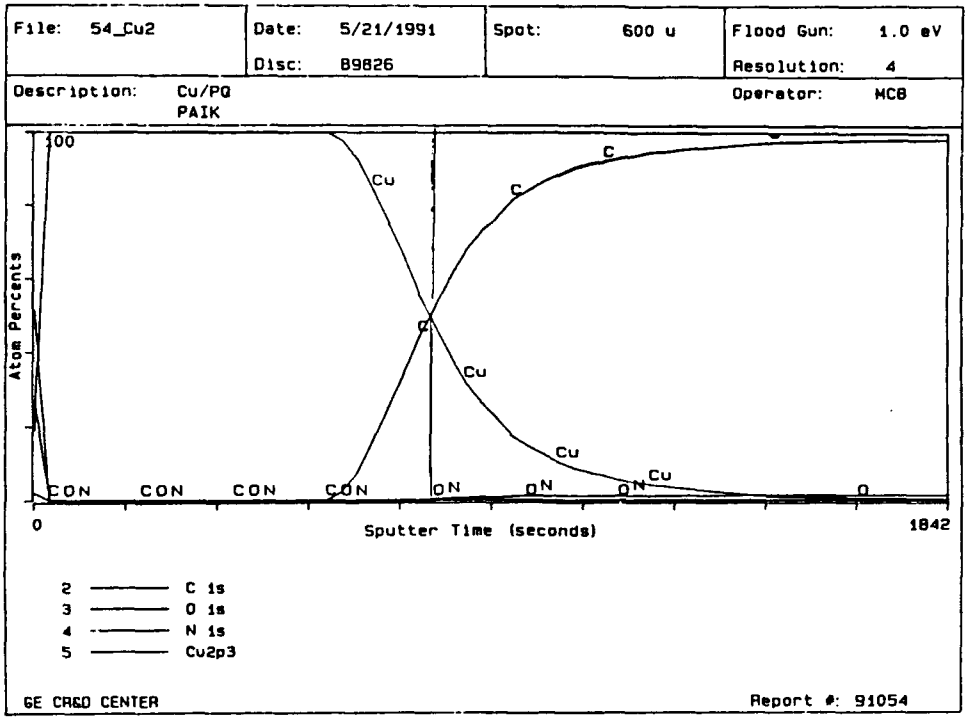

(a)

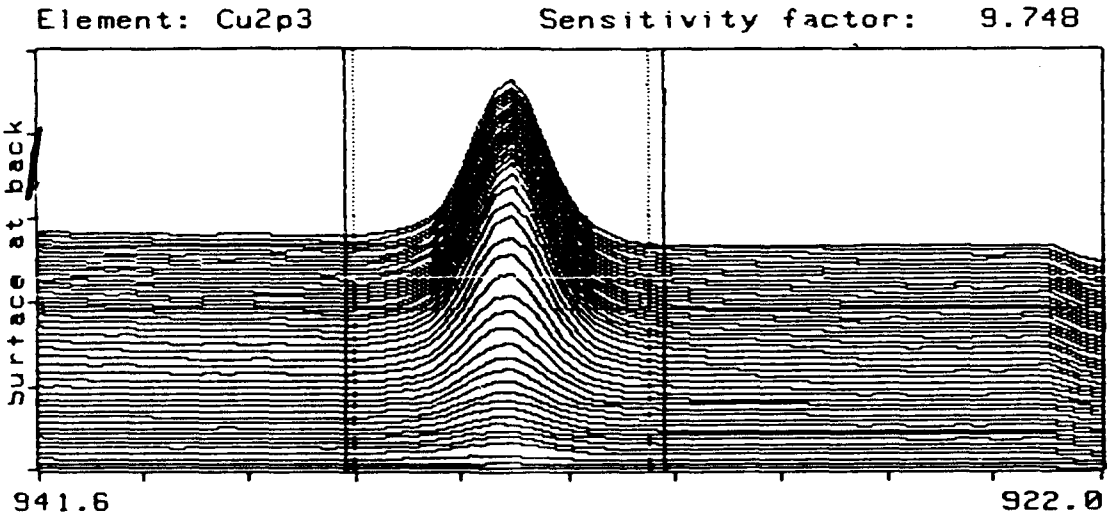

(b)

Figure 3.4-15. (a) XPS depth profile of the Cu/PQ-100 interface.
(b) Elemental depth profile of Cu_{2p} spectrum at the Cu/PQ-100 interface.

As reported in Table 3.4-6, Ti adheres well to the PQ film with all RIE treatments. As-control PQ film with Ar ion backsputtering shows the best adhesion rather than modified PQ surfaces, suggesting that the chemical bonding between Ti and PQ molecules observed by the XPS is the major adhesion mechanism between Ti/PQ.

Boiling water treatment only slightly reduces the peel strength indicating that the Ti/PQ interface is stable in the presence of water. This observation is somewhat different from the Ti/polyimide case. Ti to polyimide adhesion decreases significantly in the presence of water; however, in some instances, the adhesion restores to its original value when water is completely removed. In this case both as-RIE modified and water boiled, specimens failed at the PQ film itself, indicating the observed peel strength represents only the lower bound of the actual Ti/PQ adhesion.

Annealing at 250 °C significantly reduced the observed peel strength. In the annealed case, the failure mode was the cohesive failure of the PQ polymer itself. The glass transition temperature of the TM100 PQ polymer is reported as 257 °C, which is very close to the annealing temperature. Additional annealing studies are needed to further explain this phenomena.

3.4.5.4 Conclusion

Oxygen and O_2+CF_4 RIEs showed faster etch rate of PQ film than non-oxygen containing RIE, and caused rough surface morphology. Ti shows good adhesion to the PQ film because of the Ti-O and possible Ti-N compound formation at the interface. No diffusion of Ti and Ti-containing precipitates was observed at the Ti/PQ interface even at temperatures of 250 °C. In contrast to the Ti/PQ interface, Cu showed very poor adhesion to the PQ film because of weak chemical bonding. Cu reaction compounds were not observed at the interface even at the 250 °C annealing. Ti adhesion to the PQ film was good for as-control, as-RIE modified, and water-boiled cases. Initial studies suggest a reduction in peel strength at 250 °C annealing. To understand the exact mechanism of this process, further study needs to be continued in this area.

REFERENCES

[1] N.H. Hendricks, M.L. Marrocco, D.M. Stoakley, and A.K. St. Clair, Proceedings of the 4th International SAMPE Electronics Conference, SAMPE Pub., Covina, CA, pp. 544-555.

[2] For a review of the synthesis and properties of the original polyquinolines, see J.K. Stille, Macromolecules, 14, 870 (1981).

[3] N.H. Hendricks, et al., Proceedings of the 36th International SAMPE Symposium, April 15-18, 1991, San Diego, CA, SAMPE pub., Covina, CA.

[4] K.W. Paik and H.S. Cole, Mat. Res. Soc. Symp. Proc., Vol., 203, 309 (1991).

[5] F.S. Ohuchi and S.C. Freilich, J. Vac. Sci. Technol., A 6 (3), 1004 (1988).

[6] K.W. Paik,l Ph D thesis, Cornell University (1989).

3.5 Process Implementation

3.5.1 HDI Fabrication

Development of processing sequences that use the concept of selective electrolytic depsition (SED) for fabrication of HDI structures must be compatible with all processing steps as well as having demonstrated reliability. Key issues include yield, stability to processing chemicals and temperature, and ease of processing. A process that can meet these requirements in shown schematically in Figure 3.5-1. The process steps for this approach incorporating the SED process are compared with the current baseline GE-HDI process. The baseline process starts with thin Ti/Cu, which is electroplated to the desired thickness and then overcoated with thin Ti to provide a barrier layer between the next layer of dielectric and underlying Cu. A photoresist is then used to pattern the metal interconnect structure. The usual steps involved in resist technology include coat, prebake, expose, develop, etch, and remove resist. These steps must be completed for each layer of metal interconnect, thus complicating the reliability and yield. In the SED approach, thin Ti/Cu is sputtered and as shown in this example the thin Cu is selectively laser-ablated to provide patterned Cu on a continuous film of Ti. Using the SED concept, thick Cu is plated only in the regions containing Cu, and at this time, thin Ni is electroplated again only in the regions coantaining Cu. Finally, the thin Ti is etched in the unprotected regions to give the desired interconnect structure.

The main advantages of the "SED" process is that significantly fewer processing steps are required, thus allowing for the potential of higher yield and lower cost. In addition, the entire Cu interconnect is surrounded with barrier metal to prevent electromigration of Cu into the polyimide dielectrics. In the case of the baseline HDI process, there is the small possibility of interdiffusion at the sides of interconnect runs.

It should be pointed out this example proposes the ablation of thin Cu as the Cu patterning step, although this step could be accomplished in a variety of manners. As previously discussed in Section 3.2.6, a number of different approaches to provide patterned Cu on Ti have been investigated. To test the process sequence shown in Figure 3.5-1, a photoresist was used to pattern Cu on test devices. These devices were prepared using the GE-HDI overlay process. A silicon chip with metal pads and daisy chain structure was mounted on an alumina substrate, and a layer of Kapton was laminated over the chip and substrate. Via holes to Al pads were laser-drilled using an Ar laser at 351 nm. Thin Ti/Cu was sputtered and the Cu was patterned using photoresist and the Ar ion laser for exposure. The resultant patterned thin Cu on Ti was immersed in a Cu electroplating solution to build up the desired thickness of Cu (in this case 4 um). After rinsing in DI, the part was placed in a Ni electroplating bath to provide a barrier layer for subsequent processing. A cross section of a structure fabricated using this process is shown in Figure 3.5-2. Contact resistance measurements on via strings were found to give identical results with structures processed using the standard baseline GE-HDI process. The structures were cycled for 300 cycles between liquid nitrogen and +150 °C with no change in electrical resistivity or other visual effects.

In summary, this process provides the capability of direct write Cu deposition for HDI structures with the potential advantage of lower cost with higher yield and reliability. Additional studies are needed to optimize the Cu patterning process and demonstrate process control and reliability.

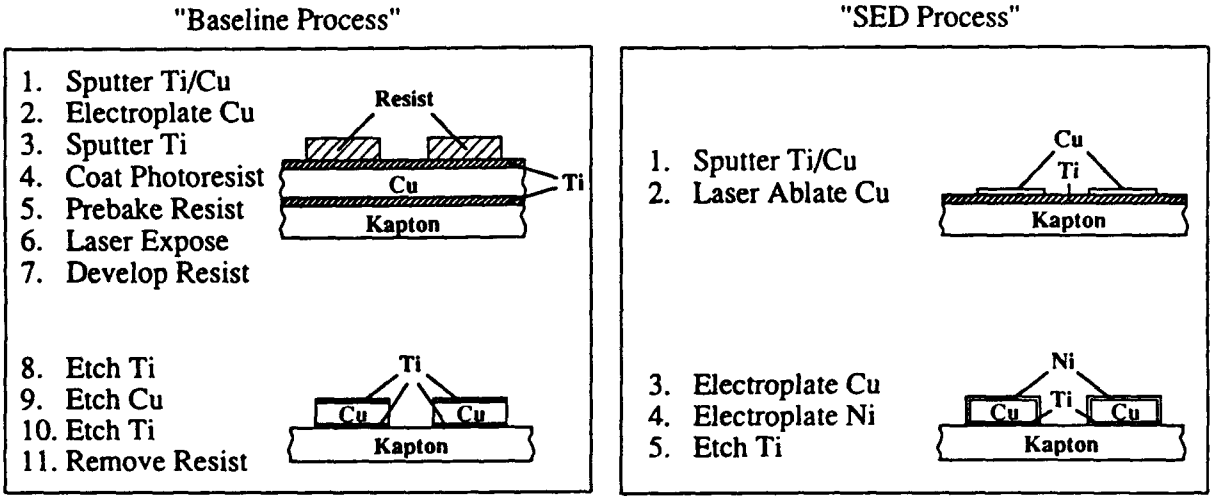

KEY FEATURES

RESISTLESS:	Less processing steps, higher yield/lower cost potential
HIGHER RESOLUTION:	Feature sizes < 1/2 mil demonstrated vs, 1 mil for "baseline process"
HIGH RELIABILITY:	Entire Cu interconnect encapsulated in barrier metal

Figure 3.5-1. Laser-activated SED process for high density interconnect.

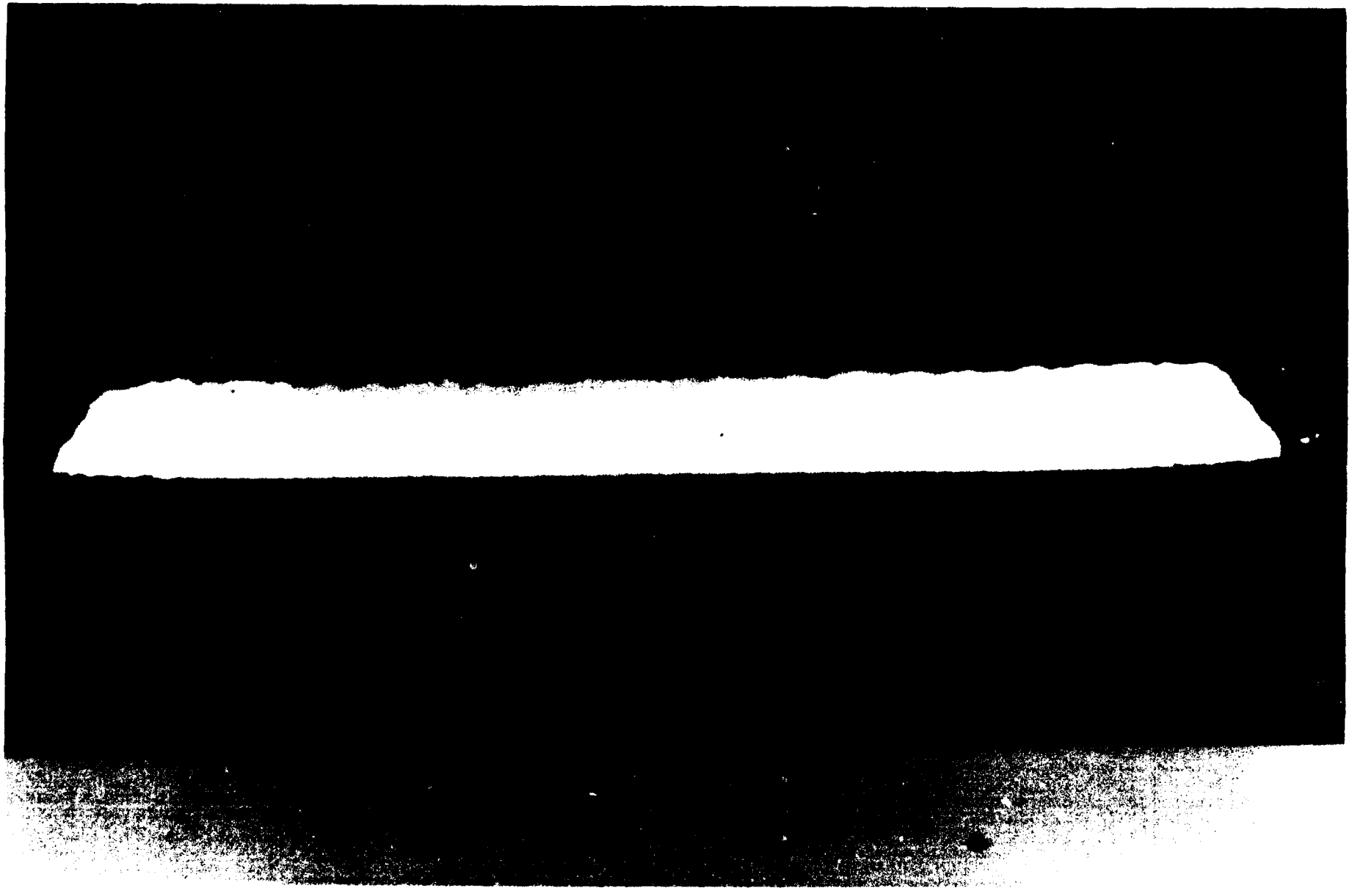

Figure 3.5-2. Cross-section of Cu interconnect structure fabricated using SED.

3.5.2 Ground Plane Metallization

As MCM modules become more complex, the options to provide interconnection for power and ground must be addressed to capitalize on certain performance advantages. For example in some instances, it is desireable to provide thruholes in the substrate and provide patterned metal from the backside to the front substrate surface through these holes. Currently, the ground plane metallization layers have been Al or in some instances Au. These metals are sputtered to desired thickness and then patterned using standard photoresist technology. One particular problem is to provide good metal coverage in the thruholes to ensure uniform electrical conductivity. Vacuum deposition or sputtering can result in holes that do not get uniformly coated, especially as hole sizes are reduced. In addition, these processes can be costly, especially if the ground plane must be Au.

The approach taken in this study was to use the thermal or photochemical decomposition of palladium acetate (PdAc) to catalyze the surface for subsequent electroless and electrolytic metal deposition. Details of PdAc decomposition can be found in Section 3.2.2. In this process, the decomposition of PdAc was used to catalize Au deposition. The process sequence is outlined below:

Process for Au Plating on Alumina

1. Clean substrates and spin thin layer of PdAc from 1% solution in chloroform.
2. Bake at 250 °C for 15 min.
3. Immerse in electroless Ni bath (Niklad 752) to deposit 0.5-μm-thick Ni.
4. Immerse in PUR-A-GOLD 540 bath for 15 min to deposit 4-μm Au.
5. Photopattern.
6. Etch in KI:I:DI.
7. Rinse in DI, spin dry.

Using this process, alumina substrates with flat, milled pockets and thruholes were successfully plated with Au. Excellent thruhole coverage was demonstrated as well as the ability to solder wire bonds. The adhesion of ULTEM/KAPTON films was also measured to be greater than 9 lb, and electrical surface conductivity was measured to be 2.9 μm-Ω cm.

In other experiments, the metal adhesion as a function of surface roughness was evaluated. Alumina substrates with 1-2, 3-5, 10, and 20 μm-inch surface roughnesses were plated using the above process. All surfaces gave good adhesion to polyimide and showed good solder pull strengths(Au wire broke under load) except the polished alumina surface with 1-2 μm-inch finish.

Laser selective patterning of PdAc on alumina resulted in poor resolution. Because of heat dissipation in the substrate and beam scattering, initial studies at 351 nm with a CW Ar laser were not successful. A few experiments were evaluated using a pulsed YAG at 266 nm with more promising results. This approach requires further work that was outside the scope of this initial study.

In summary, the above process provides a high efficiency, low cost approach to metallization of ceramic substrates. The elimination of Au sputtering targets and need for sputtering equipment can significantly reduce overall processing expenditures for MCM fabrication.

3.5.3 Multilayer Polymeric Structures

Low dielectric constant materials such as Teflon are anticipated to give high frequency performance improvements, although numerous challenging process issues must be solved to use this class of materials. These issues include method of coating, laser via formation and metal/polymer adhesion. An alternative to this method is to fabricate composite dielectric structures which incorporate low dielectric constant polymers such as Teflon and amorphous Teflon in combination with polyimide dielectrics. Through appropriate selection of composite structures, it is possible to significantly reduce the dielectric constant but still maintain adhesion and laser via processing. One such composite structure is shown in Figure 3.5-3. A single dielectric layer is shown schematically in cross section where the layer is made up of alternating thin layers of Teflon and polyimide. The presence of Teflon is used to reduce the dielectric constant, whereas the polyimide is incorporated to provide metal adhesion to substrate layers metal and upper dielectric layers. The presence of the absorbing polyimide also allows laser via drilling through the nonabsorbing Teflon layers. The thickness of the individual layers that can be coated from solution or laminated together from thin films is adjusted to ensure that efficient laser energy is absorbed to allow via ablation. Although structures such as this were not fully fabricated, modelling experiments suggest the thickness of non-absorbing Teflon must be < 5 um.

An alternative composite structure is shown in Figure 3.5-4 where only two layers make up the multilayer dielectric film. The structure shown in Figure 3.5-4 was fabricated using a laminated approach. A composite film composed of 0.5 mil Teflon and 0.5 mil Kapton was laminated over a test chip mounted in an alumina package. Via holes to bonding pads on the chip were fabricated by first laser drilling through the upper Kapton portion of the structure and then using the Kapton as a mask for RIE plasma etching of the underlying Teflon. In this process, the exposed regions of Teflon over the bonding pads are cleanly etched and at the same time, the overall thickness of Kapton is etched to give the resulting structure where up to 90 % of the remaining film can be composed of Teflon. The metallization layer is then patterned to give the desired interconnect structure. The resultant dielectric constant can approach the value for Teflon and additional layers of dielectric and metal can be applied.

The above structure was fabricated using a Test TEG with via strings containing 100 via holes. Contact resistance measurements were identical to values usually obtained using the conventional GE-HDI process sequence. Thermal shock testing of > 300 cycles between liquid nitrogen and 150 °C was performed and retesting of contact resistance showed no change.

In summary, composite structures offer unique process advantages over what is possible with conventional dielectric processing. Through appropriate choice of dielectrics and structures, it is possible to take advantage of properties not available in any one class of polymeric materials.

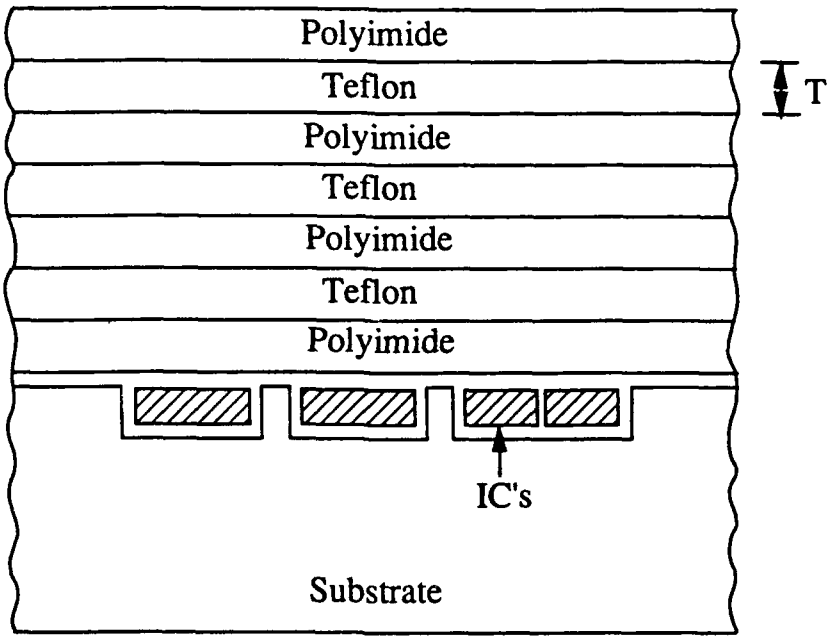

Figure 3.5-3. Multilayer dielectric structure.

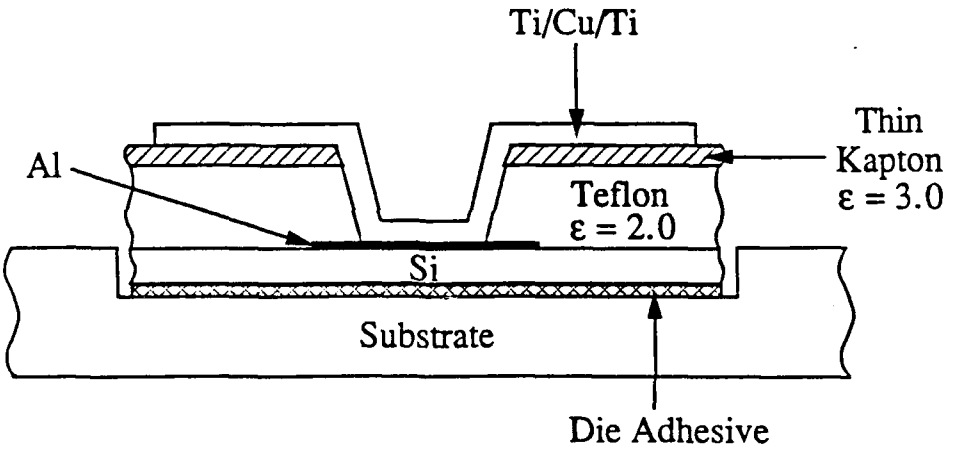

Figure 3.5-4. Low dielectric constant composite structure for HDI.

Section 4

CONCLUSIONS

Laser metal deposition and photoetching have been studied under this sponsored program. We have demonstrated that this technology is a viable adaptive interconnect technology for use in multichip module packaging. Laser direct write metal deposition processes that have been developed offer improved resolution over conventional thick film resist technology in addition to the ability to be interfaced with computers. "On the fly" repair of opens and rapid design changes are made possible with this adaptive processing technology. The concept of selective electrolytic deposition provides metallurgical interconnects and when used with laser metal patterning technology eliminates the need for photoresist processing.

Studies on laser photoetching of polymers have resulted in the development of a process for high-speed via formation using a frequency-quadrupled YAG laser at 266 nm. This development provides the capability for using a wide variety of polymeric materials as interlayer dielectrics that could not be used earlier because of insufficient absorption at the argon ion laser wavelength for via formation at 351 nm wavelength.

Studies of new low dielectric constant polymers and structures will impact device performance as future IC devices operate at much higher frequency. Process-related issues were investigated in this program, such as metal/polymer interfaces, interdiffusion, and electroless and electrolytic deposition technology, and this work will form a basis for laser-assisted processing in the gigahertz regime.

In conclusion, under this sponsored program, we have demonstrated that laser processing of polymeric materials offers unique capabilities for high density interconnect applications. As a beam source, the energy, flux, and wavelength can be conveniently controlled to expose photoresist as well as thermally ablate or modify the surface of polymeric layers at a rapid rate. Since the laser can be put under computer control, rapid engineering circuit changes are possible. This adaptive laser interconnect technology will find increasing applications in the development of application-specific electronic modules (ASEM) technology.

Section 5

APPENDIX

5.1 Publications, Presentations and Conference Proceedings

1. "Dependence of Photoetching Rates of Polymers at 193nm on Optical Absorption Depth," H.S. Cole, Y.S. Liu and H.R. Philipp, Appl. Phys. Lett. 48, 192, 1986.

2. "Optical Absorption of Some Polymers in the Region 240-170 nm," H.R. Philipp, H.S. Cole, Y.S. Liu and T.A. Sitnik, Appl. Phys. Lett. 48, 192, 1986.

3. "An X-Ray Photoelectron Spectroscopy study of PMMA and PS Surface Irradiated by Excimer Lasers," M.C. Burrell, Y.S. Liu and H.S. Cole J. Vac. Techno. 4, 2459 (1986)

4. "Laser Photoetching of Polymers," H.S. Cole, Y.S. Liu, H.R. Philipp and R. Guida, MRS Symp. Proceedings, Vol. 72 (1986)

5. "Interactions of Polymers With Excimer Lasers," Y.S. Liu, H.S. Cole and H.R. Philipp, Proceedings of International Laser Sciences, American Physical Society, (1987)

6. "Optical Properties of Bisphenol-A-Polycarbonate," H.R. Philipp, D.G. LeGrand, H.S. Cole and Y.S. Liu, Polymer Engineering Science, 27, 15, 1148 (1987)

7. "Photoetching of Polymers With Excimer Lasers," Y.S. Liu, H.S. Cole, H.R. Philipp, R. Guida, SPIE., Vol. 774, 133 (1987)

8. "Lasers in Microlithography," Y.S. Liu, H.S. Cole, H.R. Philipp, R. Guida, SPIE, Conf. Proceedings, vol. 774, p. 133 (1987).

9. "Laser Processing for Interconnect Technology," H.S. Cole, Y.S. Liu, R. Guida, and J.W. Rose, *SPIE Symposium on Optoelectronics and Laser Applications in Science and Engineering*, Vol. 877,92 (1988).

10. "Lasers in Microlithography," Y.S. Liu, H.S. Cole, H.R. Philipp, R. Guida, *SPIE, Conf. Proceedings*, Vol. 774, 133 (1987).

11. "Laser-Induced Selective Copper Deposition on Polyimide," H.S. Cole, Y.S. Liu, J.W. Rose and R. Guida, Appl. Phys. Lett. 53 (21), 2111 (1988).

12. "Theory of Polymer Ablation," G.D. Mahan, H.S. Cole, Y.S. Liu, H.R. Philipp, Appl. Phys. Lett. 53, 2377 (1988).

13. "Laser Surface Modification for Copper Deposition on Polyimide," Y.S. Liu and H.S. Cole, *Chemtronics* 4,209 (1989).

14. "Area-Selective Laser Processing Techniques for Multi-Chip Interconnect," Y.S. Liu and H.S. Cole, *Electronics Packaging Materials Science IV, Materials Research Society,* Pittsburgh, PA, 11-19 (1989).

15. "Laser Surface Modification for Copper Deposition on Polyimide," Y.S.Liu and H.S. Cole, *Materials Research Society Symposium Proceedings,* Vol. 129, *Laser and Particle-Beam Chemical Processes on Surfaces*, 579 (1989).

16. "Laser-Based Area-Selective Processing Techniques for High Density Interconnects," Y.S. Liu and H.S. Cole, MRS Fall Meeting, Conference Proceedings, Boston, MA, 1989.

17. "Laser Processing of Polymeric Materials for High Density Interconnect Structures," Y.S. Liu and H.S. Cole, *Electrochem. Soc. Conf. on Electronic Materials, Conference Proceedings,* Los Angeles, CA, 1989.

18. "Studies on the Surface Modification of Benzocyclobutene film by Plasma Ions," K. Paik, R. Saia and J. Chera, MRS Conf. on Elect. Packaging Materials, Nov. 26-28, (1990), Boston, MA (Conf. Proceedings).

19. "Interfacial Studies on Cr and Ti Deposited on Benzocyclobutene film," K. Paik and H.S. Cole, MRS Conf. on Elect. Packaging Materials, Nov. 26-28, (1990), Boston, MA (Conf. Proceedings).

20. "Laser Ablation of Dielectrics in IC Fabrication," Y.S. Liu and H.S. Cole, ASM International 4th Elect. Materials and Processing Congress, Aug. 19-22 (1991), Montreal, Canada.

21. "Laser Processing for Interconnect Technology," Y.S. Liu, Opt. Soc. Am., Conf. on Laser Processing of Materials, Nov. 4-9, (1990), Boston, Mass. (Conf. Proceedings).

22. "Studies of PQ-100 (TM) Polyquinoline Film for Multichip Module (MCM) Applications," K. Paik, H.S. Cole, N. Hendricks, to be presented at 1992 Spring MRS Meeting, San Francisco, CA.

5.2 Patents (Issued and Pending)

US #4,960,613 (October 1990)

"Laser Interconnect Process," H.S. Cole and Y.S. Liu

US #4,988,412 (January 1991)

"Selective Electrolytic Deposition on Conductive and Non-Conductive Substrates," Y.S. Liu, H.S. Cole, R. Guida and J.W. Rose.

US #5,073,814 (December 1991)

"Multi-Sublayer Dielectric Layers," H.S. Cole and Y.S. Liu

Serial No. 07/459,844 (Filed January 2, 1990)

"Area-Selective Metallization Process." H.S. Cole and J.W. Rose

Presented at Electrochemical Society Meeting, Symposium on Electronic Packaging,
Honolulu, Hawaii, October, 1987

LASER-ACTIVATED COPPER DEPOSITION ON POLYIMIDE

H.S. Cole, Y.S. Liu, J.W. Rose, R. Guida, L.M. Levinson and H.R. Philipp
General Electric Company
Corporate Research and Development
P.O. Box 8
Schenectady, NY 12301

ABSTRACT

Laser irradiation of organometallic palladium compounds with a CW argon ion laser at 351 nm is used to selectively deposit catalytic amounts of palladium on polyimide. Subsequent immersion of the irradiated samples in an electroless copper solution results in copper deposition. Since a few monolayers of palladium are sufficient to catalyze the electroless copper process, fast writing speeds of several cm/s are obtained.

INTRODUCTION

Polymeric materials have desirable features as a packaging medium for VLSI, for multichip circuitry, and as an interconnect substrate. These materials are inexpensive, can be formed in any desired shape, can withstand required solder temperatures, have excellent dielectric strength, and, most importantly, have low dielectric constant, thus reducing capacitance coupling between metallization stripes. This capacitance often determines the ultimate speed or frequency limitation of packaged devices. For high-density packaging, a major concern is the interconnect layout. Many chips are mounted on a substrate and a complex interconnect scheme is required to contact different metal layers to each other and to other chips. Generally, standard metallization and photoresist processes have been used to make interconnects and etch via holes for contact from one metal layer to another.

Recently, laser-activated chemistry has been shown to be a viable method to fabricate metal lines on various substrates (1-4). The production of metal lines by laser-induced deposition techniques offers several advantages over other thin film deposition processes. The laser process is non-contact, maskless, low temperature, selective, and relatively simple. Pyrolysis and photolysis of organometallic compounds either in the gas phase or as thin adsorbed films have been studied using CW and pulsed lasers at a variety of wavelengths. A few examples of reported reactions are shown in Table 1.

The laser deposition rate is the rate of growth in thickness, V_g, and is related to the scan rate, V_s, via the following relationship;

$$V_s = D/d\, V_g$$

where

V_s = scanning speed
V_g = growth velocity
D = beam diameter
d = film thickness

Presented at SPIE Meeting, Optoelectronics and Laser Applications in Science and Engineering,
Los Angeles, CA, January, 1988

Laser processing for interconnect technology

H.S. Cole, Y. S. Liu, R. Guida, and J. Rose

GE Research and Development Center
PO Box 8, Schenectady, New York 12309

ABSTRACT

Laser processing of polyimide dielectric layers for use in high-density interconnect structures was studied. A pulsed excimer laser was used to photoetch via holes and a CW argon ion laser operating at 351 nm was used to selectively deposit catalytic amounts of palladium on polyimide. Subsequent immersion of the irradiated samples in an electroless copper solution resulted in selective copper deposition.

1. INTRODUCTION

For high-density interconnect technology, high-performance organic polymers are used as dielectric layers instead of conventional inorganic materials. These polymers (such as polyimides), applied by spinning or laminating, are used as the interlayer dielectric because of their high thermal stability (Tg > 400 °C) and low dielectric constant (E = 3.2). Devices made using these materials show reduced capacitive coupling between metal interconnects, thus resulting in higher density packages. Several levels of metal and polymer can be used to accommodate power, ground, and signal inputs. Generally, standard metallization and photoresist processes have been used to make interconnects and etch via holes for contact from one metal layer to another. An alternate approach utilizing laser technology for hole drilling and metallization has inherent advantages such as selectivity and elimination of the need for resists; this approach is presented.

2. VIA HOLE FORMATION

Excimer laser photoetching of polymers has been shown to be a convenient, fast, selective method of producing fine patterns or holes in polymeric materials.[1-4] Numerous studies have shown that this ablation process is due to a combination of local heating, photochemistry, and bond breaking to produce volatile fragments.[5,6] Experimental data have shown that the photoetching rate is dependent on factors such as laser fluence, wavelength, structure, and absorption coefficient of the polymer at the irradiating wavelength. By appropriate adjustment of irradiating parameters, the absolute etch rate can be optimized.[7]

Typical etch rate data is shown in Figure 1. The depth of etched holes is measured as a function of fluence and number of pulses to calculate the etch depth per laser pulse. A linear plot of etch depth per pulse vs. laser fluence for three different polymers are shown. These polymers were chosen because they represent very different absorption coefficients.[8] Polyimide (PI) and poly(methyl)styrene (PS) are strong absorbers with absorption coeffficients of 4.2×10^5 and $8.0 \times 10^5 cm^{-1}$ at 193 nm. Polymethyl-methacrylate (PMMA) is a weak absorber with an absorbtion coefficient of 2.0×10^3 cm, which requires many laser pulses to start ablation. All three show a linear dependence on the laser fluence. For practical applications, the fluence should be as high as tolerable without undue damage to underlying circuitry. Etching rates of a few tenths of a micron per pulse allow hole drilling through 10-μm polyimide in less than a second using a commercially available excimer laser.

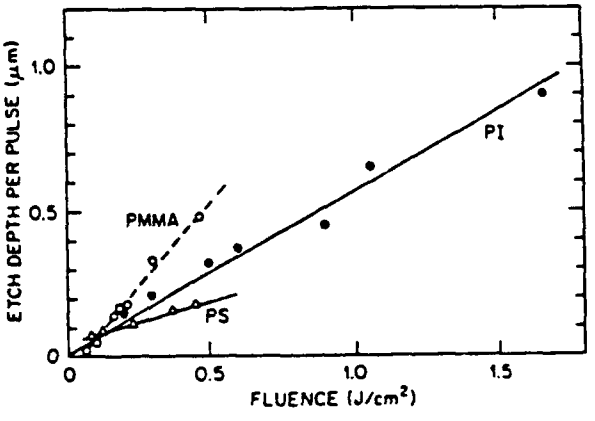

Figure 1 **Etch depth vs. laser fluence for three diferent polymers. The polyimide (PI) data is from Reference 8, while the polymethyl-methacrylate (PMMA) and poly(α-methyl) styrene (PS) data is from Reference 9.**

Laser-induced selective copper deposition on polyimide

H. S. Cole, Y. S. Liu, J. W. Rose, and R. Guida
GE Research and Development Center, P.O. Box 8, Schenectady, New York 12301

(Received 25 April 1988, accepted for publication 13 September 1988)

Laser irradiation of organometallic palladium compounds with an argon ion laser at 351 nm is used to selectively deposit catalytic amounts of palladium on polyimide. Subsequent immersion of the irradiated samples in an electroless copper solution results in copper deposition. Since a few monolayers of palladium are sufficient to catalyze the electroless copper process, fast writing speeds of several centimeters per second are obtained.

Recently, laser-activated chemistry has been shown to be a viable method to fabricate metal lines on various substrates.[1-4] The production of metal lines by laser-induced deposition techniques offers several advantages over other thin-film deposition processes. The laser process is noncontact, maskless, low temperature, selective, and relatively simple. Pyrolysis and photolysis of organometallic compounds either in the gas phase or as thin adsorbed films have been studied using cw and pulsed lasers at a variety of wavelengths. Although numerous metals have been deposited on semiconductors and insulators using the laser-activated process, little work has been reported on laser-induced selective metal deposition on polymeric materials. This area is particularly important for high-density, high-frequency interconnect assemblies and is the subject of this letter.

In general, the growth rate of laser-activated deposition processes depends on beam intensity, wavelength, and concentration of precursors. For practical line scanning applications, high growth rates are required. This is best demonstrated via the following relationship:

$$V_s = D/dV_g \qquad (1)$$

where V_s is the scan speed, V_g is the deposition rate, D is the beam diameter, and d is the film thickness.

Using a laser with a beam diameter of 10 μm to deposit a 1-μm-thick film requires a deposition rate (V_g) of 1 μm/s to scan at a rate of 10 μm/s and a deposition rate of 100 μm/s for scanning speeds of 1 mm/s.

For packaging applications, fast scanning rates are required on polymers without adverse effects such as surface damage or resultant metal features with poor electrical and mechanical properties. The approach used in this work was to laser decompose a catalytic amount of an organometallic palladium compound for subsequent immersion in an electroless copper plating solution. The process is shown schematically in Fig. 1. The advantage of this approach is that only a few monolayers of palladium atoms are needed and hence fast scan speeds are achievable.

Using a cw argon ion laser at 351 nm as the exposure source, we have studied three different palladium compounds: palladium hexafluoro acetylacetonate (PdHFAcAc), palladium acetylacetonate (PdAcAc), and palladium acetate (PdAc). Each of these compounds has particular physical properties allowing us to evaluate the gas phase (e.g., PdHFAcAc) as well as thin-film (e.g., PdAcAc and PdAc) laser deposition. Thermogravimetric (TGA) analysis data are shown for these compounds in Fig. 2.

Experiments in the gas phase (PdHFAcAc) were carried out by placing a few milligrams of the palladium compound in a stainless-steel cell fitted with a quartz window. The substrates were either polyimide films, which were spin coated on glass from solution and fully cured, or 2 mil Kapton (polyimide) films laminated on glass. These samples were placed in the cell and the surface was irradiated through the quartz window using a focused laser beam. Prior to irradiation, the cell was evacuated and heated to a temperature of about 70 °C to give the desired vapor pressure. The vapor pressure was determined by extrapolation of the data published earlier on similar compounds, suggesting that at approximately 75 °C the vapor pressure is about 1 Torr.[5] The gas pressure could be readily varied by adjustment of the cell temperature. The cell was positioned on an x-y translation stage and the laser power level and scan rate were computer controlled to allow a systematic study of deposition parameters. Less volatile palladium compounds were prepared on the polyimide surface by sublimation or by spin coating from solution. The exposure to laser took place in air ambient without special arrangement. The advantage of this approach was that no special apparatus was needed during laser exposure.

At 351 nm, polyimide has an absorption coefficient of 2.6×10^4 cm^{-1}, which results in 91% of the incident intensity being absorbed in the top 1 μm layer assuming negligible reflection loss.[6] When a sample is exposed to a focused laser

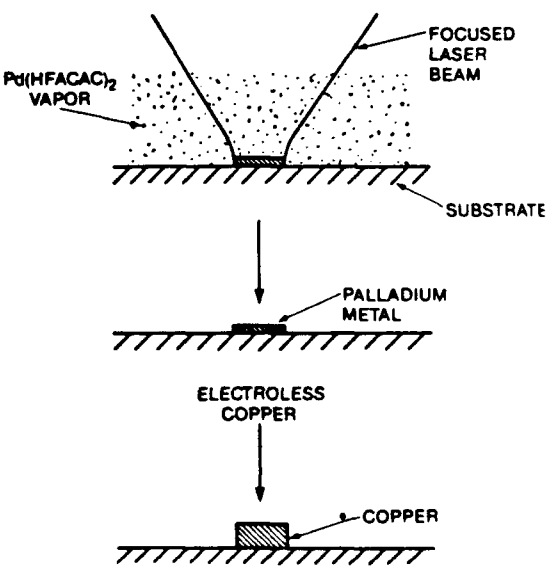

FIG. 1. Laser-activated copper deposition process.

 0003-6951/88/472111-03$01.00

NOVEMBER 1988

A CAHNERS PUBLICATION

SEMICONDUCTOR INTERNATIONAL

The Industry's Source Book for Processing, Assembly & Testing

Deposit Copper Films on Polyimide Using Laser Catalyzed Process

Researchers at the General Electric Research and Development Center, Schenectady, N.Y., selectively deposited copper on polyimide using laser irradiation of organometallic palladium compounds (Fig. 1). They irradiated organometallic palladium compounds with a CW argon ion laser at 351 nm to selectively deposit catalytic amounts of palladium on polyimide. They then immersed the irradiated samples in an electroless copper solution resulting in a selective copper deposition — as opposed to an electrodeposition. "Electroless copper deposition is a common practice in industry," says Y.S. Liu of GE. "But people have not used a laser to selectively deposit a catalyst on polymers before."

Since only a few monolayers of palladium are needed to catalyze the electroless copper process, the researchers at GE achieve fast writing speeds of up to 10 cm/s. "In the past, people tried to use lasers to direct deposit copper. But the speed is limited because you need to deposit a large amount of copper, which is difficult." The technique, developed by Y.S. Liu and H.S. Cole at GE's R&D Center, is not only unique, but fast. Copper lines with 1.5 μm thickness and resistivities of 3μΩ-cm were produced.

According to Liu, the major application for this process is for advanced packaging where speed and density can be increased. The copper can be deposited on a low dielectric constant material and the structures can be made finer so that more conducting lines per square area can be produced. *KS* □

1. By selectively depositing a very small amount of palladium as a catalyst and then using electroless copper deposition to deposit copper selectively on the polyimide, very fast writing speeds can be achieved.

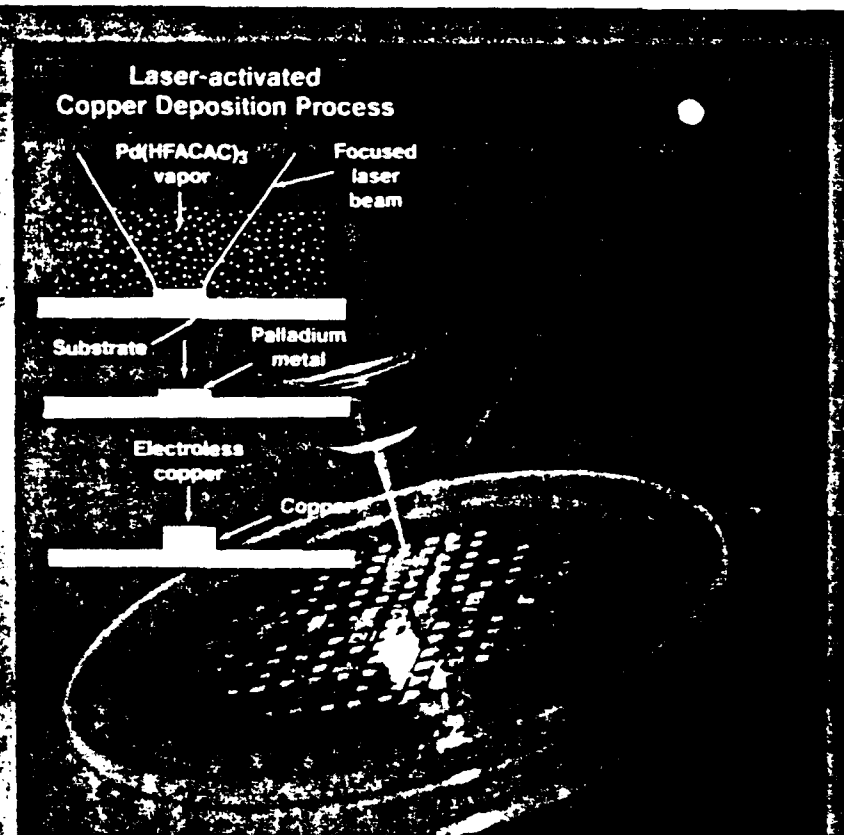

Theory of polymer ablation

G. D. Mahan
Department of Physics, University of Tennessee, Knoxville, Tennessee 37996, and Solid State Division, Oak Ridge National Laboratory, P. O. Box 2008, Oak Ridge, Tennessee 37831-6030

H. S. Cole, Y. S. Liu, and H. R. Philipp
General Electric Corporate Research and Development Center, Schenectady, New York 12301

(Received 5 October 1987; accepted for publication 28 September 1988)

A new formula is presented for the etch depth l per pulse of an excimer laser of fluence F. Incremental ablation is defined as the etch depth per pulse after many pulses. We show that l is proportional to F, rather than $\ln(F)$.

The light pulses from short-wavelength excimer lasers have been shown to etch clean holes in polymers.[1,2] This process has numerous applications in medicine and in the manufacture of integrated circuits.[3,4] Here we examine the theory of this process, and derive a new and simple formula for the etch depth l per pulse for a laser of fluence F.

Experiments have shown that the ablation process is not just due to local heating, but involves some other process which presumedly is bond breaking. Define $n(x,t)$ as the number of broken bonds per unit volume at a distance x from the surface at the time t. We follow previous theories in assuming that ablation occurs whenever this bond breaking density exceeds some threshold value n_T.[5-8]

The first laser pulse produces a damage profile given by Beer's law of $n = (f\alpha F/h\nu)\exp(-\alpha x)$, where α is the absorption coefficient, $h\nu$ is the photon energy, and f is the fraction of absorbed photons which break bonds.

$$l = (1/\alpha)\ln[F/F_T]\theta(F-F_T),$$
$$F_T = h\nu n_T/\alpha f, \tag{1}$$

where θ is the step function. This formula has been widely used to interpret ablation data.[4,6-11] The initial experiments seemed to show that l is proportional to $\ln(F)$, although the range of values for F was small. Recent experimental plots for large ranges of F show that Eq. (1) is not obeyed.[7,12]

Experimental data are usually taken by averaging over many laser pulses. A key aspect of our theory is that broken bonds remain in the unetched portion of the polymer. The exponential nature of Beer's law guarantees that substantial bond breaking density remains in that part of the polymer which is not etched away. The next laser pulse builds on this residual bond breaking density. Equation (1) is only valid for the first laser pulse, but is invalid for subsequent pulses since it ignores the residual bond breaking. This model distinguishes bond breaking from purely thermal effects. The low repetition rate of the pulses, on the order of Hertz, means that heating effects will dissipate between pulses.[13,14] However, the bond breaking which turns a polymer into a monomer seems to have a much longer relaxation time. Since the density of broken bonds is low, we can assume that their presense does not change physical parameters such as the absorption coefficient.

Ample evidence exists for the concept of residual bond breaking density. For polymers of low absorption coefficient, numerous laser pulses must be absorbed before any ablation occurs.[7] This makes sense if the polymer is accumulating residual broken bonds from each pulse. We introduce the concept of *incremental abalation depth*. It is the etch depth per laser pulse l after many pulses; that is, after the threshold processes are over and actual ablation occurs. We show below that incremental ablation has l proportional to F rather than to $\ln(F)$.

Our theory also employs the concept of a moving melt front as introduced by Keyes *et al.*[15] Typical laser pulses have a duration of 5–10 ns, during which time the ablated monomer can travel many microns away from the surface. We assume that the ablated material leaves the light path of the laser and no longer causes absorption. Let $s(t)$ be the position of the polymer surface during a single laser pulse. If the period of the laser repetition is $2t_r$, then we consider a single pulse during the duration $(-t_r, t_r)$ where the pulse is a maximum at the surface at time $t \cong 0$. The distance marker x is defined in a fixed reference frame from where the surface is at the start of a laser pulse. The distance from the actual surface is $x - s$. The rate at which bond breaking occurs is

$$\frac{dn(x,t)}{dt} = \frac{f\alpha I(t)}{h\nu}\exp\{-\alpha[x-s(t)]\}, \tag{2}$$

where the laser intensity I (J/cm^2 s) is defined in terms of the fluence F (J/cm^2) and the normalized pulse shape $i(t)$:

$$I(t) = Fi(t),$$
$$1 = \int_{t_r}^{t_r} dt'\, i(t'). \tag{3}$$

Equation (2) is solved by direct integration. The residual density of broken bonds $n_T \exp(-\alpha x)$ is taken as the initial condition

$$n(x,t) = \frac{f\alpha F}{h\nu}e^{-\alpha x}\int_{t_r}^{t} dt_1 i(t_1)e^{\alpha s(t_1)} + n_T e^{-\alpha x}. \tag{4}$$

The position of the ablation surface $s(t)$ is defined by setting $n(s,t) = n_T$ in Eq. (4). Then multiplying each term by the factor of $\exp(\alpha s)/n_T$ gives the equation for $s(t)$:

$$J(t) \equiv e^{\alpha s} = 1 + \lambda\int_{-t_r}^{t} dt_1 i(t_1)J(t_1),$$
$$\lambda = f\alpha F/h\nu n_T.$$

We differentiate this equation with respect to time, which immediately brings us to the equation:

$$\frac{\partial J(t)}{\partial t} = \lambda i(t)J(t),$$

 0003-6951/88/502377-03$01.00

LASER SURFACE MODIFICATION FOR COPPER DEPOSITION ON POLYIMIDE

Y.S. Liu and H.S. Cole
GE Research and Development Center
P.O. Box 8, Schenectady, New York 12345

ABSTRACT

Selective modification of surface reactivities with lasers, using either direct writing or projection method, is intrinsically a sensitive method to prepare a surface for high-resolution and high-speed area selective thin film deposition. In this paper, we demonstrated the use of laser direct-writing and projection patterning techniques for selective modification of the electrochemical property of a polyimide surface. High quality and high-resolution copper patterns on polyimide surfaces are produced when the surface-modified sample is subsequently placed in an electroless plating solution. These results demonstrated that the use of laser-selective-modification of surface properties in conjunction with other batch thin film deposition processes provides an attractive approach for area-selective metallization for a variety of applications in which high writing speed and high sensitivity are required.

INTRODUCTION

The demands for application-specific IC design and fabrication, yield enhancement, circuit restructuring and fast turnaround prototyping have significantly increased the interest in adaptive processing techniques using direct energy sources such as lasers [1]. Previous studies in laser processing have focused mostly on semiconductors, solid dielectrics, and metals [2]. Recent interests in multilevel and multichip high-performance electronic packaging have attracted attention on laser processing of polymeric materials such as polyimide, which has a low dielectric constant and relatively stable thermal properties [3]. The low dielectric constant reduces capacitance coupling which often determines the ultimate speed and frequency of the packaged electronic devices. Standard thin film metallization and photoresist patterning processes are being used for fabrication of interconnects layouts, followed by either additive or subtractive processes to make final multichip interconnects. Topographical nonuniformity often limits the interconnect line width to greater than 25 m using present thin film techniques. Laser-selective metal deposition on polymers, either direct-write or projection patterning, is a key processing technology for the development of a viable laser direct-interconnect for high-density and high-performance multichip interconnects for ASICs and quick turnaround prototyping applications.

A fast writing speed exceeding several millimeters per second is a key requirement for the development of a direct-write process for interconnect paths over several meters. Slower direct writing processes are useful only for short-run interconnects such as circuit alternations, local restructuring, and repairs. The laser scan speed V_s is related to the film growth rate, V_g by [4]

$$V_s = D/(dV_g)$$

where D is the beam diameter and d is the film thickness. This equation shows that with a beam diameter of 10 μm to deposit a 1-μm-thick film, a film growth rate of 100 μm/sec is required in order to achieve a writing speed of 1 μm/sec. In gas phase photolysis, growth rates are limited by the transport of reactants and products to and away from the reaction

Mat. Res. Soc. Symp. Proc. Vol. 129. © 1989 Materials Research Society

LASER-BASED AREA-SELECTIVE PROCESSING TECHNIQUES FOR HIGH-DENSITY INTERCONNECTS

Y.S. LIU and H. S. COLE
GE Research and Development Center; P.O. Box 8, Schenectady, NY, 12345

ABSTRACT

This paper reviews several laser-based area-selective processing techniques developed for high-density multichip interconnection applications. Key material and process requirements for the development of a viable laser-direct-write interconnect technique on polyimide are addressed.

1. INTRODUCTION

The rapid advances in VLSI processing technology have outpaced the development of the electronic packaging and interconnect technology. Shrinking feature sizes, increasing gate density and clock rates have made electronic devices faster, and more complex. As a result of the increasing number of pin-counts and power dissipation, the VLSI packaging and interconnect become a very complex task. The chip-to-chip delay is becoming a limiting factor of the system performance. To reduce the chip-to-chip interconnect length and improve circuit performance, multichip module packaging and high density interconnect are the key technologies.

Laser processing has been shown to be a viable technology for depositing and/or etching a variety of metals and dielectric materials and has been the subject of many research activities. [1-3]. Laser metal patterning on polymers, either direct-write or projection patterning, is particularly relevant to high-density interconnect. For HDI applications, the relatively long focal depth achievable with a Gaussian laser beam is a very important property which is unique to laser processing. [4] This property is particularly critical when the substrate surface is not completely planar, as is frequently encountered in polyimide structures. For HDI applications, key laser process steps include fabrication of micro-vias and metal interconnects. In the following sections, several laser-based processing techniques that have been developed for HDI applications are discussed.

2. HIGH-DENSITY INTERCONNECT TECHNOLOGY (HDI)

Various HDI approaches have been developed. The topic has been discussed in a review paper by Neugebaur et al [5] and the results are summarized in Table 1. The Table also illustrates the requirements of various HDI technologies in terms of substrate, metal, dielectric materials, method of patterning, chip attachment and interconnect technology. As the Table shows copper or aluminum is the most commonly used metal for high-density multichip interconnect, while polyimide is the most commonly used dielectric material due to the fact that the polymeric material is compatible with the standard IC processing technology, has good thermal stability, and more importantly, has a low dielectric constant. Therefore, it reduces capacitive coupling

Mat. Res. Soc. Symp. Proc. Vol. 158. ©1990 Materials Research Society

Laser surface modification for copper deposition on polyimide

Y.S. Liu and H.S. Cole
GE Research and Development Center, PO Box 8, Schenectady, NY 12345, USA
(Received 30 August 1989)

Selective modification of surface reactivities with lasers, using either direct writing or projection method, is intrinsically a sensitive method to prepare a surface for high resolution and high speed area selective thin film deposition. In this paper, we demonstrate the use of laser direct-writing and projection patterning techniques for selective modification of the electrochemical property of a polyimide surface. High quality and high resolution copper patterns on polyimide surfaces are produced when the surface-modified sample is subsequently placed in an electroless plating solution. These results demonstrated that the use of laser-selective modification of surface properties in conjunction with other batch thin film deposition processes provides an attractive approach for area-selective metallization for a variety of applications in which high writing speed and high sensitivity are required.

Keywords: *Lasers; surface deposition; polyimide; copper*

The demands for application-specific ic design and fabrication, yield enhancement, circuit restructuring and fast turnaround prototyping have significantly increased the interest in adaptive processing techniques using direct energy sources such as lasers[1]. Previous studies in laser processing have focused mostly on semiconductors, solid dielectrics, and metals[2]. Recent interests in multilevel and multichip high-performance electronic packaging have attracted attention on laser processing of polymeric materials such as polyimide, which has a low dielectric constant and relatively stable thermal properties[3]. The low dielectric constant reduces capacitance coupling which often determines the ultimate speed and frequency of the packaged electronic devices. Standard thin film metallization and photoresist patterning processes are being used for fabrication of interconnects layouts, followed by either additive or subtractive processes to make final multichip interconnects. Topographical non-uniformity often limits the interconnect linewidth to greater than 25 μm using present thin film techniques. Laser-selective metal deposition on polymers, either direct-write or projection patterning, is a key processing technology for the development of a viable laser direct-interconnect for high density and high performance multichip interconnects for ASICs and quick turnaround prototyping applications.

A fast writing speed exceeding several millimetres per second is a key requirement for the development of a direct-write process for interconnect paths over several metres. Slower direct writing processes are useful only for short-run interconnects such as circuit alternations, local restructuring, and repairs. The laser scan speed, V_s, is related to the film growth rate, V_g, by[4]

$$V_s = (D/d)\, V_g$$

where D is the beam diameter and d is the film thickness. It shows that with a beam diameter of 10 μm to deposit a 1 μm thick film, a film growth rate of 100 μm s^{-1} is required in order to achieve a writing speed of 1 mm s^{-1}. In gas phase photolysis, growth rates are limited by the transport of reactants and products to and away from the reaction zone. The proper laser wavelength must be used to couple the spectral properties of gaseous phase compounds or adsorbates for photodissociation with efficient quantum yields. In spite of the fact that many interesting photochemical reactions have been reported, none of these processes appeared fast enough for direct writing applications. In the pyrolytic approach, reactants of higher concentration can be used to enhance the writing speed. As a result, higher film growth rates have been demonstrated[4].

In this study, a two-step process was used to achieve a fast writing speed. In this two-step process, laser radiation is first used to selectively modify the polymer surface, followed by a batch thin film process to form interconnect patterns. Surface modification of surface reactivities with lasers, using either direct writing or projection patterning technique, is intrinsically a sensitive method for area-selective thin film deposition[5]. Surface modifications can be achieved via a variety of means, such as:

- physical *versus* chemical;
- photolytic *versus* pyrolytic;
- additive *versus* subtractive;
- catalytic *versus* inhibitive;
- adsorptive *versus* desorptive.

In the present study, we applied surface modification to copper deposition on polyimide using both direct writing and excimer laser projection techniques. In the former case, an argon laser was used to selectively deposit a trace amount of Pd on polyimide surfaces such that electroless copper deposition takes place in the surface areas exposed to laser irradiation (positive process). In the latter case, an excimer laser was used to desensitize a polyimide surface such that a negative metal pattern was formed after electroless deposition (negative process).

0267-5900/89/030209-03 $03.00

INTERFACIAL STUDIES ON CR AND TI DEPOSITED ON BENZOCYCLOBUTENE (BCB) FILM

Kyung W. Paik and Herbert S. Cole, GE Corporate Research and Development, P.O.Box 8, Schenectady, NY 12301

ABSTRACT

Interfacial characteristics such as chemical reaction, metal diffusion, and morphology were investigated for Cr/BCB and Ti/BCB structures. Using Auger and XPS depth profiling, the formation of Ti carbide and Cr oxide was confirmed at the metal/BCB interface. Annealing at 250 °C for extended time periods resulted in diffusion of Cr and Ti into the BCB and subsequent formation of $CrSi_2$ and Ti-Si compound precipitates. The reaction is a thermal diffusion controlled process which was dependent on time and temperature. It was also found that Ar backsputtering treatment on BCB film before metallization was found to roughen the surface resulting in metal spikes which penetrate into the BCB film.

1. INTRODUCTION

Thin film multichip packaging is one of the more promising techniques among various multichip electronic packaging approaches because of its fine dimensional capability, use of lower dielectric constant polymers for interdielectric, and ease of processing[1]. Polyimide has been widely used for the interdielectric material, even though it has certain disadvantages such as high water absorption and relatively higher dielectric constant than other polymers[2, 3]. Key attributes of this class of polymers include high thermal stability, excellent metal/polymer adhesion, and the ability to tailor physical properties through appropriate molecular engineering. For improved reliability and faster signal propagation, polymers with lower water absorption and lower dielectric constant will be required[4].

One class of polymers which have recently been developed for this application are the benzocyclobutenes. These polymers have relatively low dielectric constant (E=2.7), low dissipation factor (0.0008), and low water absorption (0.25%) compared to polyimides[5]. In addition, polymerization of the BCB functional monomer is a thermal process which does not require catalysts and does not generate volatile by-products. Since the coating solution is in the form of low molecular weight oligomers, a high solid content can be spin or spray coated resulting in a high degree of planarization. Full polymerization/crosslinking does not occur until the dielectric film has been coated. Use of this material as a multilayer dielectric film in high density interconnect packages has recently been reported[6].

A key requirement of any multichip module packaging approach is the issue of metal/polymer adhesion. In the case of polyimide, numerous studies have shown that to achieve good adhesion, one must use a metal primer layer such as Cr or Ti[7,8]. These metals have been shown to form chemical bonds at the polyimide interface resulting in strong bonding of the

CHAPTER 1

Sources, Optics, and Laser Microfabrication Systems for Direct Writing and Projection Lithography

Y.S. LIU

GE Research and Development Center
Schenectady, New York

Laser Microfabrication

0-12-233430-2

United States Patent [19]

Cole et al.

[11] **Patent Number: 4,960,613**

[45] **Date of Patent: Oct. 2, 1990**

[54] **LASER INTERCONNECT PROCESS**

[75] Inventors: **Herbert S. Cole**, Scotia; **Yung S. Liu**, Schenectady, both of N.Y.

[73] Assignee: **General Electric Company**, Schenectady, N.Y.

[21] Appl. No.: **253,020**

[22] Filed: **Oct. 4, 1988**

[51] **Int. Cl.**[5] **B05D 3/06**; B05D 5/12; B05D 3/02

[52] **U.S. Cl.** **427/53.1**; 427/96; 427/97; 427/229; 427/123

[58] **Field of Search** 427/53.1, 229, 304, 427/305, 306, 97, 96, 98, 99, 123, 252, 253

[56] **References Cited**

U.S. PATENT DOCUMENTS

3,772,056	11/1973	Polichette et al.	427/53.1
4,169,171	9/1979	Narcus	427/304
4,332,879	6/1982	Pastor et al.	427/229
4,340,617	7/1982	Duetsch et al.	427/53.1
4,388,517	6/1983	Schulte et al.	219/121
4,511,597	4/1985	Teng et al.	427/53.1
4,543,270	9/1985	Oprysko et al.	427/53.1
4,574,095	3/1986	Baum et al.	427/53.1
4,592,975	6/1986	Young et al.	430/5
4,606,932	8/1986	Oprysko et al.	427/53.1
4,727,234	2/1988	Oprysko et al.	219/121 L
4,830,880	5/1989	Okubi et al.	427/229
4,840,820	6/1989	Schultz et al.	427/305
4,865,873	9/1989	Cole, Jr. et al.	427/304
4,869,930	9/1989	Clark et al.	427/304
4,900,581	2/1990	Stuke et al.	427/53.1

OTHER PUBLICATIONS

Cole, H. S. et al., "Laser Processing for Interconnect Technology", SPIE, vol. 877, Micro-Optoelectronic Materials (1988), pp. 92-96.

Cole, H. S. et al., "Laser-Induced Selective Copper Deposition on Polyimide", *Applied Physics Letters*, 53(21), Nov. 21, 1988, pp. 2111-2113.

Primary Examiner—Shrive Beck
Assistant Examiner—Marianne Padgett
Attorney, Agent, or Firm—Robert Ochis; James C. Davis, Jr.; Marvin Snyder

[57] **ABSTRACT**

The uniformity of a catalyst layer produced by laser decomposition of a catalyst source compound is substantially improved for patterned substrates whose characteristics vary along the path of a conductor line by providing a buffer layer of a metal such as Ti, Cr or Ni over the substrate prior to the laser induced decomposition of the catalyst source compound.

18 Claims, 7 Drawing Sheets

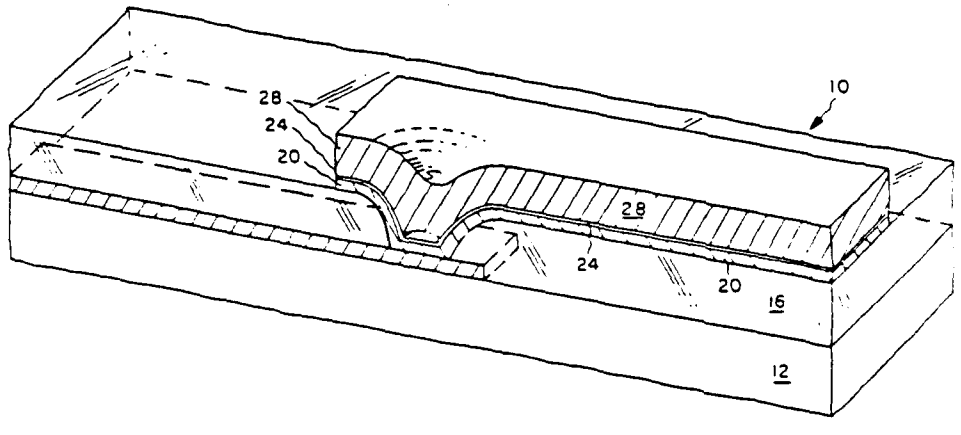

United States Patent [19]

Liu et al.

[11] **Patent Number: 4,988,412**

[45] **Date of Patent: Jan. 29, 1991**

[54] **SELECTIVE ELECTROLYTIC DESPOSITION ON CONDUCTIVE AND NON-CONDUCTIVE SUBSTRATES**

[75] Inventors: **Yung S. Liu**, Schenectady; **Herbert S. Cole**, Scotia; **Renato Guida**, Wynantskill; **James W. Rose**, Delmar, all of N.Y.

[73] Assignee: **General Electric Company**, Schenectady, N.Y.

[21] Appl. No.: **289,944**

[22] Filed: **Dec. 27, 1988**

[51] **Int. Cl.**[5] **C25D 5/02**

[52] **U.S. Cl.** **204/15**

[58] **Field of Search** 204/15

[56] **References Cited**

U.S. PATENT DOCUMENTS

1,862,231	6/1932	McFarland	204/18.1
3,388,048	6/1968	Szabo	204/15
3,507,756	4/1970	Wenger	204/15
3,809,625	5/1974	Brown	204/15
4,783,695	11/1988	Eichelberger et al.	357/65

Primary Examiner—T. M. Tufariello

Attorney, Agent, or Firm—Robert Ochis; James C. Davis, Jr.; Marvin Snyder

[57] **ABSTRACT**

Selective electrolytic deposition is provided on a body having a conductive surface comprised of two different conductive materials in which one of the conductive materials forms a surface layer upon exposure to a particular ambient environment and wherein that surface layer prevents electroplating on that material in the particular electroplating environment utilized for the electroplating of the desired pattern on the other conductive material.

9 Claims, 20 Drawing Sheets

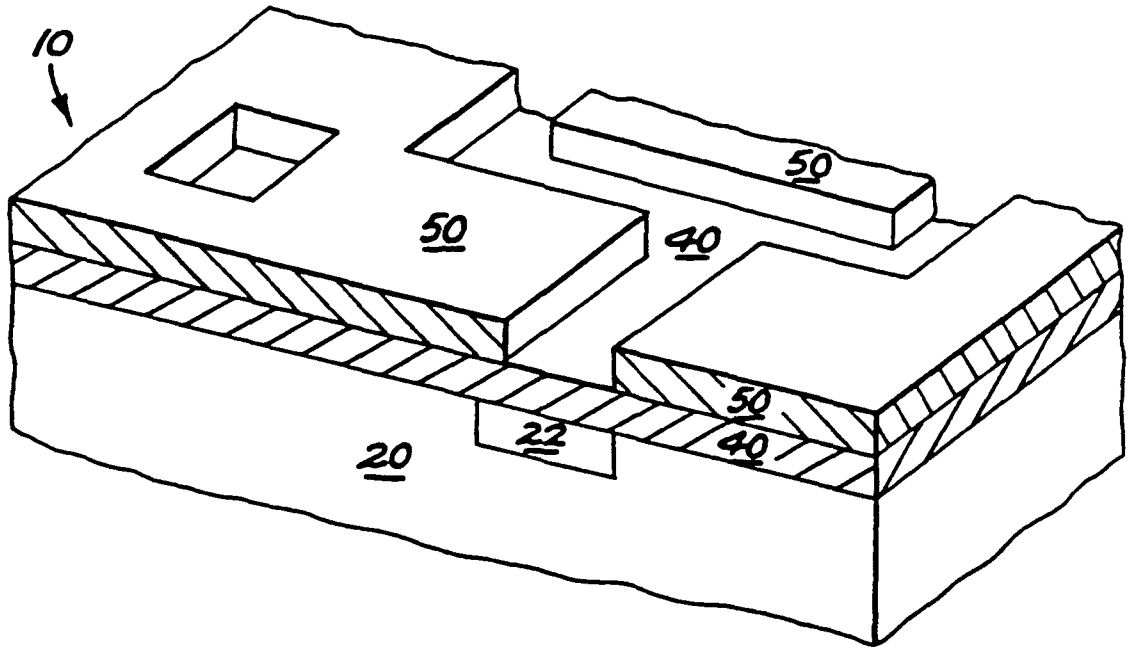

United States Patent [19]

Cole, Jr. et al.

[11] **Patent Number: 5,073,814**

[45] **Date of Patent: Dec. 17, 1991**

[54] **MULTI-SUBLAYER DIELECTRIC LAYERS**

[75] Inventors: **Herbert S. Cole, Jr.**, Scotia; **Yung S. Liu**, Schenectady, both of N.Y.

[73] Assignee: **General Electric Company**, Schenectady, N.Y.

[21] Appl. No.: **546,960**

[22] Filed: **Jul. 2, 1990**

[51] **Int. Cl.**[5] **H01L 29/34**; H01L 23/48

[52] **U.S. Cl.** **357/54**; 357/52; 357/71

[58] **Field of Search** 357/52, 54, 71

[56] **References Cited**

U.S. PATENT DOCUMENTS

4,827,325	5/1989	Orbach et al.	357/54
4,933,738	6/1990	Orbach et al.	357/51

OTHER PUBLICATIONS

S. M. Sze, *Semiconductor Devices Physics and Technology*, John Wiley & Sons, New York (1985), pp. 344, 472.

An eight page data sheet entitled "Teflon AF Amorphous Fluoropolymer", dated 01/19/90 from DuPont.

Primary Examiner—J. Carroll

Attorney, Agent, or Firm—Marvin Snyder; James C. Davis, Jr.

[57] **ABSTRACT**

A dielectric layer comprising a plurality of sublayers of alternating composition can provide a reduced dielectric constant while providing the adhesion and laser drilling properties of a higher dielectric constant material. Such multi-sublayer dielectric layers may be formed in situ on a high density interconnect structure or may be laminated thereon after their own formation.

28 Claims, 6 Drawing Sheets